Synthesis of Vertically-Aligned Zinc Oxide Nanowires and Their Applications as Photocatalysts

by

Qiong Zhou

A thesis
presented to the University of Waterloo
in fulfillment of the
thesis requirement for the degree of
Master of Applied Science
in
Mechanical Engineering - Nanotechnology

Waterloo, Ontario, Canada, 2013

AUTHOR'S DECLARATION

I hereby declare that I am the sole author of this thesis. This is a true copy of the thesis, including any required final revisions, as accepted by my examiners.

I understand that my thesis may be made electronically available to the public.

Abstract

Zinc oxide (ZnO) nanostructures, especially nanowires, have been one of the most important semiconductive materials used for photocatalysis due to their unique material properties and remarkable performance. In this project, vertically-aligned ZnO nanowires on glass substrate have been synthesized by using the facile hydrothermal methods with the help of pre-coated ZnO seeding layer. The crystalline structure, morphology and UV-Vis transmission spectra of the as-synthesized sample were characterized by X-ray diffraction (XRD), field-emission scanning electron microscopy (FE-SEM) and Ultra-violet Visible (UV-Vis) Spectrophotometer. The photocatalytic activity of the sample was examined for the photocatalytic degradation of methyl orange (MO) as the test dye in aqueous solution under UV-A irradiation. The extent of direct hydrolysis of the MO dye under UV light without the photocatalysts was first measured to eliminate the possible contribution from the undesired variables to the overall efficiency. The effects of pH and initial concentration of the MO solution, as well as the nanowire growth time, on the photocatalytic efficiency have been investigated, in order to determine the optimal conditions for photocatalytic applications of ZnO nanowires in the industry. Furthermore, the reproducibility of the experimental methods used in this project was tested to ensure the reliability of the experimental results obtained; and the reusability of the prepared ZnO nanowire arrays were also evaluated to investigate the stability of the products for photocatalytic applications in a large scale. In addition, a micro-chamber based microfluidic device with integrated ZnO nanowire arrays has been fabricated and used for photodegradation studies of MO solution under continuous-flow conditions. As expected, the micro-chamber based approach exhibited much improved photodegradation efficiency as compared to the conventional method using bulk dye solution. The effects of the flow rate and chamber height of the microfluidic device have also been investigated in order to determine the optimal experimental conditions for photodegradation reactions in microfluidic devices.

Acknowledgements

During my two years' study towards the degree of Master of Applied Science in Mechanical Engineering (Nanotechnology) in University of Waterloo, so many people offered me help that I would like to express my sincere acknowledgements here.

First and foremost, my sincere thanks to my thesis advisor, Prof. John Z. Wen, who not only gave me the opportunity to conduct research under his supervision, but also offered me continuous supervisory, guidance, and support throughout my course of research work. I appreciate much the freedom he allowed me for both my research and course studies, and his initiation and efforts to start collaborations with researchers across multiple disciplines, especially with the Waterloo Microfluidics Laboratory and Prof. William Anderson's research group. Being part of the group in Laboratory for Emerging Energy Research (LEER), I am proud and thankful that he has always been very concerned with the personal development of us, for not only supporting us for conferences each year, but also giving us chances to sharpen our research skills and presentation skills in group meetings.

Secondly, I would also like to express my grateful acknowledgement to the Waterloo Microfluidics Laboratory. Thank Prof. Carolyn Ren for her consistent coordination, guidance, and motivation on all the work towards the completion of the microfluidic project. Her enthusiasm for research is infectious and I personally appreciate her attitude towards research and the way of motivating students. Specially thanks to Ning Qin, for all his contributions and close collaborations with me on the microfluidic project. His resilience not only motivated me to work hard with him, but also directly led to the completion of preliminary studies of the microfluidic project. I would also like to thank Cody, Tom and some other people from the Waterloo Microfluidics Lab that may have also contributed to the microfluidic project but I am not aware of. For the photocatalysis project, my grateful thanks to the Waterloo Microfluidics Lab for teaching me how to and allowing me to use their spin coater.

I would also like to acknowledge Prof. William A. Anderson, for all his advises on my photocatalysis project, and his generosity for granting me the access to his lab facilities, especially the UV lamp, oven, and UV-Vis spectrometer, his continuous efforts to connect me to a number of researchers in this area, and finally for all his time and effort put in my thesis, paper, and seminar. Meanwhile, I would also like to sincerely thank Prof. Michael Mayer for sparing his time to read and comment on my thesis and attend my seminar.

In the completion of this work, there are also many other researchers who have offered me precious help in different areas. I would like to acknowledge Nina from WATLab led by Prof. Tong Leung for taking the XRD measurements of my sample, Zeinab and Dave from Prof. Ting Tsui's group for teaching me how to use their SEM equipment and Prof. Ting Tsui for granting me access to it later, Prof. Siva Sivoththaman for providing me access to his UV-Vis spectrometer and Bita from his group for assisting me to use it, and Prof. Zhongchao Tan for letting me use the oven in his lab.

Last but not least, I want to thank all my colleagues for their knowledgeable and moral support: Jinhee, Saleh, Golnaz, Kang, Sarah, and Amir. Special thanks to Golnaz who also taught me how to use the SEM and told me whom to contact for equipment, to Jinhee who has shared and taught me how to use the facilities in our lab, to Saleh who always offered good advices to my presentations and for his previous efforts in coordinating our group meetings.

Dedication

This thesis is dedicated to my family (Mom, Dad, my sister Carol and my grandpa);

and to my future family.

Table of Contents

List of Figures

List of Tables

Chapter 1

Introduction

1.1 Background

Over the past few decades, industrial effluents, as well as household wastewater, have been major sources of residual dye pollutants that are improperly disposed into the environment and are not readily biodegradable. Traditional ways of treatment, such as adsorption on activated carbon, chemical precipitation and separation, coagulation, are non-destructive methods, and only transfer dyes from one phase to another, causing secondary pollution and requiring further treatment [1–3]. Strict regulations of waste water treatment force to search for novel and efficient methods.

Since the first discovery of photocatalytic activity in TiO_2 by Fujishima and Honda [4] in 1972 through their initial work on the photocatalytic splitting of water on TiO_2 electrodes, extensive studies have been done to understand the principles of photocatalysis and to improve the photocatalytic performance of TiO_2 in many applications. In recent years, the widely concerned energy and environment-related issues have drawn intense attention onto the application of TiO_2 nanostructures as effective photocatalysts in degrading a wide range of organic pollutants into non-hazardous non-toxic byproducts under UV or Visible light irradiation. However, large-scale application of TiO_2 in industrial waste water treatment is non-economic. ZnO, on the other hand, has also been commonly used for many applications such as gas sensors [5], UV lasers [6], light-emitting diodes [7], solar cells, nanogenerators [8], and field effect transistors [9], due to their remarkable performance in electronics, optics, and photonics. It has also been found that ZnO is a suitable alternative to TiO_2, as ZnO has a similar band gap as TiO_2, and is cheaper, non-toxic, and easier to grow. Later it has been

proven that ZnO actually exhibit a higher quantum efficiency and photocatalytic efficiency than TiO_2.

The preparation of ZnO nanostructures was reported using different synthesis techniques [7], [10–13]. Among them, the hydrothermal synthesis of ZnO nanowire structures is the most extensively employed, due to the anisotropic growth nature of ZnO, the ability to be immobilized onto different substrates, and its ease of handling. The application of ZnO nanowires as photocatalysts for photodegradation of organic pollutants in water has been reported to be more efficient than other ZnO nanostructures such as nanoparticles and nanothin films, due to a high specific surface area without aggregation and the introduction of more surface defects in the structure. Moreover, the applications of the immobilized ZnO nanowires on substrates eliminate the costly post-treatment separation and recovery process.

So far, a lot of research works have been done to optimize the synthesis conditions to improve the photoactivity of ZnO nanowires, such as the precursor concentration and pH, growth temperature, and the properties of the seeding layer. However, not much information is available on the photocatalytic application side, such as the effect of the pH and concentration of the pollutant solution on the performance of the ZnO nanowire photocatalysts.

In very recent years, the miniaturization of the photodegradation process using microreactors has been proposed in order to take advantage of the high surface-to-volume ratio and continuous-flow inherent in the microfluidic devices. Some research groups have fabricated ZnO nanowire-integrated microfluidic devices with different methods for photocatalytic studies of organic dyes, and have reported enhanced photocatalytic efficiency compared to the existing conventional techniques. However, a systematic study is still lacking to optimize the device dimensions and reaction parameters, in order to achieve a maximum photocatalytic efficiency of the device in photodegradation of organic pollutant solutions.

1.2 Motivation

It is desirable to investigate the effects of pH and initial dye concentration of the dye solutions as well as the nanowire growth time on the photocatalytic efficiency of the prepared ZnO nanowire arrays, so as to tailor the properties of the products or the photodegradation reaction conditions to achieve a better photoefficiency in the environmental waste water treatment applications. It is also beneficial to miniaturize the photocatalytic degradation reactions into a micro-chamber based microreactor using the fabricated ZnO nanowire-integrated microfluidic device, and study its dependence of photoefficiency on the parameters such as chamber height and flow rate, aiming to optimize the device for a maximum photoefficiency in the photocatalytic applications.

1.3 Objectives

The objectives of this thesis project are:

(1) To prepare vertically-aligned ZnO nanowire arrays on glass substrate and test their photocatalytic efficiency in photodegradation of MO solutions.

(2) To investigate the effects of pH and initial concentration of MO solutions, and the growth time of the nanowires, on the photocatalytic efficiency of the ZnO nanowires.

(3) To evaluate the reproducibility of the experimental methods used, and to test the reusability of the prepared ZnO nanowires as photocatalysts for multiple cycles.

(4) To fabricate the micro-chamber based microfluidic device integrated with ZnO nanowire arrays, and compare its photoefficiency with the conventional methods.

(5) To investigate the effects of chamber height and flow rate on the photocatalytic efficiency of the integrated microfluidic device for photodegradation applications.

1.4 Thesis Organization

This thesis report has been organized as follows:

Chapter 1 gives a brief introduction to the background, basic properties and applications of ZnO, development and advantages of applying ZnO nanowires for photocatalysis, development of photocatalyst-integrated microfluidic devices, and the motivation and objectives of the project.

Chapter 2 presents a comprehensive review of literature on the principles of photocatalysis, types of photocatalysts, structural properties and synthesis methods of ZnO semiconductor, and the development of microfluidic devices for photocatalytic applications. The first part of this chapter explains the principles of the photocatalysis by describing in detail the processes taking place after photoexcitation of ZnO semiconductor. The second part compares different types of the commonly used photocatalysts, with a focus on ZnO versus TiO_2. The third part analyzes the crystal structures of ZnO, compares the nanostructures, and summarizes the synthesis techniques. The last part of this chapter reviews the current progress of fabrication and photocatalytic applications of the nanostructure-integrated microfluidic devices.

Chapter 3 describes the detailed experimental procedures in this project. The first part gives all the materials used, and the second part describes the steps of synthesizing ZnO nanowire arrays. The characterization techniques and equipment used are mentioned in the third part. The fourth part gives the experimental set-up, procedures adopted and their theoretical support to evaluate the photocatalytic efficiency of the samples. The last part describes the steps to fabricate the ZnO nanowire-integrated microfluidic device and to evaluate its efficiency in photodegradation reactions.

Subsequently, Chapter 4 presents the results obtained from the various characterization techniques and the photocatalytic activities of the ZnO nanowire arrays and the integrated microfluidic device under different conditions. An in-depth analysis and comparison of the results are also presented in this part.

Chapter 5 concludes the work done in this project and gives recommendations for possible improvement.

Finally, the Bibliography part provides the references used in this thesis report.

Chapter 2

Literature Review

In this chapter, a comprehensive review of literature will be presented on the principles of photocatalysis, different types of photocatalysts, structural properties of and photocatalytic performance comparison between TiO_2 and ZnO, synthesis methods of ZnO semiconductor, discussion of main parameters that affect the photoefficiency, and the development of microfluidic devices for photocatalytic applications. In the first part, the principles of the photocatalysis and the processes taking place after photoexcitation will be described in detail. The second part compares different types of the commonly used photocatalysts, with a focus on TiO_2 vs. ZnO, as detailed in the third and fourth part, respectively. The fourth part also analyzes the crystal structures of ZnO, compares the different nanostructures, and summarizes the synthesis techniques. The fifth part presents a detailed discussion of some of the main parameters that affect the photocatalytic efficiency of the catalysts in decomposing organic pollutants. The last part reviews the current progress of fabrication and photocatalytic applications of the nanostructure-integrated microfluidic devices.

2.1 Principles of Heterogeneous Photocatalysis

In chemistry, homogeneous catalysis refers to a series of reactions that are catalyzed by a catalyst in the same phase as the reactants. Usually, homogenous catalysts are dissolved together with the reactants in a solvent, most commonly water. Due to the technically difficult and economically undesirable process of post-reaction separation, heterogeneous reaction is more preferred, where the catalyst is in a different phase with the reactants and is hence more easily to be separated. In general, in order for a heterogeneous reaction to occur,

five steps are necessary [14]: (1) diffusion of reactant molecules from the bulk to the surface, (2) adsorption onto the surface, (3) reaction on the surface, (4) desorption of products from the surface, and (5) diffusion of products to the bulk.

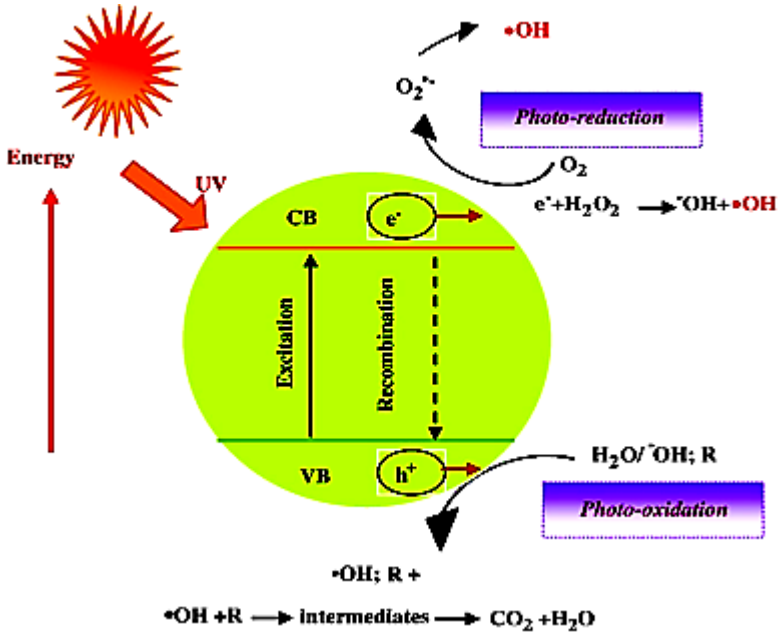

Figure 2.1: A schematic diagram illustrating the principle of photocatalysis (reproduced from [15]**).**

Photocatalysis generally involves the process of photosensitization, where a photochemical reaction occurs in one chemical species due to the absorption of photonic energy by another species called photosensitizer [16], which, in most cases, refers to a semiconductor. The mechanism of photocatalysis is illustrated in Figure 2.1. When incoming photons with energies larger than the band gap energy (ΔE) of the photocatalyst are absorbed, the electrons in the valence band (VB) of the semiconductor photocatalyst are excited into the conduction band (CB), leaving behind an equal number of holes in the VB (Eq. (2.1)). Apart from the recombination that may occur in the bulk or on the surface of the catalyst, the photo-generated electron-hole pairs will separate from each other and migrate to catalytically active sites at the semiconductor/liquid interface and then react with any adsorbed species. The

holes, with high oxidative potential, will either oxidize the organic species directly (Eq. (2.2)), or form very active hydroxyl radicals (*OH·*) by decomposition of water (Eq. (2.3)) or reaction with hydroxyl ions (*OH-*) in water (Eq. (2.4)). The electrons in the conduction band on the catalyst surface, on the other hand, can reduce adsorbed oxygen into superoxide anions (Eq. (2.5)) or peroxides (Eq. (2.6)), which may subsequently form hydroxyl radicals (*OH·*) (Eq. (2.7))[15], [17]. The hydroxyl radical is a highly powerful, non-selective oxidant (E° = +3.06 V) which gives a partial or complete decomposition of many organic compounds (Eq. (2.8)) [18], and hence acts as the primary cause of organic species mineralization in the photocatalytic reactions [3], [19], [20]. Table 2.1 gives the relative rate constants of the oxidation reactions of various organic compounds by ozone and hydroxyl radicals, and the data confirms the potency of the hydroxyl radicals.

Table 2.1: Relative rate constants ($dm^3mol^{-1}s^{-1}$) of ozone and hydroxyl radical (reproduced from [21]**).**

Compound	O_3	*OH*
Chlorinated Alkenes	10^{-1}–10^{3}	10^{9}–10^{11}
Phenols	10^{3}	10^{9}–10^{10}
N-containing organics	10–10^{2}	10^{8}–10^{10}
Aromatics	1–10^{2}	10^{8}–10^{10}
Ketones	1	10^{9}–10^{10}
Alcohols	10^{-2}–1	10^{8}–10^{9}
Alkanes	10^{-2}	10^{6}–10^{9}

The process of photocatalytic degradation can also be represented by a series of equations. The photoexcitation of ZnO semiconductor by proper UV light irradiation, followed by the formation of electron-hole pairs can be expressed below:

$$ZnO + h\nu \rightarrow ZnO\ (e^- + h^+) \qquad (2.1)$$

The photogenerated holes and electrons are strong oxidizing and reducing agents, which will cause a series of subsequent oxidative and reductive reactions, respectively, as illustrated by:

Photooxidation reactions:

$$h^+ + \text{dye} \rightarrow \text{dye}^{\cdot+} \rightarrow \text{degradation of the dye} \quad (2.2)$$

$$h^+ + H_2O \rightarrow H^+ + OH\cdot \quad (2.3)$$

$$h^+ + OH^- \rightarrow OH\cdot \quad (2.4)$$

Photoreduction reactions:

$$e^- + O_2 \rightarrow O_2^{\cdot-} \quad (2.5)$$

$$2e^- + O_2 + 2H^+ \rightarrow H_2O_2 \quad (2.6)$$

$$e^- + H_2O_2 \rightarrow OH^- + OH\cdot \quad (2.7)$$

The primary degradation of dye is caused by the hydroxyl radicals generated through the previous processes, as represented by Eq. (2.8):

$$OH\cdot + \text{dye} \rightarrow \text{intermediates} \rightarrow CO_2 + H_2O \quad (2.8)$$

It is worth noting that the presence of adsorbed oxygen molecules prevents the recombination of the photogenerated electron-hole pairs. In a typical photocatalytic reaction, if the reduction of adsorbed oxygen does not take place simultaneously with the oxidation of organic dyes, there is a large chance that the electrons are accumulating on the catalyst surface, leading to an increased recombination rate of the electrons and holes. Hence it is very important to prevent electron accumulation by introducing oxygen molecules into the reaction mixture to achieve an efficient photocatalytic reaction.

2.2 Types of Heterogeneous Photocatalysts

2.2.1 Noble Metal-Based Photocatalysts

In the history of heterogeneous photocatalysis, a lot of noble metals, such as Pt, Pd, Ru, Ir and Rh, and some metal oxides, such as Ti, Zn, W, Cu, Mn, Cr and Co, have been used as photocatalysts [14]. A good photocatalyst should be photoactive, able to harness visible and/or near UV light energy, biologically and chemically inert, stable towards photocorrosion, low in cost and toxicity [21]. It is well known that noble metals are generally more active catalysts than metal oxides in majority of applications. However, noble metals are less resistant to poisoning than metal oxides, and can be a potential hazard to the environment. Moreover, due to the absence of band gap and the continuum of electronic states in the noble metal structures, the photogenerated electron-hole pairs can be readily recombined, which leads to deactivation of the active sites and a reduction in photocatalytic efficiency. Hence, metal oxides are more suitable to be used in various applications as photocatalysts. In fact, according to Matatove-Metal and Sheintuch [22], there are some criteria for catalysts to be used in industrial applications, such as high activity, resistance to poisoning and stability over time at elevated temperatures, mechanical stability and resistance to attrition, non-selectivity, physical and chemical stability under various conditions.

2.2.2 Semiconductor-Based Photocatalysts

In recent years, semiconductors, such as TiO_2, ZnO, WO_3, Fe_2O_3 and ZnS, have drawn increasing interest as effective photocatalysts in the photocatalytic process, due to their higher stability than metals and higher electrical conductivity than insulators. For semiconductors, the band gap energy is very critical in the photocatalytic process. Table 2.2 and Figure 2.2 show the band gap energies and the band gap edge positions of a range of common semiconductor photocatalysts, on a potential scale (V) versus the normal hydrogen

electrode (NHE) [11, 13-14] . Figure 2.2 also indicates the redox potentials of the H^+/H_2 and O_2/H_2O half reactions versus NHE by dashed lines. In order for a semiconductor to be active as a photosensitizer in the photocatalytic processes, the photogenerated holes in VB should have more positive potential than the O_2/H_2O potential so that they have sufficient energy to generate *OH·* radicals (Eq. (2.3-2.4)) and subsequently oxidize the organics (Eq. (2.8)); similarly, the potential of photogenerated electrons in CB should be sufficiently negative to be able to reduce adsorbed oxygen molecules into superoxide anions (Eq. (2.5)) or peroxides (Eq. (2.6)). In other words, the band gap of the semiconductors should straddle their respective redox potentials, as exemplified by ZnO, TiO_2, $SrTiO_3$, ZnS, CdS, and CdSe (Figure 2.2).

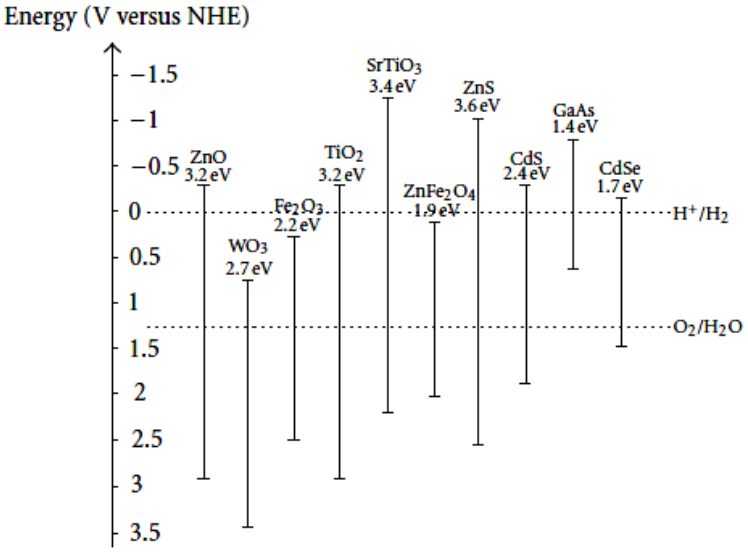

Figure 2.2: Band gap edge positions and band gap energies of common semiconductor photocatalysts (dashed lines indicate the redox potentials of the H^+/H_2 and O_2/H_2O half reactions) (reproduced from [23]**).**

Table 2.2: Values of band bap energies of various semiconductor photocatalysts (reproduced from [21]**).**

Photocatalyst	*Bandgap energy (eV)*	*Photocatalyst*	*Bandgap energy (eV)*
Si	1.1	ZnO	3.2
TiO_2 (rutile)	3.0	TiO_2 (anatase)	3.2
WO_3	2.7	CdS	2.4
ZnS	3.7	$SrTiO_3$	3.4
SnO_2	3.5	WSe_2	1.2
Fe_2O_3	2.2	α-Fe_2O_3	3.1

However, some semiconductors listed above are not very stable, such as CdS in aqueous media, or photocorrosion of metal sulfides and α-Fe_2O_3 [25]. Some have poor photooxidation kinetics such as n-Si and WO_3 [26]. Smaller band gap is usually more preferred than wide ones as the minimum wavelength required to excite electron-hole pairs depends on the band gap energy of the semiconductor photocatalysts, as described by Eq. (2.9):

$$\lambda_{min} = 1240 / E_{bg} \qquad (2.9)$$

2.3 Titanium Oxide Photocatalysts

Titanium oxide, or titania (TiO_2) is commonly used as a while pigment in producing cosmetics or paints, due to its very high refractive index (anatase is 2.5-3 and rutile is 3.87) [16]. In the past few decades, TiO_2 has been widely used as one of the most efficient photocatalysts for many environmental applications [27], since the discovery of using TiO_2 photoanode for successful photolysis of water under UV light with a wavelength smaller than 190nm by Fujishima *et al* in 1972 [4]. So far, TiO_2 has a wide range of applications in many fields, such as photocatalytic decomposition of organic pollutants in environmental purification processes, photoelectrochemical splitting of water for generation of hydrogen gas, decomposition of carbonic acid gases, and dye-sensitized solar cells [26]. In recent years, the most intensively pursued research on TiO_2 is its use for photocatalytic degradation

of organic pollutants in environmental cleaning system. This section reviews the common crystal structures of TiO_2 and its photocatalytic performance.

2.3.1 Crystal Structures

Titanium dioxide is a semiconductor that crystallizes in eight polymorphs under different conditions. Among them, rutile, anatase, and brookite nanocrystals are the three naturally existing polymorphs. The anatase and brookite phase are generally thermodynamically metastable, and upon annealing at high temperatures, could transform into the much stable rutile phase [28]. Anatase and rutile are the most common phases and much research has been conducted on their synthesis and applications. In contrast, brookite is the rarest phase in nature and is very difficult to be synthesized in laboratories [29]. Thus not much information on the properties of pure brookite is known.

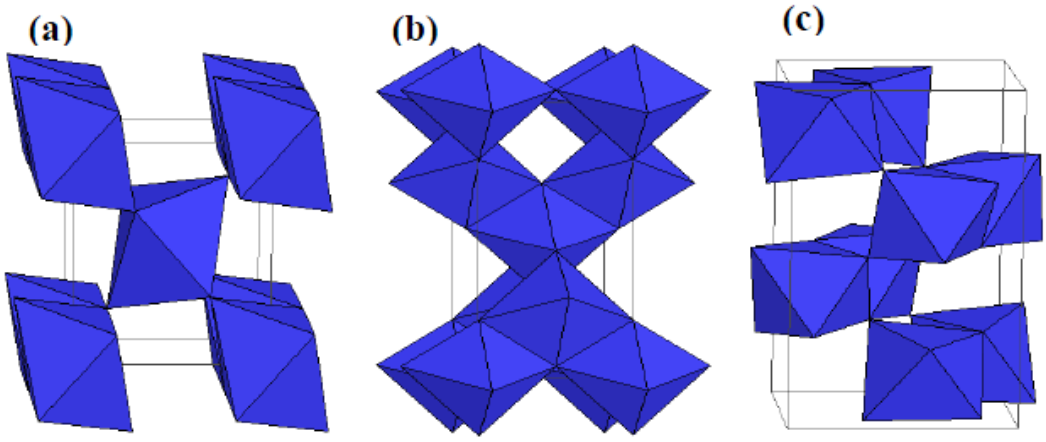

Figure 2.3: Crystal structures of (a) rutile, (b) anatase, and (c) brookite TiO_2.

As shown in Figure 2.3, rutile and anatase have tetragonal structure, while brookite is orthorhombic [30]. Although they all consist of TiO_6 octahedra, different bond formation mechanisms distinguish these three phases. In rutile crystal structure (Figure 2.3(a)), only two

out of the twelve edges of each octahedron are connected to form a linear chain, which is also connected together by sharing of oxygen atoms at the corner. For anatase (Figure 2.3(b)), four edges of each octahedron are connected to form the crystal structure without sharing of oxygen atoms. In brookite (Figure 2.3(c)), three edges per octahedron are shared [31]. A more detailed analysis of the three phases is displayed in Table 2.3 below.

Table 2.3: Bulk properties of three different TiO_2 crystal structures (reproduced from [30]**).**

Crystal structure	System	Lattice constants (nm)			Molar Volume	Density (kg/m^3)
		a	b	c		
Rutile	Tetragonal	0.4584	-	0.2953	18.693	4240
Anatase	Tetragonal	0.3733	-	0.937	20.156	3830
Brookite	Orthorhombic	0.5436	0.9166	0.5135	19.377	4170

2.3.2 Photocatalytic Performance

TiO_2, as a semiconductor photocatalyst, has high UV light absorption and high stability, and has been widely used in photocatalytic degradation of organic pollutants in environmental cleaning system. It can be used in the form of a water suspension, or a thin film in waste water treatment, and has different crystal structures. In photocatalytic applications, it has been reported that anatase is more photoefficient than rutile due to its more open structure, but anatase is not stable and can easily transfer into the less efficient rutile phase upon heating to temperatures above 70ºC [28].

Ever since Frank and Bard first investigated the possibility of using TiO_2 to decompose cyanide in water in 1977, increasingly research interests have been focused on environmental applications. For example, Zhang *et al.* have reported complete photodegradation of RhB dye

over TiO_2 bilayer films under the wavelength of 365nm [32], Dolamic *et al.* have efficient photodegradation of amino acids over TiO_2 nanoparticles [33]. In order to avoid the post-treatment separation process of TiO_2 powders from water, researchers began to try to immobilize the TiO_2 particles onto substrates, such as in the thin film form [34].

Although TiO_2 is the most widely used material in heterogeneous photocatalysis as it is cheap, chemically inert, and has high photoefficiency [35], [36], some drawbacks do exist which undermine its photoefficiency in practical applications. One important drawback is its wide bandgap energy of 3.2 eV, which necessitates the irradiation of UV light for photoexcitation [37]. Since the UV light is only a very small portion of the entire solar energy (5%) and the rest is predominantly visible light, any observable shift in the photo response of TiO_2 from UV to visible light regime would enhance much its photocatalytic activity [38]. Recently, many researches have been carried out to extend the photocatalytic activity of titania into the visible light regime, through doing with transition metals [39] or non-metal elements [40]. However, although doping with transition metals decreases the photoexcitation energy of TiO_2 to some extent, the metal ions also act as the recombination centers for the electron-hole-pairs, thus to undermine the overall efficiency of the photocatalyst [41]. Moreover, doping to TiO_2 is generally difficult and involves high temperatures, under which the anatase phase is likely to undergo phase transformation into the less active rutile phase.

2.3.3 Comparison of Photocatalytic Activities of TiO_2 and ZnO

In addition to what mentioned in the previous section, a large-scale application of TiO_2 in industrial waste water treatment operations is very non-economic due to its high price and rareness in existence [18]. Hence, ZnO has been increasingly recognized as a suitable alternative to TiO_2, as its band gap energy is comparable with that of TiO_2 and its photocatalytic degradation mechanism has been proven to be similar to that of TiO_2 [14], [42–44]. In contrast to TiO_2, ZnO is abundant in nature, non-toxic, has a lower cost of

production, and is easier to grow either in the form of powders [45] or on top of various substrates [46–48]. In fact, ZnO has been reported to be more efficient than TiO_2 in some cases, for instance, in the advanced oxidation of pulp mill bleaching wastewater [49], and photocatalyzed degradation of phenol [50], [51] and 2-phenylphenol [19]. In the field of dye-sensitized solar cells (DSSCs), ZnO-based DSSC techniques are also preferred than TiO_2-based ones due to a faster electron transport rate in ZnO with a reduced recombination rate, and its ease of crystallization and anisotropic growth [52].

Semiconductor photocatalysts like TiO_2 and ZnO are generally capable of exhibiting photoactivity under UV light irradiation, and even under visible light if there exist enough inherent crystalline defects in the crystal structures [53] or by artificial creation of defect sites through doping with metals and/or transition metals [54–57]. The defect sites, either inherent or engineered, create quasi-stable energy levels within the band gap, which lower the required transition energy for electrons and enhance electron trapping, leading to a higher optical absorption and a lower recombination rate; in other words, more electron-hole pairs are generated and migrated onto the surface to form more hydroxyl radicals. And ultimately the quantum efficiency and photocatalytic efficiency of the photocatalysts are increased [53]. Compared to TiO_2, ZnO nanostructures have a larger number of inherent active defect sites on the surface [58], which makes ZnO capable of absorbing a larger fraction of the solar spectrum and exhibit a higher quantum efficiency and photocatalytic efficiency than TiO_2 [19], [20], [51], [59], [60], due to its effectiveness in generation and separation of photon-induced electron-hole pairs [43], [61], [62]. In contrast, the undoped TiO_2 is not very active, especially under visible light irradiation. It has been reported that the commonly used TiO_2 nanoparticle (Degussa P25) aqueous solution exhibits an absorption peak at around 220nm but with nearly zero absorption after 370nm [63].

Since doping of semiconductors with metal and/or transition metals increases surface defects, the doping of both ZnO and TiO_2 with various metals have been investigated separately by many research groups, with an effort to enhance their optical absorption and shift into visible light regime (400-700nm). It has been reported that ZnO nanostructures

doped with silver (Ag) [54], lead (Pb) [55], cobalt (Co) [56] and manganese (Mn) [57] have shown enhanced visible light absorption and photocatalytic activity. However, doping of TiO_2 is more difficult, and it has been reported by Martin *et al.* [64] that the vanadium (V)-doped TiO_2 shows a reduced quantum efficiency than the undoped TiO_2, probably due to an undesired phase transformation of TiO_2 from anatase to rutile at elevated temperatures. Klosek and Raftery [65] reported later that the photocatalytic degradation of ethanol using V-doped TiO_2 showed higher efficiency but produced undesired hazardous byproducts. Another major problem reported with TiO_2 is that its reaction photoefficiency is very low possibly due to scattering of light by the TiO_2 particles dispersed in the water suspension [66].

2.4 Zinc Oxide Photocatalysts

2.4.1 Crystal Structures of ZnO

Zinc oxide (ZnO) is a II-VI semiconductor with a wide direct band gap of 3.37 eV (i.e. in the near-UV range) and a large exciton binding energy of about 60 meV at 300 K [13]. It is important to note that the values for ZnO band gap energy reported in literatures are not necessarily the same, due to the existence of different levels of oxygen vacancies in the ZnO samples [67].

ZnO can be crystallized in three forms under different conditions: hexagonal wurtzite, cubic zinc blende, and rock-salt structure [68]. The rock-salt crystal structure (Figure 2.4 (a)), similar to the common NaCl crystal structure, is only stable under relatively high pressures of about 10GPa; while the cubic zinc blende-type structure (Figure 2.4 (b)) can only be stabilized by epitaxial growth of ZnO on substrates with cubic lattice structure [69]. In the rock-salt structure, each of the two individual ion types forms a separate face-centered cubic (fcc) lattice, interpenetrating each other to form a 3D checkerboard pattern, which can also be

viewed as a face-centered cubic structure with its octahedral positions occupied by another type of ions. In the zinc blend structures (typical example: ZnS), the two types of ions also form two interpenetrating fcc lattices, similar as in the rock-salt structure, but it differs in terms of the positions of the two lattices. As illustrated in Figure 2.4 (b), the zinc and oxygen ions have tetrahedral coordination, i.e., each zinc ion is surrounded tetrahedrally by four oxygen ions and vice versa.

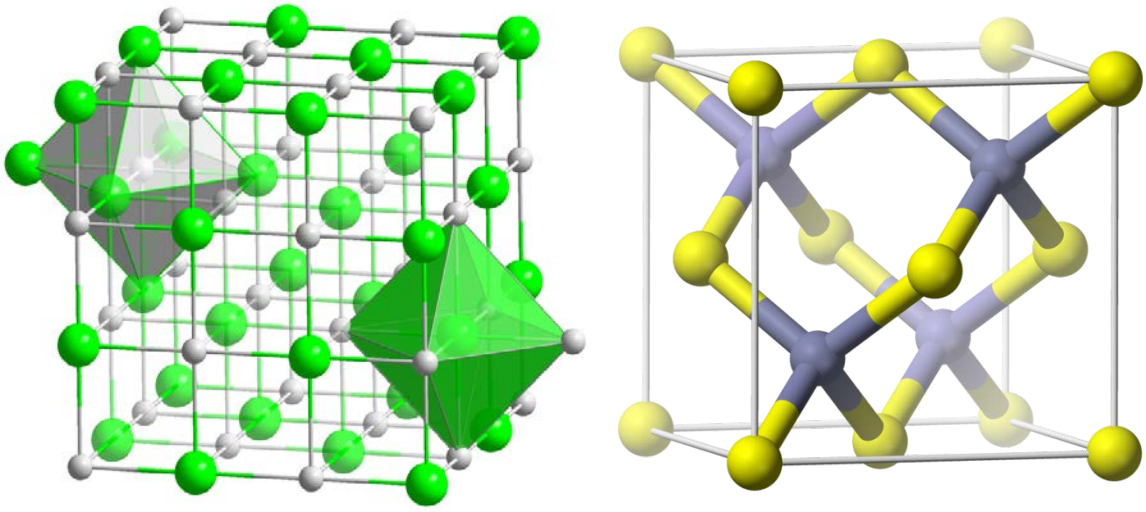

(a) ***(b)***

Figure 2.4: Stick and ball representation of ZnO crystal structures: (a) the rock-salt structure; (b) the cubic zinc blende unit cell. The light grey or yellow spheres denote oxygen, and dark or blue ones denote zinc, respectively (retrieved from http://www.wikipedia.org/).

The hexagonal wurtzite structure of ZnO is the most thermodynamically stable and hence most common among the three structures. Under general conditions, ZnO crystallizes into the wurtzite structure with great preference. As in the zinc blende structure, the ions in the wurtzite structure are also tetrahedrally coordinated (Figure 2.5 (b)), but each type of ions forms a separate hexagonal closed pack (hcp)-type lattice, instead of fcc-type for zinc blende structure. The entire structure can be simply described as a series of alternating planes composed of tetrahedrally coordinated oxygen and zinc ions, stacked alternately along the *c*-

axis, as illustrated in Figure 2.5 (a). According to Mehrabian *et al.* [70], the crystalline properties of the as-synthesized ZnO well match the indexed ZnO hexagonal structures on JCPS card no. 36-1451, with lattice constants to be a = 0.32498 nm, b = 0.32498 nm, c = 0.52066 nm. The corresponding c/a ratio is calculated to be around 1.60, which deviates merely slightly from the ideal value for a hexagonal unit cell ($c/a = \sqrt{8/3}$ =1.633) [68]. The Zn-O bonding in ZnO is polar and largely ionic, and the entire structure has no central symmetry, which together account for the preferred growth of wurtzite structure and the strong piezoelectricity of ZnO [71].

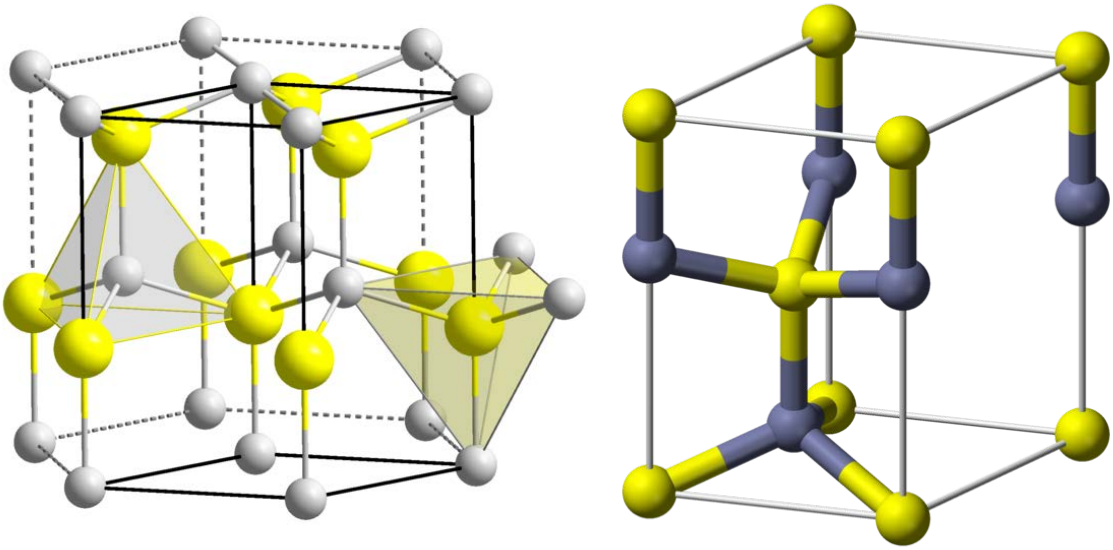

(a) *(b)*

Figure 2.5: Stick and ball representation of ZnO crystal structures: (a) the wurtzite structure; (b) the wurtzite structure unit cell. The light grey or yellow spheres denote oxygen, and dark or blue ones denote zinc, respectively (retrieved from http://www.wikipedia.org/).

2.4.2 Typical Nanostructures

Heterogeneous photocatalysis involves photoreactions occurring at the surface of a semiconductor, such as the contaminant species molecules need to be adsorbed onto the surface of the photocatalysts before the reactions could take place, and the active radicals are generated on the catalyst surface as well. Thus, surface area is a critical parameter to determine the activity of a photocatalyst. In order to achieve high surface area, a wide range of membranes with high porosity have been developed. However, only a small portion of incident light would actually penetrate into the membrane, and hence the effective surface area of the membranes is small and limited to the surface. Nanomaterials, on the other hand, offer a relatively high surface-to-volume ratio due to their nano-scale nature, and hence increase the effective surface area for photoexcitation.

Nanomaterial structures have drawn tremendous attention in recent decades and have exhibited superior performance in many applications. Generally, nanomaterials can be categorized into three groups based on their morphologies: zero-dimensional (0D), one1-dimensional (1D), and two-dimensional (2D) nanostructures. Nanoparticles or quantum dots, as typical 0D nanostructures, give a larger surface area with an aspect ratio of around one, and have been widely used in various biological applications [37-38]. Their surface area is usually measured by the Brunauer-Emmett-Telle (BET) surface area technique using the dry powders form. However, there are some important limitations associated with nanoparticles. Since nanoparticles are mostly used in the form of water suspensions, they tend to aggregate in the solution which results in a severe surface area reduction. So the actual specific surface area of the nanoparticle photocatalysts dispersed in the solution is dependent on the degree of aggregation of the powders. Moreover, it is a well-known difficulty to separate and recover nanoparticles from water suspensions. Additional costs and equipment are needed for these post-treatment processes, which limits their practical use in the industry [74]. The difficulty in recovering all the nanoparticle catalysts from water suspensions also raises concerns regarding to the consequences of releasing nanoparticles to the environment or end users.

One way to eliminate this issue of post-treatment for catalyst removal is to immobilize the catalysts onto a steady substrate, using various thin film deposition techniques [39-40]. Nanothin films, as 2D nanostructures, have also been extensively used as optical coatings, corrosion-resistant coatings, and semiconductor thin film-based devices. However, it exhibits a much lower photocatalytic performance due to the reduced surface area. 1D nanostructures, on the other hand, not only offer a specific surface area that is much larger than that of nanothin films and is comparable to that of aggregated nanoparticles, but it also eliminates the post-treatment process for catalyst removal. In the history of academic research and also industrial applications, 1D semiconductor nanostructures, such as nanowires, nanotubes, nanorods, nanofibers, and nanobelts, have drawn extensive interests and have been extensively used as building blocks for other structures [76], or for investigation of effects of electrical, thermal, and mechanical properties on the dimension and size reduction of materials [43-44].

Among all these 1D nanostructures, ZnO nanowires have been recognized as one of the most significant nanostructures for research and applications in the nanotechnology fields [79]. Table 2.4 gives a summary of comparison between three different ZnO nanostructures used in photocatalytic applications. ZnO nanowires could either be grown independently, or be grown and well aligned onto a wide range of substrates including polymer, glass, semiconductor, metal and other organic substrates such as polydimethylsiloxane (PDMS) [80] and polystyrene (PS) [81]. A vertically well aligned growth of ZnO nanowires on a substrate not only offers a much improved photocatalytic efficiency due to an enhanced specific surface area compared to direct catalyst deposition on the substrates, it also offer many advantages, such as introducing more surface defects and oxygen vacancies, which make nanowire structure a strong photocatalyst in photocatalytic applications [48-49]. Surface defects usually play an important role in determining photocatalytic efficiency of photocatalysts, and the crystalline defects in ZnO nanowires are primarily in the form of oxygen vacancies [53]. As a wide band gap semiconductor, ZnO is normally photoactive under blue to UV light irradiation. But it has been reported by Baruah and Dutta that ZnO

nanowires with inherent crystalline defects are capable of exhibiting visible light photoactivity even without of doping with transitional metals [82].

Table 2.4: Comparison of different ZnO nanostructures for photocatalytic applications (reproduced from [23]**)**

	Advantages	Disadvantages
0D Nanoparticles	• Large surface area-to-volume ratio	• Reduced effective surface area due to particle aggregation • Additional cost associated with post-treatment and recovery • Difficult to recover all catalyst
1D Nanowires	• Larger surface area-to-volume ratio than nanothin films • Growth well aligned on most substrates • post-treatment not required • Lower crystallinity and more surface defects, increases efficiency	• Lower surface area compared to nanoparticles, but similar effective surface area (aggregation of nanoparticles) • Restricted growth conditions
2D Nanothin films	• Coated on certain substrates • Post-treatment for catalyst removal is not required	• Small surface area, gives low performance

2.4.3 Synthesis Techniques

In the development of techniques to synthesize different nanostructures, the most important issue is to control the dimension, morphology and uniformity of the products simultaneously. In the past few decades, a large variety of "bottom-up" techniques have been employed to generate 1D nanostructures. Some of the strategies are summarized and illustrated in Figure 2.6, such as use of intrinsically anisotropic crystalline structure of a material (Fig. 2.6A), confinement of a liquid droplet by introducing a liquid-solid interface as in the vapor-liquid-solid process (Fig. 2.6B), use of a 1D template to direct the growth (Fig. 2.6C), control of the growth kinetics on different facets (Fig. 2.6D), and control of supersaturation levels in hydrothermal methods.

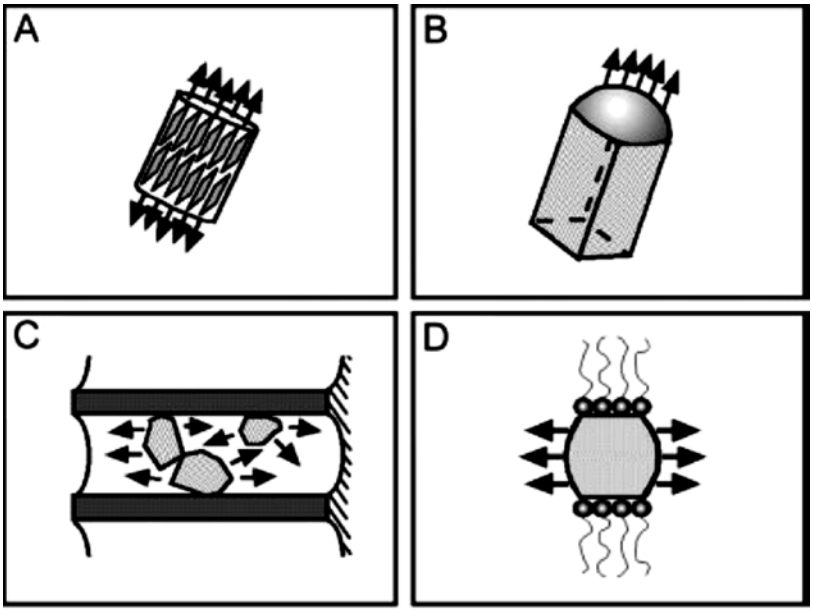

Figure 2.6: Illustration of four different strategies to achieve the growth of 1D nanostructures (reproduced from [77]**).**

Since ZnO is one of the solid materials that will naturally grow into 1D nanostructure due to its high anisotropy in the crystalline structure and ease of crystallization, extensive studies have been focused on fabricating 1D ZnO nanostructures and investigating the dependence of

electrical, thermal and optical properties on their morphologies. A wide variety of ZnO nanostructures have been fabricated so far, as illustrated in Figure 2.7, such as nanowires, nanorods, nanobelts, nanotubes, nanorings, nanohelixes, hierarchical nanowire junction arrays, comb-like cantilever arrays and polyhedral cages and shells [83]. The anisotropic growth of ZnO 1D nanostructures mainly takes place along the c-axis in the [0002] direction [84]. The final shape and aspect ratio of the resultant ZnO nanostructures are dependent on the relative growth rates on the different crystalline faces. For ZnO, the growth rates under the hydrothermal synthesis conditions are v[0001] > v[1011]> v[1010] [85].

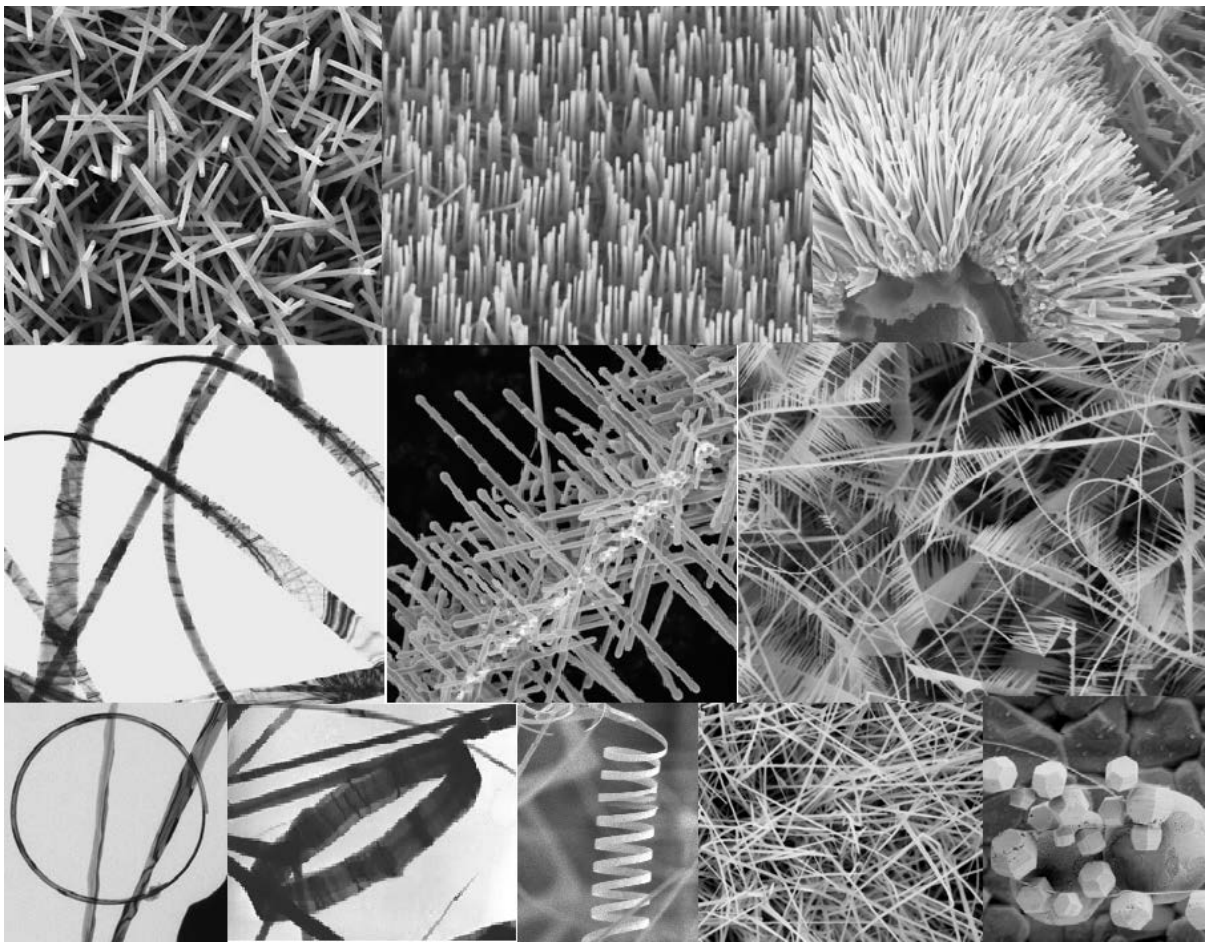

Figure 2.7: A collection of ZnO nanostructures synthesized under different controlled conditions (reproduced from [83]**).**

The synthesis methods of ZnO nanostructures could be broadly classified into two categories:

(1) The Vapor (or Gas) Phase Synthesis

The vapor phase synthesis is the most extensively used approach to synthesis 1D nanostructures. Many research groups, such as Kong *et al* [10], Yao *et al* [86] and Zhang *et al* [87], have used this technique to fabricate ZnO nanorods or nanowires with high quality, single-crystalline . A typical process takes place in a closed chamber at high temperatures from 500°C to 1500°C, with the gaseous species first generated by thermal evaporation, chemical reduction or gaseous reaction, and then transported and condensed onto a solid substrate surface [78]. The most common vapor synthesis methods include vapor liquid solid (VLS) growth [88], physical vapor deposition (PVD) [89], chemical vapor deposition (CVD) [90], metal organic chemical vapor deposition (MOCVD) [91], molecular beam epitaxy (MBE) [92], pulsed laser deposition (PLD) [93], and so on. Among all these methods, the VLS and MOCVD are the two most commonly and extensively used methods for ZnO nanowires fabrication.

Since first developed by Wagner and Ellis in the 1960s to fabricate micrometer-sized whiskers [94], the VLS method has been recognized as a very simple and cheap method and has been widely used for synthesis of ZnO nanowires and nanorods on large substrates such as Si, GaN, and AlGaN [95]. In a typical process, the gaseous reactants are dissolved into nanosized liquid metal droplets, which act as metal catalysts to facilitate nucleation and growth of single crystalline nanorods or nanowires, as illustrated in Figure 2.8 (a). The typical metal catalysts used in VLS methods include Au [96], [97], Cu [98], Ni and Sn [99].

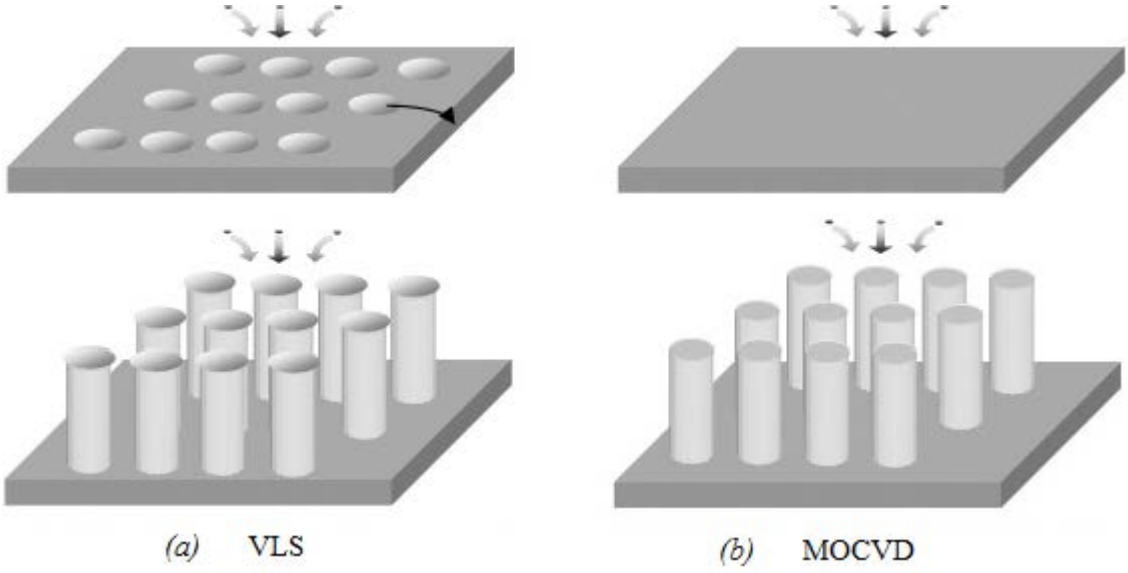

Figure 2.8: Schematic illustration of ZnO nanowires/nanorods growth from *(a)* VLS method and *(b)* MOCVD method [78]**.**

As contrast to VLS method, the MOCVD method is a very recently developed technique for ZnO nanowire fabrications, and no catalyst is used here, which eliminates the possible inclusion of catalyst impurities as in the catalyst-assisted VLS method and hence produces high-purity ZnO nanowires [94], [100]. The growth temperature of MOCVD is around 400 – 500°C, which is much lower than a typical catalyst-assisted VLS process of 900°C [96]. The advantages of producing high-purity ZnO nanowires at lower temperatures make the MOCVD-synthesized structures more useful and efficient for electric and photonic device applications [78]. The exact mechanism of MOCVD of ZnO nanowires is not thoroughly revealed, but it is believed to be mainly attributed to the anisotropic surface energies existent in the ZnO wurtzite structure and the higher growth rate on the nanowire tips than on the side walls (Figure 2.8*(b)*). The resultant structures from MOCVD, as observed from Figure 2.9 (b), exhibit more needle-like tips at the top of the nanowires, as compared to VLS-synthesized structures (Figure 2.9 (a)), as the vertical growth rate for ZnO nanostructures is much higher the lateral one [101].

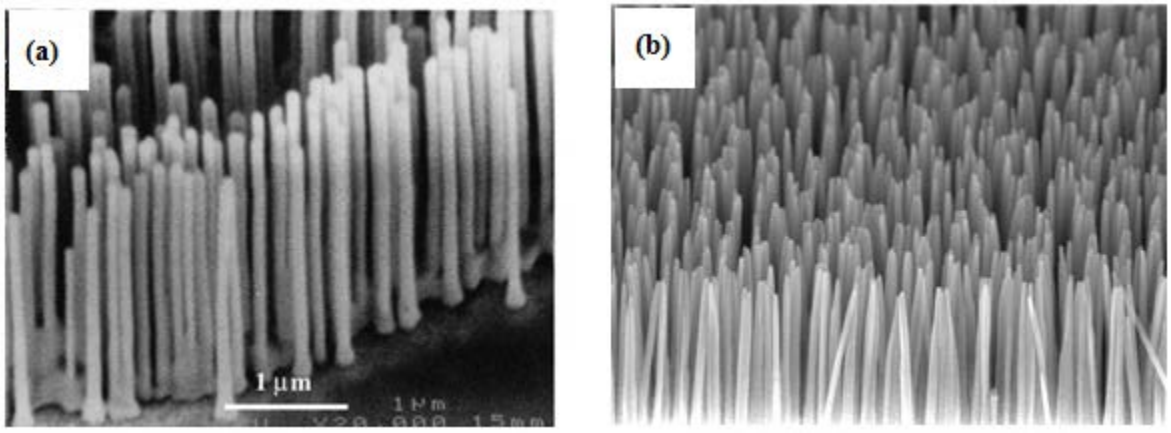

Figure 2.9: FE-SEM images of (a) VLS-grown [102] **and (b) catalyst-free MOCVD-grown ZnO nanostructures** [100]**.**

(2) The Solution Phase Synthesis

Although the vapor phase synthesis methods can produce high-quality, single-crystalline nanowires with several micrometers in length, these methods have some disadvantages such as requiring high temperatures, having limited substrate choice, low product uniformity, and low product yield [103]. In contrast, the solution phase synthesis has been reported to be advantageous due to its low growth temperature, low cost, ease of handling and potential scalability for producing high-density arrays (number density above 10^{10} cm^{-2}) [12]. A typical solution phase synthesis process takes place at a much lower temperature of about less than 200°C, thus offering a wider choice of substrates including both inorganic and organic ones. The synthesis process can take place in either aqueous [104] or organic solutions [105] or even a mixture of the two [106].

If the synthesis process takes place in an aqueous solution, it is referred to as hydrothermal synthesis. Hydrothermal synthesis method has received much attention and is increasingly widely used to synthesize 1D nanostructures, not only due to the advantages mentioned earlier for the solution phase synthesis methods, but also due to

the fact that the hydrothermally grown 1D nanostructures have more inherent crystalline defects. For ZnO nanowires particularly, the crystalline defects are primarily due to oxygen vacancies [53], which enable the ZnO nanowires to be photoactive under visible light irradiations without doping of transition metals [82]. Another major advantage of hydrothermal synthesis method is that almost any kind of substrates can be used to synthesize vertically aligned ZnO nanowires with the help of seed layers, such as polymer, glass, semiconductor, metal, and also organic substrates like polydimethylsiloxane (PDMS) [80] and polystyrene (PS) [81].

A general process of growing vertically aligned ZnO nanowires on a substrate using the hydrothermal method is summarized below:

(a) A thin layer of ZnO nanoparticle seeds is coated onto a certain substrate, and these nanoparticles act as catalyst to direct the nucleation and growth of nanowires as a result of thermodynamic barrier reduction [107].

(b) Zn^{2+} salt (such as $Zn(NO_3)_2$, $ZnSO_4$) and alkaline reagent (such as NaOH, hexamethylenetetramine) in aqueous solution is used as precursor.

(c) The substrate with ZnO seed layer is immersed in the precursor solution at certain temperature for a certain period of time.

(d) The substrate with ZnO nanowire arrays is washed and dried.

2.5 Effects of Main Parameters on Photocatalytic Performance

Since photocatalytic degradation of organic dyes is reactions taking place on the surface of the photocatalysts, any parameter that will affect the surface properties of catalysts will have

an influence on the overall photocatalytic efficiency. This section reviews some of the main parameters that have been reported to affect the photoefficiency.

(1) Catalyst Types and Compositions:

The efficiency of photocatalysts is dependent on surface and structural properties of the semiconductor, such as specific surface area, particle size, porosity, crystal compositions, band gap and surface hydroxyl density [15]. Particle size influences the photocatalytic efficiency through the definition of specific surface area (diameter/length). A variety of commercially available photocatalyst have been investigated for photocatalytic degradation of phenolic compounds and dyes in aqueous solutions. Table 2.5 gives the composition, measured BET surface area and particles size of three commonly used commercial TiO_2 samples. The Degussa P25 is the mostly widely used and readily available TiO_2 sample in industry for most of the experimental studies; other photocatalyst, such as Hombikat UV 100 and PC 500 are also used for photodegradation studies of toxic organic dyes. From Table 2.5, it shows that P25 is composed of 75% anatase and 25% rutile with a measured specific surface area of 50 m^2/g and a main particle size of around 20 nm; both Hombikat UV 100 and PC 500 contain 100% anatase, with specific surface area of 250 and 287 m^2/g, and particle size of 5 and 5-10 nm, respectively [108].

Table 2.5. Compositions and Structural properties of three commercial TiO_2 samples (data from [108]**).**

TiO_2 samples	Measured BET surface area (m^2/g)	Measured Particle size (nm)	Compositions
Degussa P25	50	20	75% Anatase + 25% Rutile
Hombikat UV 100	250	5	100% Anatase
PC 500	287	5-10	100% Anatase

It has been reported that the photodegradation rates of various dyes are fastest with the presence of Degussa P25, followed by Hombikat UV 100, and finally PC 500, i.e. the order of photoefficiency is reported to be: P25 > UV100 > PC500 [109–115]. It has been demonstrated that the higher photoefficiency of Degussa P25 is mainly due to a slower recombination rates of photogenerated electron-hole pairs; and the Hombikat UV 100 is more efficient than PC 500 due to a faster interfacial electron transfer. In summary, the variation in the photocatalytic efficiency of different photocatalysts can be attributed to the difference in specific surface area, existence of impurities and structural defects and density of surface hydroxyl groups. All these factors will also affect the surface adsorption/desorption of organic dyes and their degradation intermediates [110]. Salah *et al.* [116] have also conducted experiments to compare the photocatalytic efficiencies of the three commercially available TiO_2 catalysts Degussa P25 (20 nm), TiO_2-A1 (160 nm) and TiO_2-A2 (330nm) in the anatase phase and also ZnO for photodegradation of Phenol. After five fours, it was reported that the photoefficiency of the two catalysts was as follows: ZnO > P25 > TiO_2-A1 > TiO_2-A2. The observed difference in the photoefficiency was attributed to the structures, particle sizes and electrical properties of the catalysts.

(2) Light Intensity and Wavelength

Light intensity, by definition, is a measurement of the rate at which light energy is delivered to a unit of surface, or energy per unit time per unit area. The intensity of the incoming light is a crucial parameter to determine the photocatalytic efficiency of the catalysts, as it affects the extent of light absorption by the photocatalysts at a certain wavelength and the rate of photogeneration of electron-hole pairs [117]. Light intensity distribution over the wavelength range determines the overall photodegradation efficiency of the organic dyes [118]. Thus, the dependence of the photocatalytic efficiency on the light intensity has been extensively studied in photodegradation of various organic dye pollutants in water [35], [119]. Three different research groups

have reported that the photodegradation rate is linearly proportional to the light intensity flux under 25 mW/cm^2; and above that value, a square root dependency of the photodegradation rate is observed [35], [119], [120]. It was explained that at low intensity, the photogeneration of electron-hole pairs is predominant, and the recombination rate is negligible; while at higher intensities, the recombination increases, and when the light intensity is too high, the degradation rates become independent of the light intensity. Venkatachalam *et al.* [121] have compared the photodegradation rates of 4-Chlorophenol (4-CP) catalyzed by TiO_2 under the incoming wavelength of 365 nm and 254 nm, and reported that the photodegradation rate at 254 nm is slightly faster than at 365 nm, likely due to the fact that the photogenerated electrons and holes in TiO_2 by the light of 254 nm wavelength process higher kinetic energy and can migrate to the catalyst surface more easily and faster with less recombination compared with the 365 nm. Shukal *et al.* [122] had an extensive study on the effect of light intensity in the range of 160-330W on the photodegradation efficiency of phenol catalyzed by ZnO under artificial light. It was observed that 95% degradation of phenol was achieved after 3 hours with 330W light irradiation, while 4 hours was required using the 160W lamp, indicating an increase in the degradation rate of phenol with increasing lamp power.

(3) Initial Dye Concentration

The initial concentration of the dye solutions will also affect the photocatalytic efficiency of the catalysts, as proven by many research groups. Hong *et al.* [123] have investigated the effect of initial concentration in the range of 50-400 ppm on the photodegradation rate of phenol catalyzed by TiO_2 in aqueous suspension, and a maximum degradation rate was observed at the concentration of 50 ppm. Shukla *et al.* [122] have done a similar experiment with concentration range to be 12.5-37.5 ppm using ZnO, and the highest rate was achieved at the concentration of 12.5 ppm. However, Priya and Madras [124] have reported different results from studying the

effect of initial dye concentration (10-76 ppm) on the photodegradation rate of 2,4-dinitrophenol in the presence of combustion synthesized TiO_2 and P25, as the maximum rate was observed at concentration of 76 ppm. Pardeshi and Patil [125] reported that the photodegradation rate of phenol in aqueous ZnO suspension under sunlight decreases with increasing phenol concentration from 25 to 300mg/L, as more phenol molecules get adsorbed onto the surface of the ZnO catalyst but the relative amount of radicals attacking the phenol molecules decreases under the same conditions. Moreover, the adsorption of reaction intermediates onto the catalyst surface also lead to the deactivation of surface active sites, resulting in a decrease in photodegradation rate. Several studies also adequately described the dependence of the photodegradation rates on the initial concentrations of phenols and other types of dyes by the Langmuir-Hinshelwood (L-H) kinetics model [126–128], although the parameters for the model is strongly dependent on the composition of the dyes and the reaction conditions.

(4) Catalyst Loading

There are also a lot of studies to investigate the effect of catalyst loading on the photocatalytic efficiency of catalyst, mainly in the aqueous suspension form. It has been reported by many groups after studies of photodegradation of various dyes using different light sources and photocatalyst that the photodegradation rate generally increases initially with low catalyst loading and then decreases at high values [45], [122], [125], [129]. Although the total surface area and hence number of surface active sites will increase with catalyst loading, there is a counter effect with excessive catalyst concentration that a higher tendency of particle aggregation and light scattering by the particles will lead to a drop in the effective surface area available for light absorption and photodegradation. The trade-off between these two phenomena will usually give an optimum catalyst loading for a maximum photodegradation rate [130]. Similar trends have been observed for both ZnO and TiO_2 aqueous suspensions. Table 2.6 gives a

summary of experimental conditions and results achieved by some groups for the study of the effect of catalyst loading on the photocatalytic degradation rates of different types of organic dyes.

Table 2.6: Effect of catalyst loading on photodegradation rates of different dyes.

Research Group	Organic dyes	Light source	Photocatalysts used (in aqueous suspension)	Range of catalyst loading (g/L)	Optimum loading found (g/L)
Parida *et al.* [45]	4-Nitrophenol	Solar light	ZnO	0.2 - 2.0	0.6
Barakat *et al.* [131]	2-Chlorophenol	UV	Co-TiO_2	0.005 – 0.03	0.01
Lathasree *et al.* [132]	Phenol	UV	ZnO	1.0 – 3.0	2.0

(5) Medium pH

The pH of wastewater usually varies significantly. And the pH of the aqueous solution has a significant impact on the photodegradation efficiency of various organic pollutants, as the pH in the solution affects the surface charge of the photocatalysts and the extent of aggregation of nanoparticle photocatalysts [133], [134]. Many research groups have studied the effect of pH in the reaction medium on the photodegradation rate of various dyes using different photocatalysts. Table 2.7 presents the studies and results reported by some groups. Parida *et al.* [45] investigated the effect of pH in the range of 2-7 on the photodegradation rate of 4-nitrophenol in the presence of ZnO and

solar light. It was reported that the degradation rate increased to 92% at the pH of 6.0 and decreased with further increase in the solution pH. It was explained that at pH of 6.0, the surface of ZnO is positively charged and is hence able to attract large number of negatively charged anions of 4-nitrophenol; while at higher pHs, the ZnO surface is negatively charged and hence hinders the adsorption of 4-nitrophenol molecules onto the catalyst surface for degradation. Khodja *et al*. [19] have reported a slightly different effect of pH (6.6-12) on the photodegradation rate of 2-phenyl phenol in the presence of ZnO. The results showed that the degradation rate increases with higher pH, likely due to the abundance of hydroxyl ions available at higher pH to react with the holes to form more hydroxyl radicals, hence enhancing the photodegradation efficiency. In summary, different organic dyes exhibit different activities in the photocatalytic degradation reactions due to their different nature. Some dyes can be decomposed faster in the acidic solutions, while others are decomposed faster in alkaline solutions. Therefore, it is essential to study the nature of the organic dyes to be degraded before determining the optimum pH for a maximum photodegradation rate.

Table 2.7: Effect of medium pH on photodegradation rates of different dyes.

Research Group	Organic dyes	Light source	Photocatalysts used (in aqueous suspension)	pH range	Optimum pH
Parida *et al.* [45]	4-Nitrophenol	Solar light	ZnO	2.0 – 7.0	6.0
Barakat *et al.* [131]	2-Chlorophenol	UV	Co-TiO_2	4.0 – 12.0	9.0
Khodja *et al.* [19]	2-Phenyl phenol	UV	ZnO	6.6 – 12.0	12.0

2.6 Microfluidic Devices for Photocatalytic Reactions

In recent years, increasing research efforts have been devoted to the integration of surface-functional nanostructures, such as TiO_2 nanoparticles or ZnO nanowires, into photocatalytic microfluidic devices, and the results achieved have demonstrated improved photoreaction efficiency than the conventional reaction set-up. Compared to the photocatalytic reactions taking place in the bulk solution using immobilized nanowires vertically-aligned onto a flat substrate, whose efficiency is usually limited by the diffusion and adsorption process of the contaminant molecules onto the nanostructure surface, the miniaturization of the photocatalytic reactions using microfluidic devices exhibits significant advantages, such as an inherently high surface-to-volume ratio, short diffusion distance, easy interfacing with UV light source, and rapid, efficient mass transfer and heat dissipation [135]. Moreover, the continuous-flow feature inherent in the microfluidic devices supplies fresh dye solutions with precise control, easily establishes the adsorption/desorption equilibrium of organic dye on the nanostructure surface, and enables incorporation of on-line analytics to monitor the processes more closely [136].

The design and fabrication of the nanostructure-integrated microfluidic reactors is very critical for their application in photocatalytic reactions. One has to consider the following characteristics such as a capacity to overcome the mass transfer, a large surface-to-volume ratio in order to get a good contact of the dye molecules with the catalyst surface, and a homogeneous irradiation on the whole surface of the micro-reactor [137]. Recently, several research groups have reported successful fabrication of microfluidic devices for photocatalytic applications. He *et al.* have fabricated aligned TiO_2 nanoparticle-coated ZnO nanorod arrays on the inner wall of capillaries (IWC) and showed a great performance in photocatalytic degradation of methylene blue (MB) solution [136]. Charles *et al.* have utilized a TiO_2 thin film-integrated microchannel reactor for photocatalytic decomposition of salicylic acid solution [137]. Other microfluidic-based microreactors with integrated nanostructures were reported to be prepared by irreversibly bonding the glass substrate pre-coated with vertically-aligned ZnO nanowire arrays and a PDMS substrate pre-patterned with

a microchamber ($50 \times 15 \times 0.1mm^3$) using soft lithography technique [138], or by simply sealing the nanofibrous TiO_2 electrospun onto a glass slide with the PDMS substrate pre-patterned with a microchannel (100μm in depth, 500μm in width) using the same technique [139]. Both microfluidic devices with different integrated nanostructures have exhibited a high photocatalytic activity in degradation of MB solutions. Kim *et al.* have also suggested a novel and simple method for *in situ* synthesis and integration of ZnO nanowires within the microfluidic device by using controlled hydrothermal reaction, and demonstrated the applications of the device for particle trapping and chemiresistive pH sensing [140].

A typical experimental set-up for photocatalytic degradation reactions in the microfluidic devices is suggested by Charles *et al.* as shown in Figure 2.10 [137]. A flow of the dye solution is continuously injected into the micro-reactor with a syringe at a certain speed. A light source, usually UV light with proper irradiation wavelength, is located above the reactor to initiate the photodegradation reaction. A flexible tube at the outlet of the reactor allows collection of the post-irradiated solutions for the subsequent UV-Vis absorbance measurement.

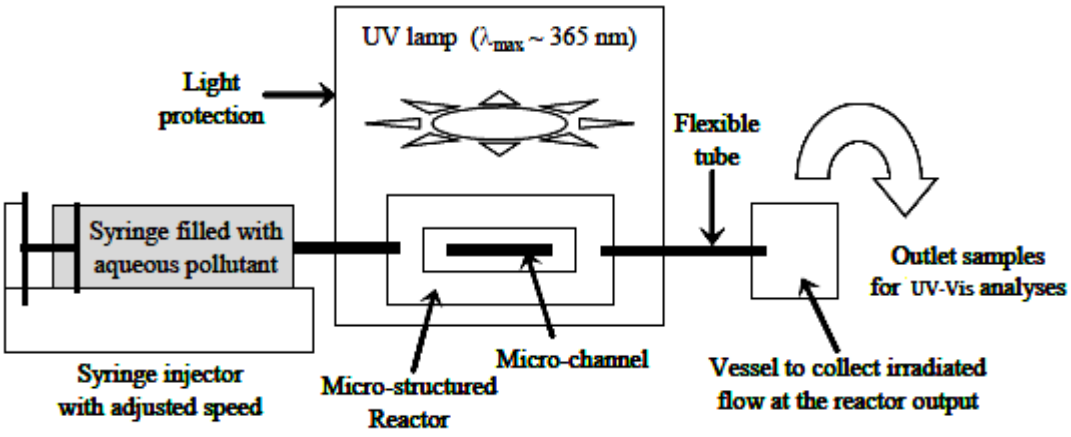

Figure 2.10: Schematics of a typical experimental set-up for photodegradation in micro-reactors (reproduced from [137]**).**

The main drawbacks for the photocatalytic reactions miniaturized into microfluidic devices are the difficulty in device fabrication and low output. Many researchers are currently working on design of the devices to simplify the fabrication process. A prototype for scaling up through the operation of multiple systems in parallel is also suggested, aiming to increase the output and accelerate the commercialization of photocatalysis of organic pollutants in aqueous solutions [136].

Chapter 3

Experimental

In this chapter, a detailed description of the experimental procedures adopted in this project will be presented, to ensure the repeatability of the project by others. The first part gives all the materials used, with a focus on structural properties and UV-Vis absorption spectra of the photocatalytic test compound (Methyl Orange) used in this experiment. The second part describes the main steps taken to synthesize the vertically-aligned ZnO nanowires on substrate. After that, the as-synthesized samples are characterized using the different characterization techniques as mentioned in the third part. The fourth part gives the experimental set-up, procedures used and their theoretical support to evaluate the photocatalytic efficiency of the samples. Finally, the last part describes the steps to fabricate the ZnO nanowire-integrated microfluidic device and to evaluate its efficiency in photodegradation reactions.

3.1 Materials

In this project, all materials were used as received without further purification unless otherwise noted. The chemicals including Zinc acetate dihydrate ($Zn(CH_3COO)_2 \cdot 2H_2O$), ethanolamine, Zinc sulphate heptahydrate ($ZnSO_4 \cdot 7H_2O$), Methyl Orange ($C_{14}H_{14}N_3NaO_3S$, M*w*=327.33g/mol) were purchased from Sigma-Aldrich; and Ammonium chloride (NH_4Cl), Sodium hydroxide pellets (NaOH, min. 97.0%), ethonal and standard glass slides (Fisherfinest® Premium Microscope Slides, Plain, Cat. No. 12-544-1, 3” x 1” x 1mm) were purchased from the Chemical Store in University of Waterloo. The deionized (DI) water available in Prof. Anderson’s lab in E6, University of Waterloo, was used to make all the aqueous solutions.

3.1.1 Properties of Methyl Orange

In this project, the photocatalytic test compound used was Methyl Orange (MO), i.e. the photocatalytic activity of the as-synthesized ZnO nanowires were tested based on the photodegradation rates of methyl orange solutions. It is important to study the nature of the model compound before carrying out the experiments, as the structure of such model compounds will affect the photodegradation processes, such as peak absorption wavelength and optimum pH. Different test compounds will usually give different results with regards to photocatalytic efficiency of the same catalyst, as discussed in Chapter 2.

Methyl Orange (MO) is a very intensely colored compound and is commonly used in dyeing and printing textiles in the industry. It is also known as Acid Orange 52, Orange III, Helianthin, and 4-[(4-Dimethylamino)phenylazo]benzenesulfonic acid sodium salt. Its molecular formula is $C_{14}H_{14}N_3NaO_3S$ with molar mass of 327.33 g/mol, and its molecular structure is shown in Figure 3.1:

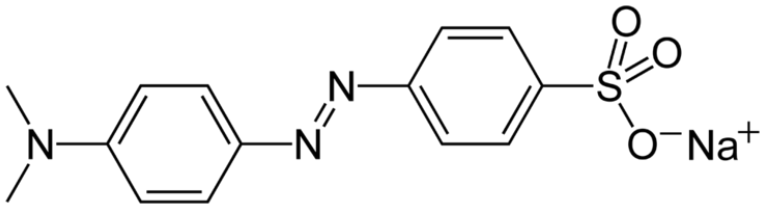

Figure 3.1: Molecular structure of Methyl Orange.

Methyl Orange is usually used as a pH indicator in the titration of weak bases by strong acids due to its clear and distinct color change from red (below pH 3.1) to orange-yellow (above pH 4.4). Figure 3.2 shows the change in the molecular structure of methyl orange in acidic solutions, where a hydrogen ion is attached to one of the nitrogens in the nitrogen-nitrogen double bond and the resultant positive charge in delocalized especially towards to the terminal nitrogen. This molecular structure absorbs blue-green light, which gives its

solution a red color. When dissolved in alkaline solutions, the hydrogen ion is lost from the –NN– bridge between the rings, and the electron used to bind the hydrogen ion neutralizes the positive charge on the terminal nitrogen, which gives the structure showing in Figure 3.1 and gives the solution a yellow color.

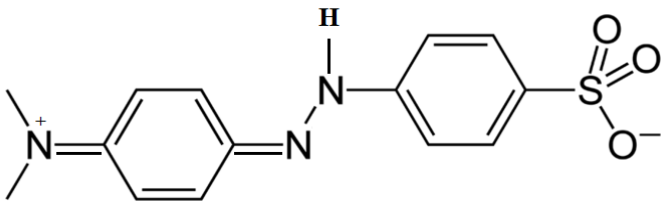

Figure 3.2: Molecular structure of methyl orange in acidic solutions.

Figure 3.3 shows the typical UV-Vis absorption spectra of 5ppm methyl orange in aqueous solutions. It can be observed that the peak absorption occurs at the wavelength of 464 nm, and absorption of light with longer and shorter wavelengths both decreases. The small increase of absorbance in the UV-range approaching 300 nm is mainly due to absorption caused by the non-UV-transparent, disposable, plastic cuvette used in the experiments.

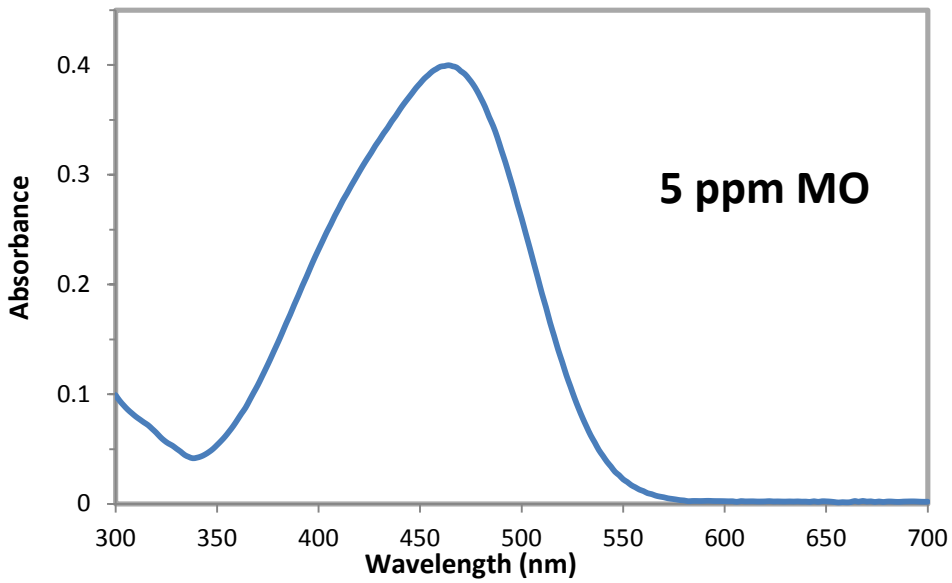

Figure 3.3: UV-Vis absorption spectra of 5ppm MO aqueous solution

3.2 Synthesis of Vertically-Aligned ZnO Nanowires

ZnO nanowires were synthesized by a typical seed layer-assisted hydrothermal method suggested by J. Joo *et al.* [141], in which two steps were involved, as illustrated by Figure 3.4.

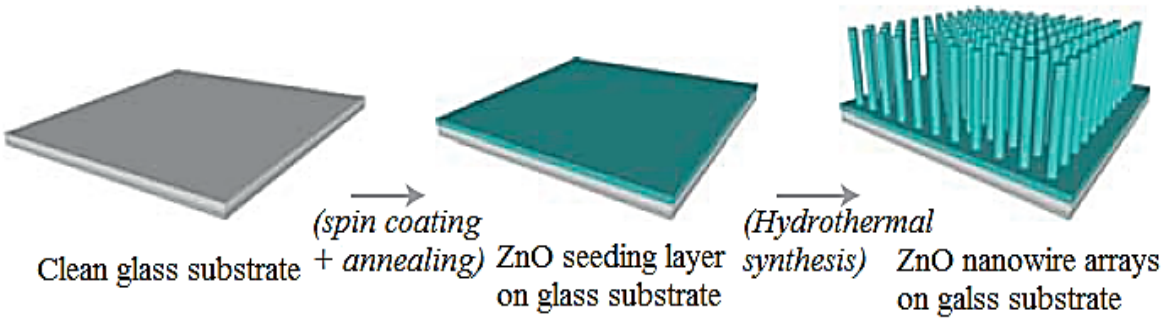

Figure 3.4: Schematic diagram illustrating the synthesis processes of ZnO nanowire arrays.

3.2.1 Growth of ZnO Seeding Layer

The first step is fabrication of ZnO seeding layer on a certain substrate. Typical methods for grow seeding layers include thermal decomposition of zinc acetate, spin coating of ZnO nanoparticles, sputter coating, and physical vapor deposition (PVD). In this experiment, spin coating of a sol-gel solution containing zinc acetate onto a glass substrate followed by thermal decomposition was adopted due to its ease in handling and low cost. The glass slides were first cut into the size of 2" x 1" x 1mm, cleaned using isopropanol (IPA) to eliminate any dust or contaminant, and then rinsed with DI water and blow-dried. A sol-gel solution was prepared using 0.7M zinc acetate dehydrate [$Zn(CH_3COO)_2 \cdot 2H_2O$)] as precursor, 0.7M monoethanolamine as stabilizer and 100mL ethanol as the solvent. The resultant solution was stirred with a magnetic stirring bar for 10 minutes to yield a clear, homogeneous and transparent solution. Then the sol-gel solution was spin-coated onto the pre-cleaned glass

substrates at 3000rpm for 40 sec, followed by annealing on a 250°C hotplate for 10 minutes to evaporate the solvent, remove the organic residuals in the films, improve the ZnO particle adhesion onto the substrate and the subsequent nanowire vertical growth alignment. During the annealing at high temperatures, the zinc acetate crystallites decomposes to form ZnO particles with their (002) planes aligned parallel to the substrate surface. This alignment does not depend on the substrate, and can take place on any flat surface regardless of the surface crystallinity or chemistry.

3.2.2 Growth of Vertically-Aligned ZnO Nanowires

The second step is to grow vertically well aligned ZnO nanowires onto the glass substrates. The precursor solution for the hydrothermal synthesis method was prepared by dissolving 10mM zinc sulfate ($ZnSO_4$) and 300mM ammonium chloride (NH_4Cl) into 100mL deionized water, with pH adjusted to 11 by diluted sodium hydroxide (NaOH) solution. The substrate pre-coated with ZnO seeding layer was then immersed upside down in the precursor solution in a closed jar, and kept in a convection oven at 60°C for 6 hours. The substrate with hydrothermally grown ZnO nanowires was then rinsed with deionized water for several times to eliminate residual salts or amino complexes, and blow-dried in air.

The chemical reactions taking place in the precursor solution containing $ZnSO_4$, NH_4Cl, and NaOH are very complicated but the main reactions can be summarized in the following equations:

Hydroxyl buffer reaction:

$$NH_4^+ + OH^- \leftrightarrow NH_3 + H_2O \qquad (3.1)$$

Supersaturation reaction:

$$Zn^{2+} + 2OH^- \rightarrow Zn(OH)_2 \qquad (3.2)$$

ZnO nanowire growth reaction:

$$Zn(OH)_2 \rightarrow ZnO + H_2O \qquad (3.3)$$

(a) ***(b)***

Figure 3.5: Comparison of the ZnO nanowire growth solution after 1 hour at 60°C with pH of (a) 11.0 and (b) 11.70.

One of the key parameters in the hydrothermal growth of ZnO nanowires is to control the supersaturation level of the reactants, which are believed to be the indicator of the driving force for hydrothermal growth. In the case of excessive driving force, i.e., high supersaturation levels, homogeneous nucleation and growth is favored, and the ZnO nanostructures primarily form in the bulk solution and then condensed onto the substrate, as opposed to the desired heterogeneous nucleation and growth at the interface between the ZnO seeding layer and the aqueous solution [76]. The supersaturation level is affected by many parameters, such as pH of the precursor solution, temperature and concentrations of the reactants. Figure 3.5 is a photograph of the ZnO nanowire growth solutions with pH of (a) 11.0 and (b) 11.70, but with the same precursor concentration (10mM $ZnSO_4$, 300mM NH_4Cl), after 1 hour at the temperature of 60°C. It is obvious that the one with pH of 11.70 (Figure 3.5(*b*)) formed a turbid solution, indicating high levels of homogeneous nucleation and growth products suspended in the solution. In this solution with higher pH, too much OH^- ions were present and the Zn^{2+} ions will precipitate out very fast as described by Equation (3.2), resulting in a fast consumption and depletion of the reactants and prohibiting the growth of ZnO nanowires [142]. J. Joo *et al*. have also reported a similar undesired

homogeneous growth of ZnO nanostructures observed at a high temperature of 90°C in their supplementary information [141]. Therefore, it is very critical to control the supersaturation level during the whole nanowire growth process, by optimizing the pH of the precursor solution and the treatment temperature. Moreover, the substrate pre-coated with ZnO seeding layer was immersed in the precursor solution upside down, to avoid any undesired condensation of the homogeneously grown ZnO nanostructures from the bulk solution.

3.3 Characterization Techniques

After synthesis of the vertically-aligned ZnO nanowires on glass substrate, the obtained sample was characterized by various techniques to investigate its crystal structure, morphology and size, and light absorption properties. In brief, the crystalline structure of the synthesized ZnO nanowire arrays was analyzed by the powder X-ray diffraction (XRD) using XPERT-PRO diffractometer system with Cu Kα radiation (λ = 1.54056 Å) at 45kV and 35 mA, by scanning from 20 to 90˚ (2θ) using a step size of 0.05˚ and 1.0s per step. The morphology and size of the grown ZnO nanowires were characterized by the field-emission scanning electron microscopy (FE-SEM, LEO 1550). Finally, the Ultra-violet visible (UV-Vis) transmission spectra of the synthesized ZnO nanowire arrays were recorded by the HP Hewlett Packard 8452A Diode Array Spectrophotometer over the wavelength range of 200-800nm.

3.3.1 X-Ray Diffractometer

In materials synthesis field, in order to properly identify the structures of the materials synthesized, X-ray diffraction (XRD) technique is usually used as a finger-printing tool. In this project, the crystalline structure of the as-synthesized ZnO nanowire arrays on glass substrate was analyzed by the powder XRD using XPERT-PRO diffractometer system with

Cu Kα radiation (λ = 1.54056 Å) at 45kV and 35 mA. The patterns were obtained by scanning from 20 to 90˚ (2θ) using a step size of 0.05˚ and 1.0s per step. This technique is also used to identify any impurity phase, if exists. After scanning was completed from 20 to 90˚, the obtained XRD patterns of the sample was compared and matched to the published standard patterns in the literature by using specific software, in an effort to identify the crystal structures present in the sample and if there is any impurities present.

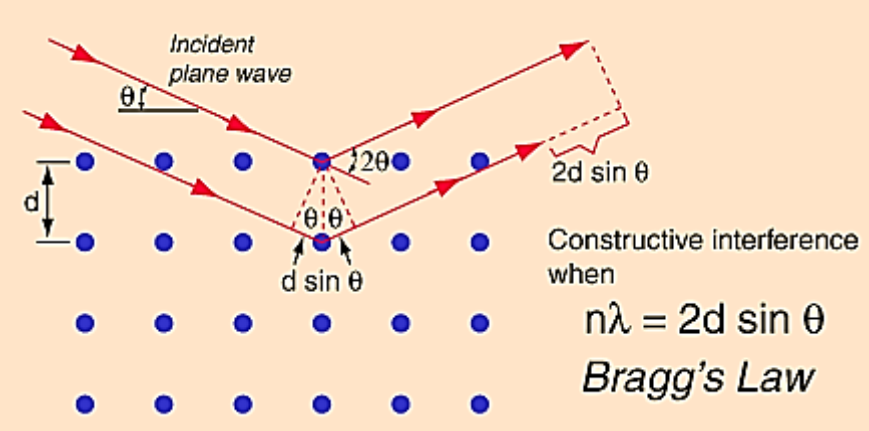

Figure 3.6: Illustration of Bragg's Law (Retrieved from http://hyperphysics.phy-astr.gsu.edu/hbase/quantum/bragg.html).

XRD patterns are obtained when the incoming X-rays interact with the crystalline planes in the material structures, and constructive interference of the X-rays is only possible at certain angles determined by the wavelength of the incoming X-rays and the distance between the planes in the crystal structure, as the relationship described by the Bragg's Law:

$$n\lambda = 2d\sin\theta \qquad (3.4)$$

Where n is an integer usually fixed at 1, λ is the incoming wavelength of the X-rays, d is the interplanar distance, and Θ is the incident angle. The construction of the Bragg's Law is illustrated by Figure 3.6.

3.3.2 Scanning Electron Microscope

The morphology and size of the as-synthesized ZnO nanowires were characterized by the field-emission scanning electron microscopy (FE-SEM, LEO 1550). Since most oxide materials become positively charged when interacting with the incident electron beam, a thin layer of gold (Au, 9nm) was first coated onto the surface of the sample using the sputter-coating technique to keep the voltage in the sample down as much as possible, in order to lead to clear SEM images of the sample. Then the SEM chamber was vacuumed until the inside pressure reached 1.5E-5 mbar. The voltage was then set to 10V and the working distance was set to 10mm. After centering the sample under the TV mode by adjusting the x-, y-, and z-adjustment knobs, InLens or SE (secondary electron) mode was turn on to capture the SEM images that have been well focused and magnified. The basic principle of a SEM is as illustrated in Figure 3.7, where an electron beam is focused onto the sample and a specific detector collects the related emitted photons and electrons to generate images.

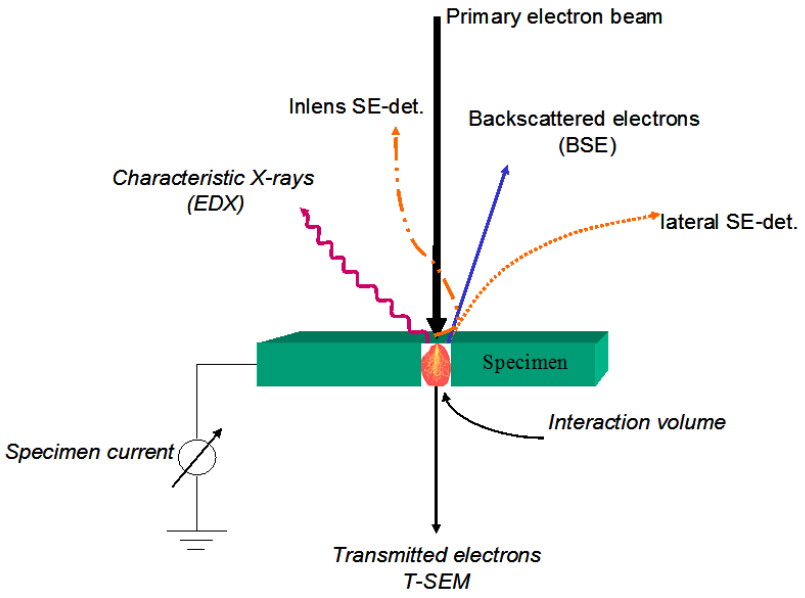

Figure 3.7: Illustration of electron-specimen interactions in SEM and related detection modes (Reproduced from [143]**).**

3.3.3 Ultra-violet Visible Spectrometer

For synthesis and photocatalytic applications of materials, the Ultra-violet Visible (UV-Vis) Spectrometer is indispensable. The UV-Vis spectra not only uniquely define the material, but also identity the possibility of using the materials for photocatalytic studies either in the UV or visible light range. To be more specific, the UV-Vis Spectra give the information necessary to decide the maximum wavelength (minimum frequency and energy) required in the incoming light source in order to excite the photocatalyst. The spectra generated here is due to the optical transitions from the ground state to an excited state of the catalyst molecules, i.e. a transition of electrons from valence band to conduction band, as described in the first part in Chapter 2. The UV-Vis spectra is also a signature for a molecule with conjugated pi-electrons such as methyl orange dye, the test dye we used to evaluate the photocatalytic properties of ZnO nanowires in this project. From the spectra, we can decide important information like the maximum absorption wavelength of the test dye solutions, and evaluate any change in the absorbance of the dye after irradiated for certain period of time.

In this project, the UV-Vis transmission spectra of the as-synthesized ZnO nanowire arrays were recorded by the HP Hewlett Packard 8452A Diode Array Spectrophotometer over the wavelength range of 200-800nm, in order to determine the proper wavelength of the incoming light source. The UV-Vis absorption spectra of MO solutions before and after irradiation were also obtained using the same equipment, as described in detail in the following section.

3.4 Photocatalytic Experiments

The photocatalytic efficiency of the synthesized ZnO nanowire arrays was tested by measuring the photocatalyzed discoloration rate of MO in aqueous solution. So the experiment for photodegradation of MO solution under the near-UV light source was first set up. Samples of degraded MO solutions were taken after different time intervals and their

absorbance were measured by the UV-Vis Spectrometer to evaluate their concentration change, i.e. degradation rates of MO.

3.4.1 Experimental Set-up for Photodegradation

A glass substrate with vertically-aligned ZnO nanowires was placed in a Petri dish with a diameter of 60mm and a depth of 15mm. 10mL of 5ppm MO solution was added into the Petri dish. Constant stirring of the solution was achieved by using a magnetic stirring bar, and the Petri dish was capped to minimize evaporation of the solvent. The set-up is shown in Figure 3.8.

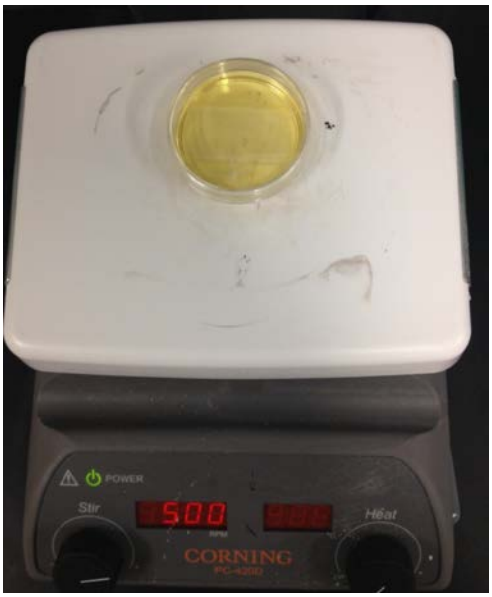

Figure 3.8: Photograph of the experimental setup for the reaction in Petri dish on stirring plate.

The UV light source used here to excite the ZnO nanowire catalysts was three 40W Philips low-pressure UV-A fluorescent lamps with main emission wavelength at 365 nm and an incident light intensity of about 70 mW/cm^2. Prior to irradiation, the solution was stirred magnetically in dark for 10 minutes to improve adsorption of the dye onto the catalyst surface. The first sample was taken right after the dark adsorption period to determine the

peak absorbance (A_0), which was related to the initial concentration of MO (C_0). Samples were taken from the solution at regular time intervals (0.5 hours).

3.4.2 Photodegradation Rates Measurement

The samples taken at each half an hour during the photodegradation reactions were immediately analyzed with the HP 8452A UV-Vis Spectrophotometer to determine its instantaneous absorbance (A) at 464 nm, which is the maximum absorption wavelength of MO as illustrated by Figure 3.3. After each absorbance measurement, the samples were put back into the solution and irradiation continued.

The absorbance of a solution is directly proportional to the concentration of the compound in the solution, as described by the Beer-Lambert Law:

$$\boldsymbol{A = \varepsilon b C} \qquad \textbf{(3.5)}$$

where A is absorbance (no units), ε is the molar absorptivity (L $mol^{-1}cm^{-1}$), b is the path length of the sample solution in the cuvette (cm), and C is the concentration of the compound in the solution (mol L^{-1}). To confirm that the absorbance of the MO solution used in this experiment obeys the law, four MO aqueous solutions with different concentrations (1ppm, 5ppm, 10ppm, and 20ppm, respectively) were prepared, as shown in Figure 3.9.

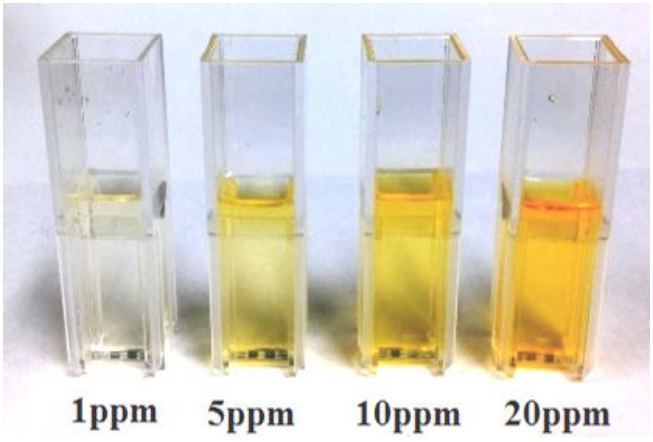

Figure 3.9: Photograph of four different concentrations of MO solutions in cuvettes.

It is obvious that with increasing concentration, the MO solution exhibits an increasingly darker orange color. Their UV-Vis absorption spectra were measured as results being displayed in Figure 3.10. By taking the peak absorbance value at 464nm from each curve in Figure 3.10 and plot the absorbance versus individual concentration, we get a straight line passing through the origin (Figure 3.11), indicating a good linear relationship between the absorbance and concentration of the MO solutions in the range of 0-20ppm.

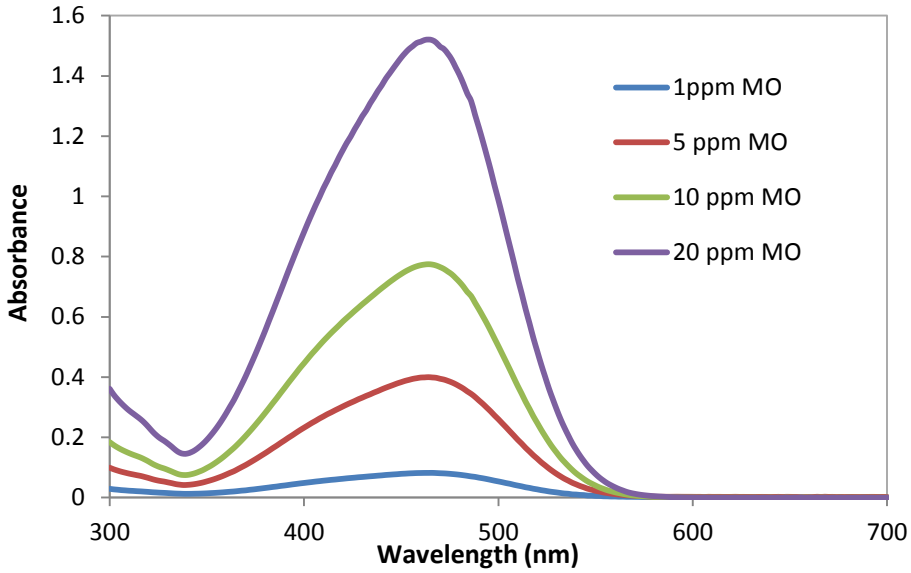

Figure 3.10: UV-Vis spectra of MO aqueous solutions with different concentrations.

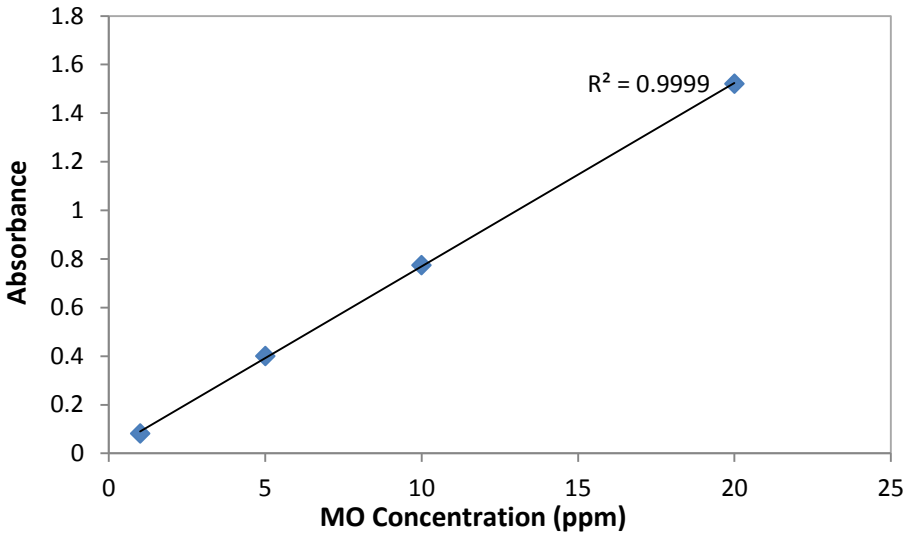

Figure 3.11: Plot of absorbance of MO solutions versus their concentrations.

After confirmed by experiment data that the absorbance (A) of MO solution used in this experiment is directly proportional to its concentration (C), we are well in the safety zone to use the following equation to calculate the photodegradation efficiency:

$$\textbf{\% Degradation} = \frac{C_0 - C}{C_0} \times 100 = \frac{A_0 - A}{A_0} \times 100 \qquad \textbf{(3.6)}$$

where C_0 and C are the initial and post-irradiation concentration of the dye, respectively; and A_0 and A are the initial and post-irradiation absorbance of MO solution at 464nm as measured by the UV-Vis spectrophotometer, respectively.

3.5 Microfluidic Device for Photocatalysis

In this study, a microfluidic device integrated with ZnO nanowires vertically-aligned on a glass substrate synthesized following the same steps described in Section 3.2 is fabricated and used for photodegradation studies of MO solutions. Some experimental equipment and materials used, if not mentioned otherwise, are the same as in the bulk reaction experiment described earlier in Section 3.4.

3.5.1 Fabrication of Microfluidic Device Integrated with ZnO Nanowires

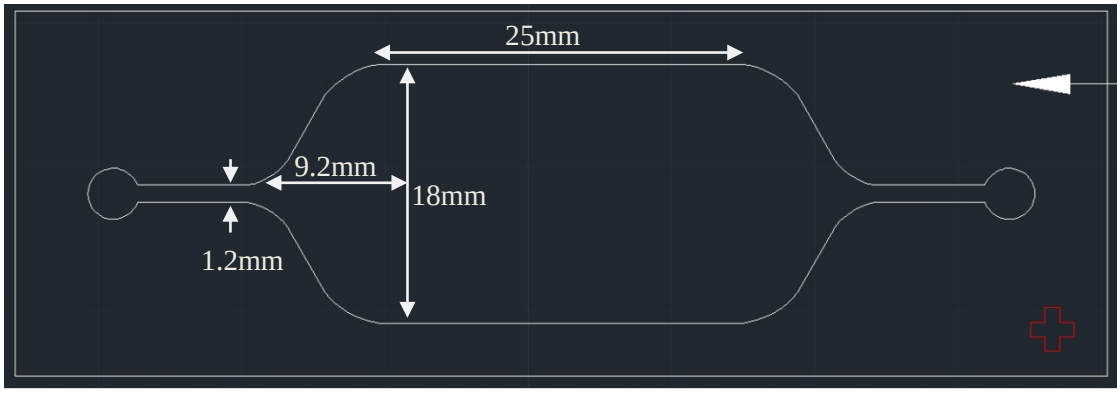

Figure 3.12: Dimension of the micro-chamber designed for the microfluidic device.

A chamber of the shape and dimension depicted in Figure 3.12 was first designed for a homogeneous fluid distribution and large reaction surface. The chamber pattern was then realized into a thin PDMS layer with designated thickness, through spin-coating of the PDMS liquid mixture prepared at a ratio of 5:1 onto a standard glass slide (3" x 1" x 1mm), curing at 95°C for at least 24 hours and pealing the chamber by hand. The height of the chamber was controlled by the speed of spin-coating, and three different chambers with height of 400μm, 600μm and 800μm were prepared separately. In order to irreversibly bond the patterned PDMS layer on glass with the glass substrate pre-coated with ZnO nanowire arrays obtained in Section 3.2, the PDMS surface was treated with plasma, and cleaned with isoproponal, acetone and DI water. Afterwards, the two layers were assembled with the nanowire side facing the chamber, and silicon glue was first used to seal the gaps in between and liquid PDMS was used as a second sealing agent for better sealing quality. After baking, two flexible tubes were inserted into inlet and outlet of the device to direct the flow, followed by sealing any gap between the tubes and the inlet/outlet. Figure 3.13 shows the structures of the fabricated microfluidic devices integrated with ZnO nanowires.

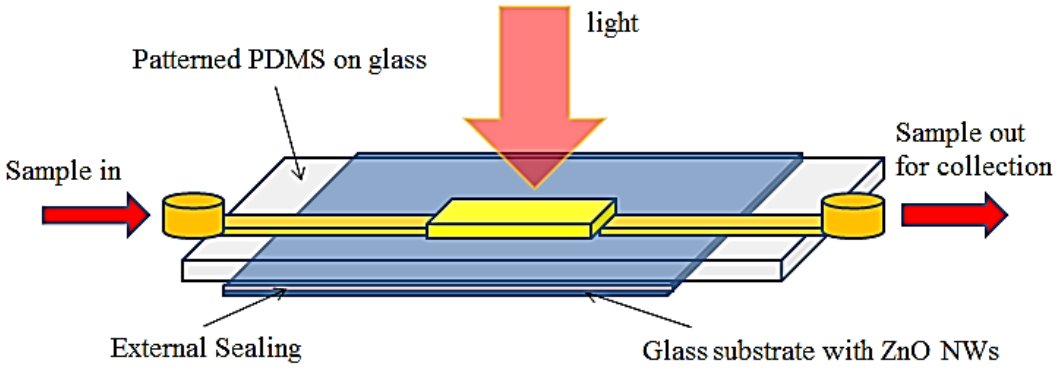

(a)

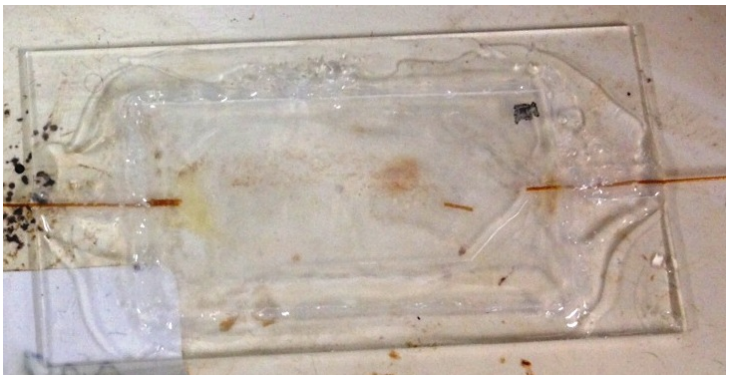

(b)

Figure 3.13: Schematic diagram (a), and photograph (b) of the fabricated microfluidic device with integrated ZnO nanowires.

3.5.2 Application of the Microfluidic Device for Photodegradation

To evaluate the photocatalytic efficiency of the microfluidic device fabricated, photodegradation rates of MO solution in the micro-chamber was measured. The experimental set-up for photodegradation is similar to the one illustrated in Figure 2.10. First, 1mL MO (5ppm) aqueous solution was injected into the micro-chamber with chamber height of 400μm through the inlet tube at a flow rate of 10μL/min controlled by the syringe pump. The whole micro-chamber filled with MO solution was irradiated with the same UV light source used for bulk reactions (365nm, 70mW/cm^2). The post-irradiated solution was collected through the outlet tube and its UV-Vis absorption spectra were recorded using the same UV-Vis spectrophotometer mentioned earlier. The experiment was repeated at three different flow rates (10, 23, and 50μL/min) using each of the fabricated microfluidic devices with chamber height of 400μm, 600μm and 800μm, in order to investigate the effects of micro-chamber height and flow rate on the photocatalytic efficiency of MO solution.

Chapter 4

Results and Discussion

4.1 Characterization Results

This section presents the results achieved by the characterization techniques mentioned in the previous experimental section, including the XRD, SEM and UV-Vis transmission spectra.

4.1.1 Crystal Structures

The as-prepared ZnO nanowire arrays on the glass substrate pre-seeded with a thin layer of ZnO nanoparticles grown by using the hydrothermal method at the pH of 11.0 at 60ºC for 6 hours were used for structural measurement with XRD technique.

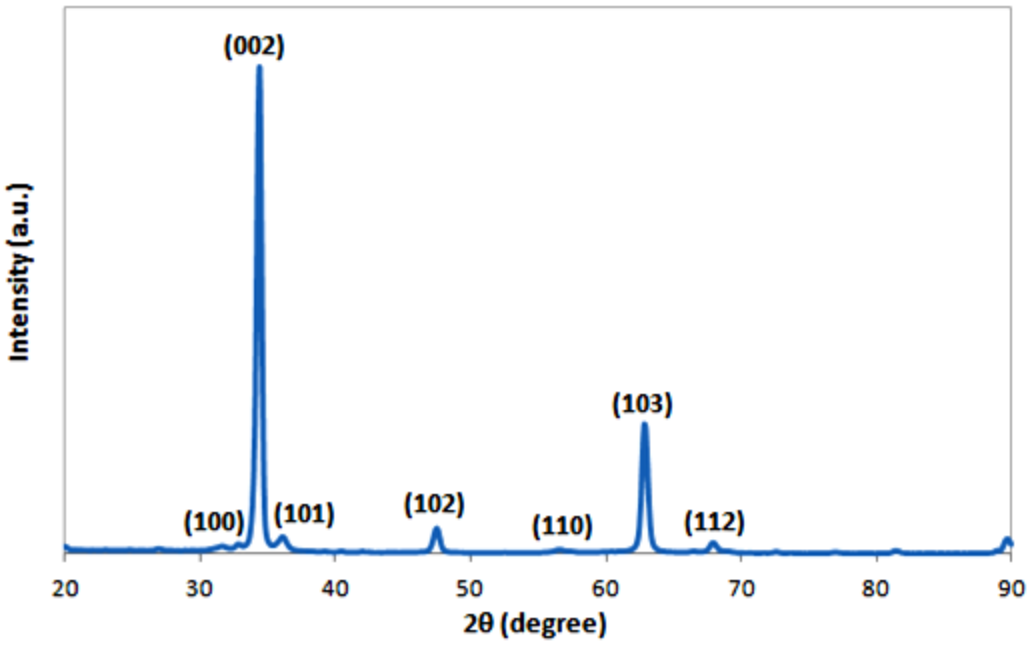

Figure 4.1: XRD patterns of the synthesized ZnO nanowire arrays (pH 11.0, 60ºC and 6 hours).

Figure 4.1 depicts the XRD patterns of the as-obtained ZnO nanowire arrays. It is observed that all the diffraction peaks are in good agreement with the standard ZnO hexagonal wurtzite crystalline structure on the JCPDS card, with measured lattice constants ($a = b$ = 3.2498 Å, c = 5.2066 Å) being the same as the indexed ones [70]. A dominant diffraction peak for the (002) plane at $2\theta = 34.43°$ indicates a high degree of anisotropic growth of ZnO nanowires along the *c*-axis vertical to the glass substrate surface. The peak is very strong and narrow, demonstrating a high degree of crystallinity of the prepared ZnO nanowires. Moreover, there are no other distinct peaks from impurities detected, indicating that the product is very pure.

4.1.2 Morphologies

The ZnO nanowire arrays on glass substrate hydrothermally grown at the same conditions, i.e. at the pH of 11.0 at 60ºC for 6 hours, were used to investigate their morphology and size using scanning electron microscope. Figure 4.2 shows the SEM images of the top view and cross-sectional view of the prepared ZnO nanowire arrays. It can be easily seen that the nanowires are very well vertically aligned and closely packed onto the substrate, with an average diameter of around 100nm and an average length of about 1.5μm. From the high magnification image inserted in Figure 4.2 (a), it can also be observed that the synthesized nanowires demonstrate the hexagonal wurtzite structure, which confirms the XRD results shown in Figure 4.1.

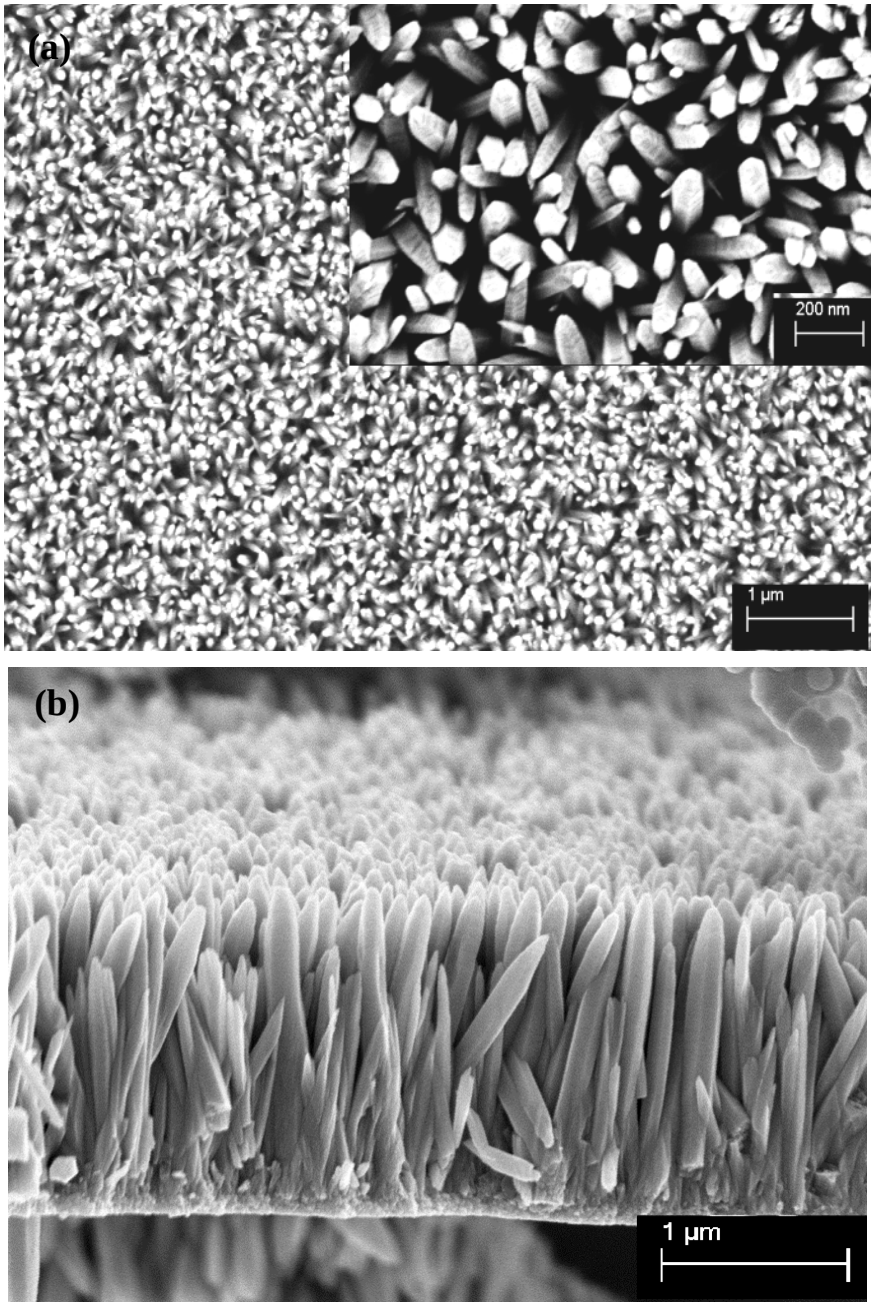

Figure 4.2: SEM images of the as-synthesized ZnO nanowire arrays (pH 11.0, 60°C and 6 hours): (a) top view, (b) cross-sectional view.

Figure 4.3 depicts the SEM images of different ZnO structures hydrothermally grown in the precursor solution when synthesis conditions are not optimized. Figure 4.3(a) shows that flower-like ZnO microstructures were formed when the pH of the precursor solution is 11.70, instead of the optimized value of 11.0 [141]. The flowers are composed of hexagonal ZnO nanorods petals with diameter of 300-700nm and length of 2-4μm, as shown by the inserted image on the right. It can also be observed that some petals of the flower-structures are formed by a cluster of closely-packed nanorods each with diameter of around 200nm. As mentioned earlier, when the pH of the solution is above the optimized value, the supersaturation level is too high, resulting in an undesired homogeneous nucleation and growth of ZnO flower-like structures emerging from a single centre in the bulk solution, which are then condensed onto the substrate. Since the flower-like microstructure is much larger than the nanowires, the solution is turbid as illustrated in Figure 3.5. The SEM image shown in Figure 4.3 (b) was obtained by immersing the glass substrate in the solution with seed layer facing upward. It can be clearly observed that trunk-like ZnO microstructures with length of 6-8μm were formed and deposited on the surface of the vertically-aligned nanowire arrays. The trunks are consisting of a cluster of closely-packed nanorods with similar length of 6-8μm and diameter of 300-500nm, plus some nanorod branches extruding horizontally from the middle of the trunk. The trunk-like structures were formed homogeneously in the bulk solution and then condensed onto the nanowire arrays, which were formed heterogeneously from the substrate. Thus, to avoid the undesired trunk-like ZnO microstructure formation and condensation onto the nanowire arrays, it is essential to immerse the pre-seeded substrate upside down into the precursor solution.

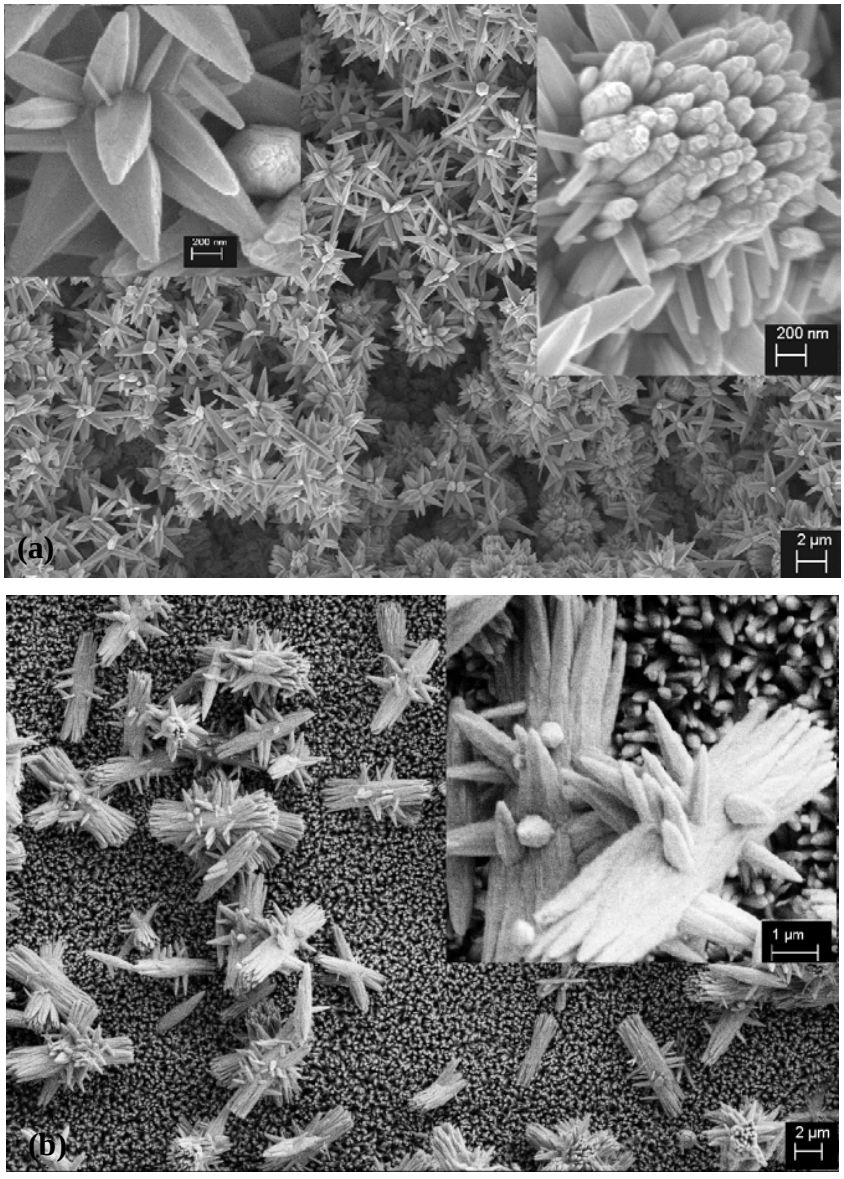

Figure 4.3: SEM images of ZnO structures formed when growth solution was at (a) pH=11.70, and (b) pH = 11.0, respectively (For both cases, the substrate was placed with seeding layer facing upwards, and all other conditions are the same, such as 60°C and 6 hours).

4.1.3 UV-Vis Transmittance

The UV-Vis transmission spectra of the ZnO nanowire arrays hydrothermally prepared under the pH of 11.0, at 60ºC for 6 hours and the standard glass substrate used in this project were recorded and compared, in order to find out the excitation wavelength threshold of the ZnO nanowires and the portion of absorption by glass substrate alone.

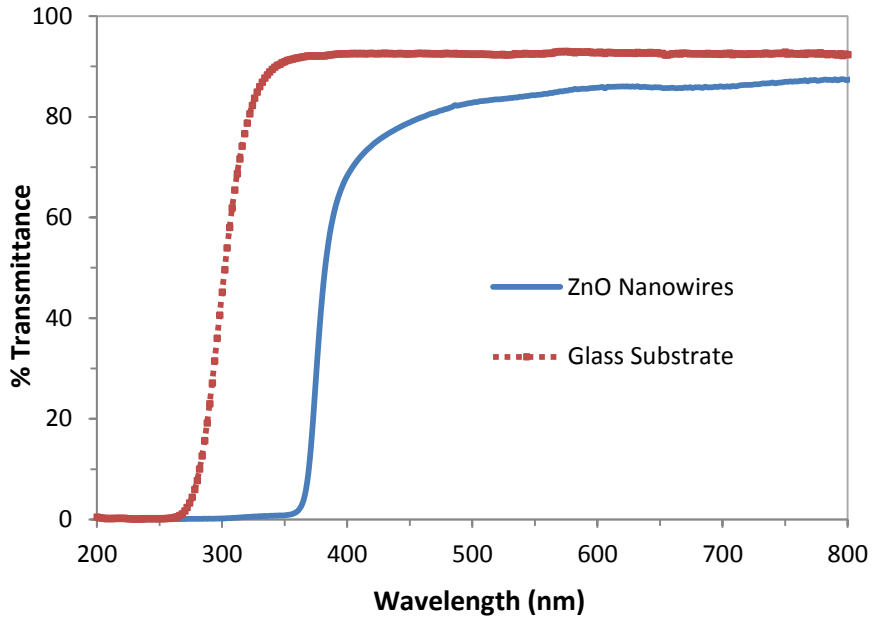

Figure 4.4: UV-Vis transmittance spectra of the prepared ZnO nanowire arrays (pH 11.0, 60ºC and 6 hours) and the standard glass substrate.

The UV-Visible transmission spectra of the prepared ZnO nanowire arrays and the glass substrate are presented in Figure 4.4. It shows clearly that the glass substrate is highly transparent (92% Transmittance) in the visible region (400-700nm) while the ZnO nanowires are capable of absorbing small amount of visible light (86% Transmittance); both the ZnO nanowires and their glass substrate exhibit a sharp absorption band in the UV region (transition is 350-400nm for ZnO nanowires, and 260-350nm for glass slides). In this project, under the light source with main emission wavelength of 365nm, 96% of the incoming light

is absorbed by ZnO nanowire arrays for photocatalytic reactions, while the absorption by glass substrate is negligible (8%).

4.2 Photocatalytic Activities of ZnO Nanowires

4.2.1 Control Experiment

Since some dyes can be degraded by direct UV irradiation without the assist from catalysts [144], it is important to find out the extent to which the degradation of MO in aqueous solution used in this project is caused directly by the UV light, or in other words, to find out the extent of direct photolysis of MO with respect to photocatalysis. So, some control experiment was carried out in the absence of the ZnO nanowire catalysts, while holding all other parameters the same. And their respective photodegradation rates were measured and compared as below. The error bars for each point was constructed based on the standard deviation of the degradation results under each condition.

It can be observed from Figure 4.5 that in the presence of the prepared ZnO nanowires (pH=11.0, T=60ºC, and t=6 hours), 96% of MO dye was degraded after 4 hours of irradiation; while in the presence of ZnO nanoparticle seeding layer, 86.7% of dye was degraded after 4 hours. In contrast, there was no degradation of MO observed after 4 hours for the same experiment performed in the absence of ZnO nanowires and ZnO seeding layer, which proves that the extent of MO photolysis solely due to UV irradiation is very negligible in this project. Based on this result, we can conclude that the degradation rates measured in the following experiments are mainly due to the photocatalytic decomposition of MO molecules in the presence of the ZnO nanowires as photocatalysts and the UV light, not due to the photolysis of MO molecules.

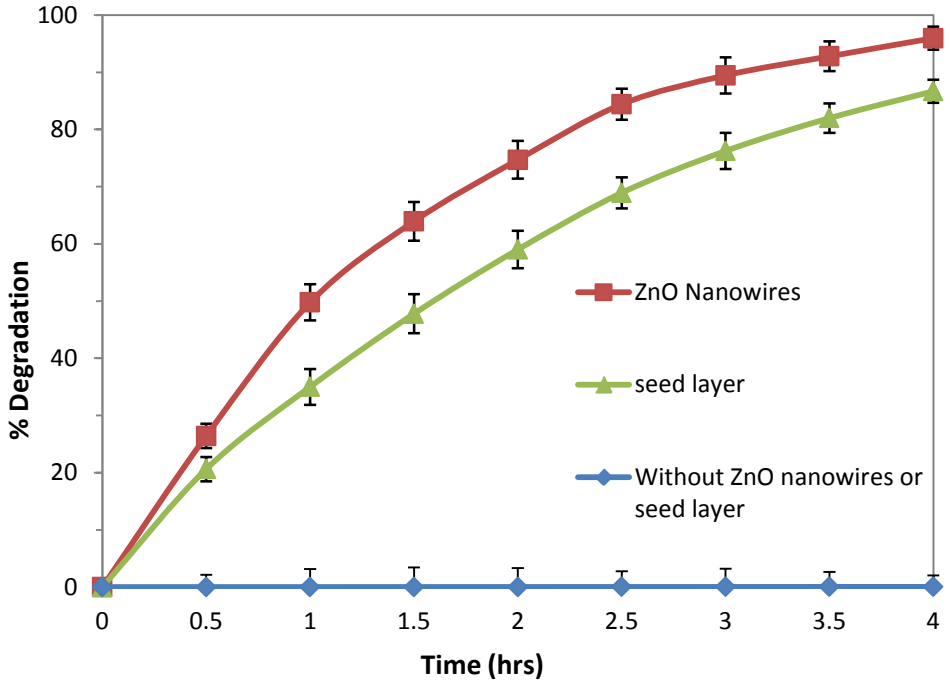

Figure 4.5: Photodegradation rates of MO solutions in the presence of ZnO nanowires, ZnO seed layer, and without both (error bars: standard deviation).

4.2.2 Reproducibility Test

To obtain more reliable result when studying the effect of the synthesis parameter such as pH and initial dye solution on the photocatalytic efficiency of the ZnO nanowire samples, it is very important to evaluate the reproducibility of the synthesis method in the first place. Thus in this project, three batches of ZnO nanowire arrays on glass slides were prepared separately using exactly the same conditions reported in the experimental section (pH 11.0, at 60ºC for 6 hours), and their photocatalytic activities for degradation of MO dye solutions were evaluated and compared.

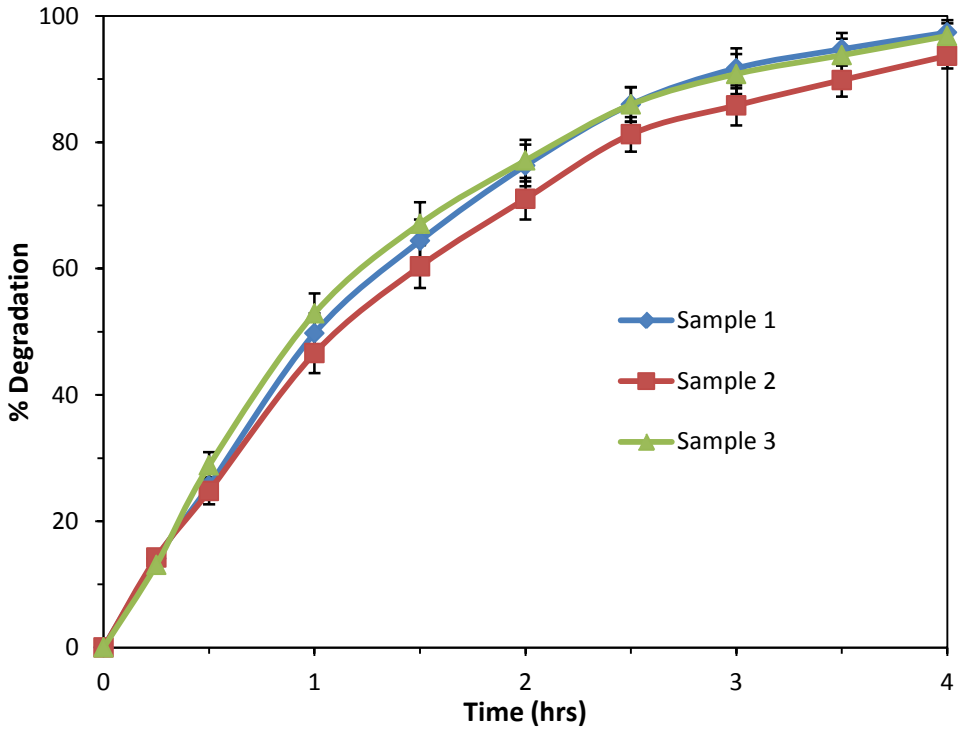

Figure 4.6: Photodegradation rates of MO solutions catalyzed by three ZnO nanowire samples prepared separately under the same conditions (error bars: standard deviation).

Figure 4.6 shows the photodegradation results of 5ppm MO solution catalyzed by the ZnO nanowire samples from each batch synthesized separately using the same methods. A series of error bars based on the standard deviation of the degradation results were constructed for each point. It can be found that the degradation rates of the three samples were consistent throughout the experiment, varying only by a maximum of around 3% over the 4 hours period. This indicates that the synthesis method used in this study gives a very consistent result, which makes further parametric study more liable. It could also be found that the variation in the degradation rates is much smaller when the reaction just starts, and becomes larger as the reaction progresses. This is likely because at the beginning of the degradation, the MO molecules need to diffuse and adsorb onto the catalyst substrate, which serves as the limiting factor in this stage. As a result, the effect of variation in the structures of the

synthesized ZnO nanowires on the photodegradation rates is not significant in the beginning. After about an hour of reaction, the effect on the degradation rates from the structures of the individually prepared ZnO nanowire samples becomes more obvious. The variations in the ZnO nanowire structures may include the differences in the specific surface area, degree of crystallinity, and defect level. But the deviation is only 3%, indicating a good uniformity of the surface area, degree of crystallinity and defect level for the synthesized ZnO nanowire samples. When the reaction has been going beyond three hours, the deviation in the degradation rates becomes smaller again. This is possibly because after three hours, nearly 90% of the MO molecules in aqueous solution have been degraded, and the supply of the MO molecules from the bulk solution onto the catalyst surface, instead of the structures of the catalysts, becomes the limiting factor for the photodegradation reaction.

4.2.3 Effect of pH on Photocatalytic Activity

Due to the amphoteric property of many semiconductor oxides, it is very important to investigate the effect of pH in the dye solution on the reactions that take place on the semiconductor surfaces, as pH is a main factor that influences the surface charge profile of the photocatalysts [145]. Furthermore, the industrial and household waste water is usually discharged at various pH values, and it is hence of practical use to study the effect of pH on the degradation rates of dyes. In this study, experiments were carried out at the same conditions except that pH of the MO aqueous solution was adjusted within the range of 4-12 using diluted NaOH or HCl solution. The photocatalysts used for each experiment were ZnO nanowire arrays on glass substrate prepared under the same conditions, e.g. pH was 11.0 for precursor solution, and temperature was set to 60 º C for 6 hours). A control experiment was also conducted using the same MO solution with pH of 12 but without ZnO nanowire catalysts, to investigate the extent of hydrolysis of MO in alkaline solutions.

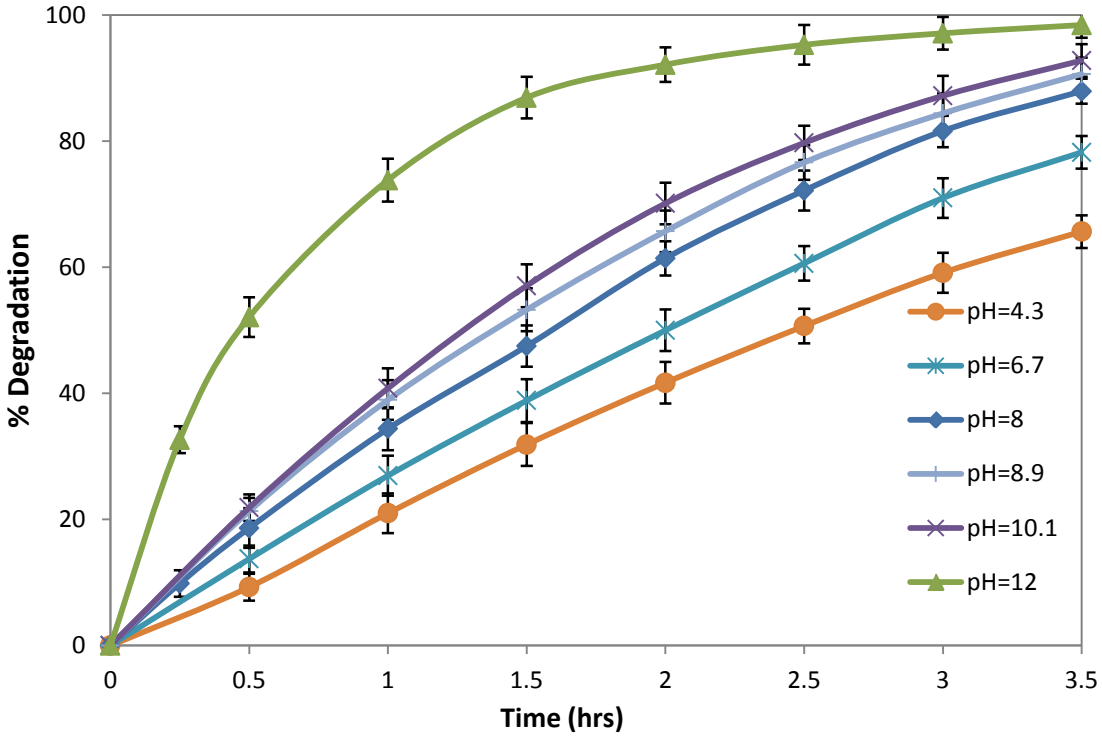

Figure 4.7: Photodegradation rates of MO solutions with different pH values catalyzed by ZnO nanowires prepared at the same conditions (pH 11.0, 60°C and 6 hours) (error bars: standard deviation).

Figure 4.7 depicts the degradation rates of MO solutions with different pH values photocatalyzed with the prepared ZnO nanowire arrays under the same conditions. It is observed the extent of photocatalysis increases with increasing pH, exhibiting a maximum rate of degradation at pH 12. Kansal *et al.* [146] have also observed similar results in their studies on pararosaniline chloride dye. It was also observed that no obvious reduction in the absorbance of the MO solutions sampled at each half hour in the 4 hours period, indicating that no severe hydrolysis of MO occurs in the solution with pH of 12, and the observed fast degradation rate of MO under pH 12 is mainly due to photocatalysis using ZnO nanowires.

In acidic environment, photodecomposition of ZnO takes place according to Equation (4.1):

$$ZnO + 2H^+ \rightarrow Zn^{2+} + H_2O \quad (4.1)$$

The photocorrosion of ZnO is most rapid in a strong acidic environment (pH lower than 4) [18]. In alkaline environment, photocorrosion of ZnO is less severe with increasing pH and no photocorrosion takes place at pH higher than 10 [18]. More importantly, in alkaline solution, large quantities of OH^- ions are present on the catalyst surface and in the reaction medium, which promotes the formation of hydroxyl radicals (OH·) [62], the species which have been widely accepted as the primary cause for organic dye degradation in photocatalytic reactions [51], [147], [148]. The mechanism is indicated by Equation (4.2) below:

$$OH \cdot + dye \rightarrow degradation\ byproducts \quad (4.2)$$

4.2.4 Effect of Initial Dye Concentration on Photocatalytic Activity

Successful application of the photocatalytic degradation system requires investigation of the effect of initial dye concentration of the dye solutions on the photocatalytic efficiency, as the industrial or household waste water comes in different concentrations. So in this project, the effect of initial dye concentration on the photodegradation rates of MO catalyzed by the prepared ZnO nanowire arrays was also investigated.

Figure 4.8 shows the photocatalytic degradation rates of MO solutions with different initial concentrations (1-20ppm) following the same treatment process. The results showed that the photocatalytic degradation rate decreased with increasing initial concentration of MO solution. By taking the percent degradation data after two hours of irradiation for each concentration curve from Figure 4.8, we can get a plot as shown in Figure 4.9.

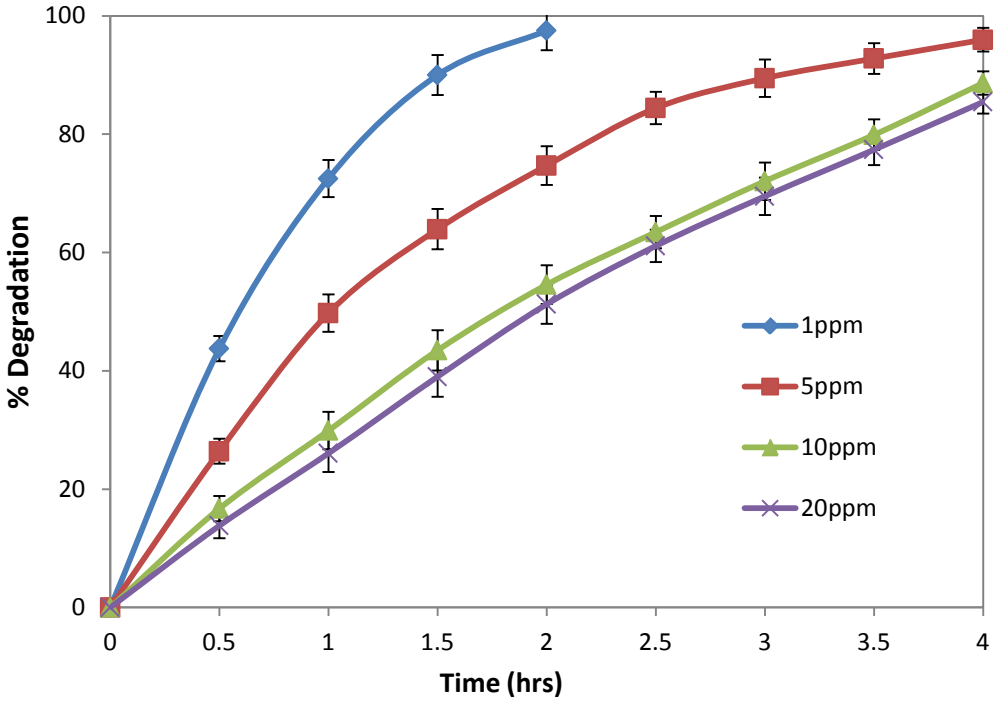

Figure 4.8: Photodegradation rates of MO solutions with different initial dye concentrations catalyzed by ZnO nanowires prepared at the same conditions (pH 11.0, 60°C and 6 hours) (error bars: standard deviation).

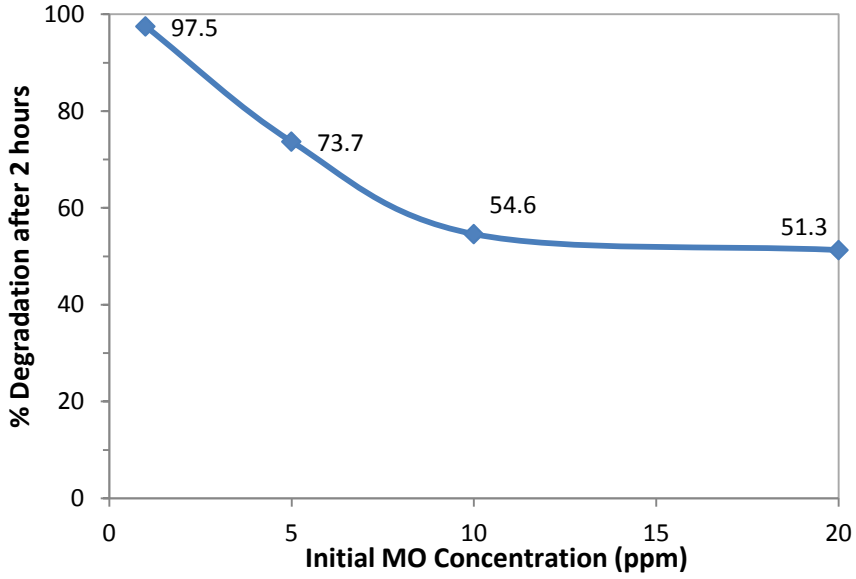

Figure 4.9: Percentage degradation after 2 hours of irradiation for each MO concentration.

From Figure 4.9, it is observed that the percentage of degradation dropped from 97.5% to 73.7% when the initial dye concentration increased from 1ppm to 5ppm after two hours of irradiation, and to 54.6% for 10ppm dye solution. Beyond 10ppm, the reduction in photodegradation efficiency is not very significant. As the dye concentration increases, more and more dye molecules get adsorbed onto the surface of the photocatalyst. Hence, the need for highly active species including hydroxyl radicals ($OH\cdot$) and superoxide anions ($O_2^{\cdot -}$) required to achieve a similar rate of dye degradation also increases [108]. However, for a given constant catalyst amount and irradiation time, the generation of the active species on the photocatalyst surface actually decreases with increasing dye concentrations, as the light intensity able to reach the catalyst surface to initiate the photoreaction decreases, as indicated by the reduction in the percentage transmittance of the incoming light intensity at 365nm in Figure 4.10. As a result, the active species available are inadequate for the photodegradation of dye at higher concentrations, and the deficit becomes more severe with increasing concentrations, which leading to the decrease in photodegradation rates of dye with increasing dye concentrations as observed in Figure 4.8. Moreover, the increase in the dye concentration can lead to the generation of more reaction intermediates as given by Equation (2.8), which can adsorb onto the catalyst surface. The slow diffusion of the generated intermediates from the catalyst surface can lead to the deactivation of the active sites on photocatalyst surface, and finally contribute to the reduction in the photodegradation efficiency with increasing dye concentrations [15]. In addition, when the dye concentration is very high (above 10ppm in this experiment), further increase in dye concentration will not lead to a significant reduction in photodegradation efficiency, as the catalyst surface is already saturated with the adsorbed dye molecules.

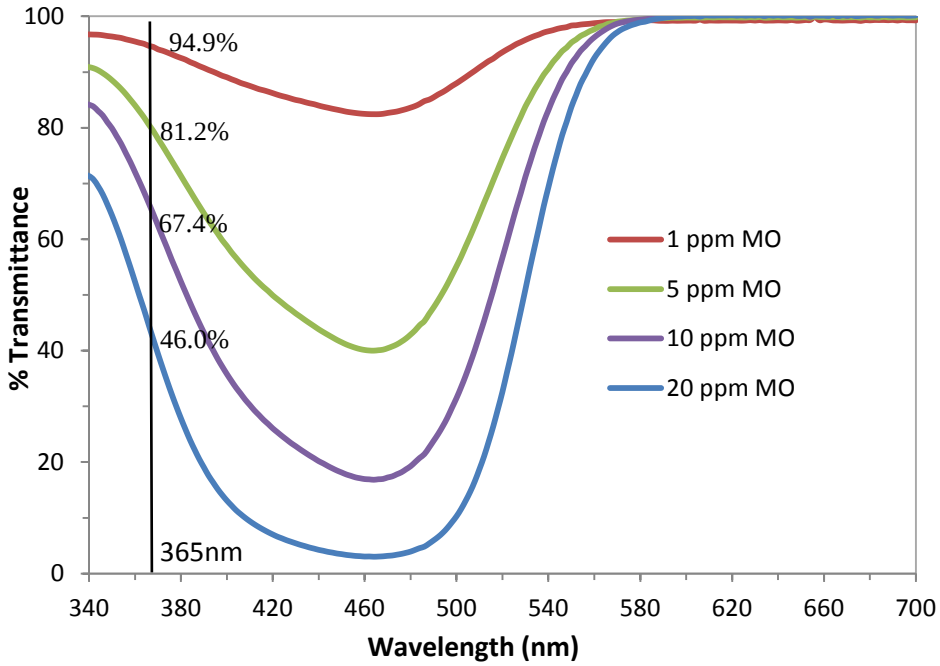

Figure 4.10: UV-Vis transmission spectra of MO solutions with different concentrations.

4.2.5 Effect of Synthesis Time on Photocatalytic Activity

As mentioned in the Section 2.5 before, the efficiency of a photocatalyst is highly dependent on its surface and structural properties, especially its specific surface area, as the photocatalytic degradation of organic pollutants usually takes place on the surface of the catalysts. Hence it is worth the effort to investigate the effect of the hydrothermal growth time duration on the morphologies of the resultant ZnO nanowires and in turn on their respective photocatalytic activities.

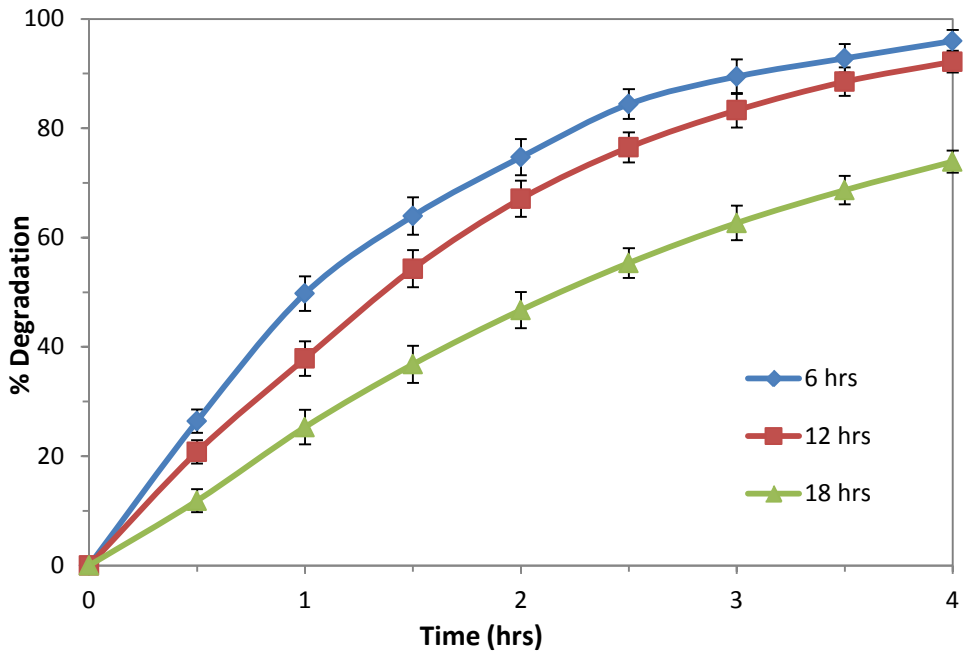

Figure 4.11: Photodegradation rates of MO solutions catalyzed by ZnO nanowires prepared for different growth durations (6, 12, and 18 hours) in the precursor solutions at the same conditions (pH 11.0, 60°C) (error bars: standard deviation).

Figure 4.11 shows the photodegradation rates of the same concentration MO solutions catalyzed by the ZnO nanowires obtained after three different time durations (6, 12, and 18 hours) in the hydrothermal precursor solutions with pH of 11.0 at 60°C, respectively. It can be observed that with longer growth duration, the obtained nanowire arrays exhibited a reduction in the photocatalytic efficiency. As reported by Joo *et al.* [141], there is a rapid growth of ZnO nanowires in the first 4 hours (initial stage), and then a low growth rate for up to 20 hours (growth stage). The growth rate is slowed down after the initial stage due to a depletion of the precursors in the growth solution. With increasing growth duration time, it is reported that both length and diameter of the prepared nanowires are increasing but the overall aspect ratio (L/D) is reduced [149]. In this experiment, the aspect ratios of the nanowires grown for different durations are found to be 15 for 6 hours, 10 for 12 hours and 8 for 18 hours. Hence, with longer growth duration, the aspect ratio of the nanowires decreases,

which gives a smaller surface-to-volume ratio of photocatalysts, and leads to a reduced photocatalytic activity.

4.3 Reusability of ZnO Nanowires

One of the main advantages of immobilizing the nanostructured photocatalysts onto a steady substrate, as mentioned earlier, is to eliminate the costly post-treatment process for catalyst separation and removal, as the immobilized form of catalysts on substrates can be easily taken out from the reaction bulk and recovered for reuse. As a next step, it is also of practical importance to evaluate the degree of reusability of the photocatalysts for degradation of organic pollutants.

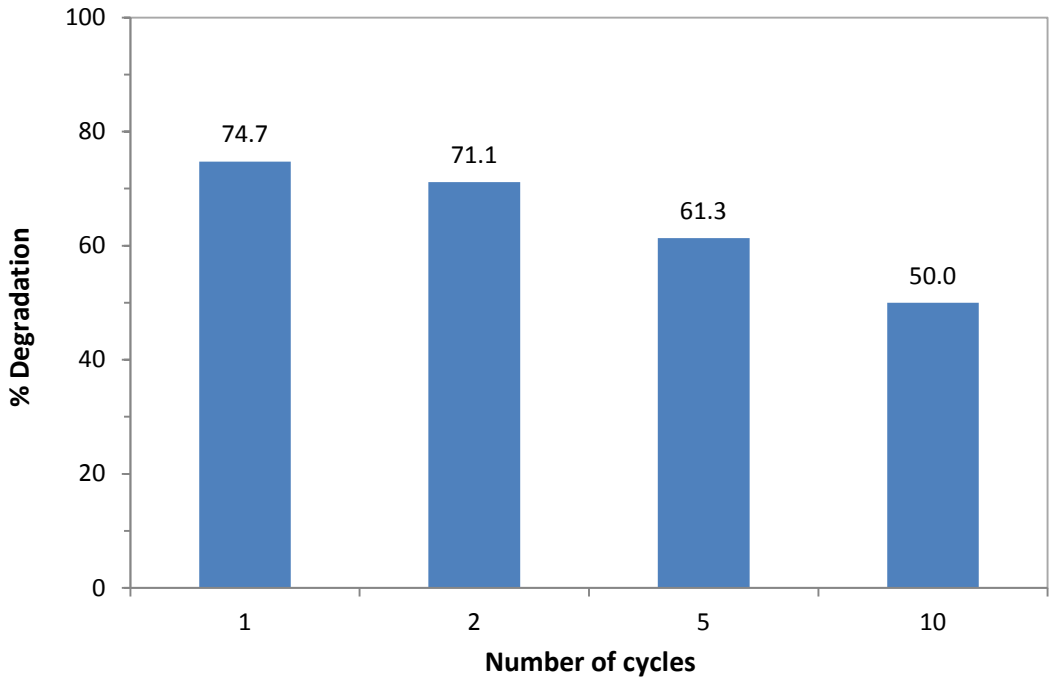

Figure 4.12: Percentage degradation values of MO solutions after 2 hours of irradiation using the same ZnO nanowire sample after multiple cycles.

In this project, in order to evaluate the reusability of the synthesized ZnO nanowire arrays for photocatalytic applications, the glass substrate with aligned ZnO nanowires was collected after each photodegradation of the 10mL MO solution (5ppm) for two hours, cleaned with DI water for several times and blow-dried in air. The dried catalyst sample was used again as photocatalysts for degradation of the same fresh dye solution following the same experimental conditions. The step was repeated for up to ten times, and the percentage degradation data after two hours of irradiation for the first, second, fifth and tenth cycles were calculated based on their absorbance data measured by the UV-Vis spectrophotometer, as shown in Figure 4.12. It can be observed that the photocatalytic efficiency of the synthesized ZnO nanowire arrays only exhibited a small reduction after each cycle (around 3%), and the samples still showed considerable photocatalytic activity even after ten cycles. The results reveal the stability of the synthesized ZnO nanowire arrays as photocatalysts for photocatalytic applications and a good potential for recycle and reuse in the industry.

4.4 Photocatalytic Efficiency in Microfluidic Device

4.4.1 Photodegradation Rate Comparison

The photocatalytic activity of the fabricated microfluidic device was evaluated by measuring the UV-Vis absorption spectra of the MO solution after UV irradiation. Figure 4.13 shows the recorded UV-Vis absorption spectra of the MO solutions after photodegradation in the ZnO nanowire-integrated microfluidic device with chamber height of 400μm at three different flow rates, in contrast to the 5ppm MO solution. By taking the peak absorbance from each curve and using Equation (3.6), the percentage degradation (%Degradation) can be calculated for each flow rate, as shown by the third row in Table 4.1. The residence time, τ, in Table 4.1 is calculated by the following equation:

$$\boldsymbol{\tau = V/Q} \qquad \textbf{(4.3)}$$

Where V is volume of the MO solution, which is 1mL in this experiment, and Q is the flow rate (µm/L).

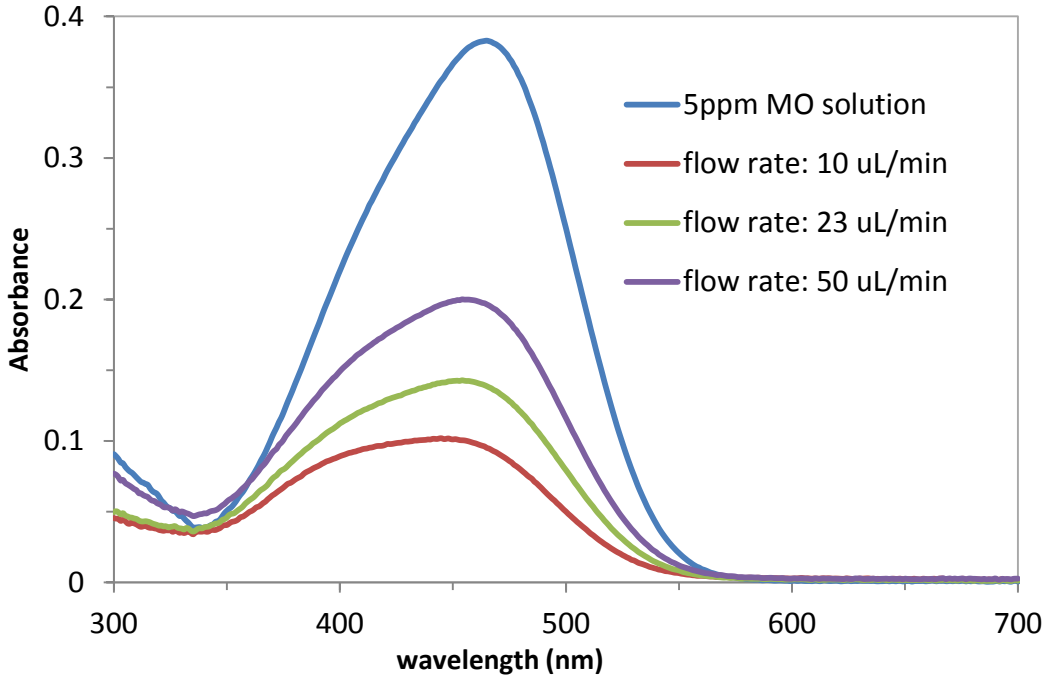

Figure 4.13: UV-Vis absorption spectra of the MO solutions measured after photodegradation in the same microfluidic device (chamber height: 400µm) with different flow rates.

Compared to the photodegradation rate of MO solution in the bulk as presented by the curve in Figure 4.5, the irradiation time required to achieve the same amount of percentage degradation is found and shown in Table 4.1. It is obvious that the irradiation time required to achieve the same amount of photodecomposition of MO is much longer in the bulk solution as compared to time required in the microfluidic device. To be more specific, the results show that the photodegradation rate of MO solution in the microfluidic device is 1.2 times faster under flow rate of 10µL/min, and twice under flow rate of 23µL/min, and triple under flow rate of 50µL/min, due to a much larger surface-to-volume ratio and other features inherent in the microfluidic devices mentioned earlier. In addition, the micro-chamber

environment for the photodegradation reactions to take place is much more optimized than the bulk solution, as constant stirring is not required and undesired evaporation of water solvent is not an issue here. Moreover, the diffusion distance of the dye molecules in the micro-chamber is much shorter than that in the bulk solution, which improves the photocatalytic efficiency in degrading organic pollutants in waste water.

Table 4.1: Photodegradation results for the microfluidic device with 400µm chamber height under different flow rates, and comparison with the results from bulk reaction.

Flow Rate, Q (µL/min)	**10**	**23**	**50**
Residence Time, τ (min) = V/Q	100	43.48	20
% Degradation	73.39	62.68	47.74
Required time in bulk reaction, t (min)	120	90	60
Efficiency improved (t/ τ)	1.2 x	2 x	3 x

4.4.2 Effects of Chamber Height and Flow Rate

The project studies the effects of chamber height and flow rate on the photocatalytic efficiency of MO solution in microfluidic device. Three microfluidic devices were fabricated individually with different chamber heights (400µm, 600µm, 800µm), and a set of photodegradation experiments were conducted for each device by varying the volumetric flow rate with a constant concentration of MO solution (5ppm, 1mL).

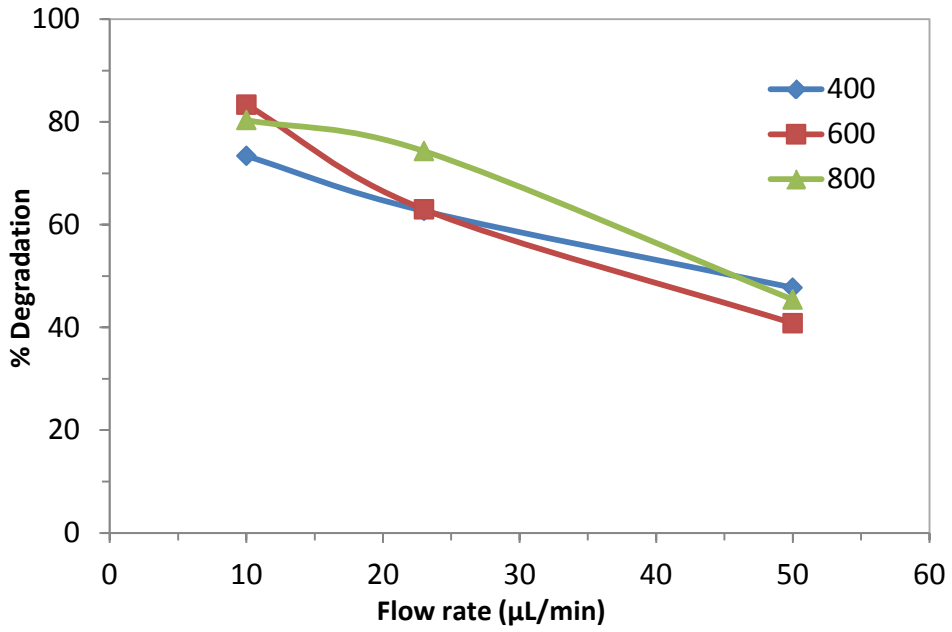

Figure 4.14: Effect of flow rate on the photocatalytic efficiency in each microfluidic device with different chamber heights (400, 600, and 800µm).

Figure 4.14 depicts the effect of the flow rate of the MO solution in the microfluidic device on the photocatalytic efficiency. The volumetric flow rate was controlled by the syringe pump and set to 10, 20, and 50µL/min, respectively. The reactions under each of the three flow rates were carried out in each of the microfluidic devices with different chamber heights (400, 600, and 800µm). The after-irradiated MO solution samples were collected and their UV-Vis absorbance was measured separately to determine their percentage degradation in each experiment, as plotted in Figure 4.14. It can be observed that the degradation rate decreases with increasing flow rate of the MO solution, for each of the three devices with different chamber heights. This is likely due to the fact that the actual reaction time for photodecomposition of MO molecules under UV irradiation, or namely, the residence time (τ) of the dye molecules in the micro-chamber, as calculated from Equation (4.3), is reduced under a higher flow rate, leading to a decreased photocatalytic efficiency.

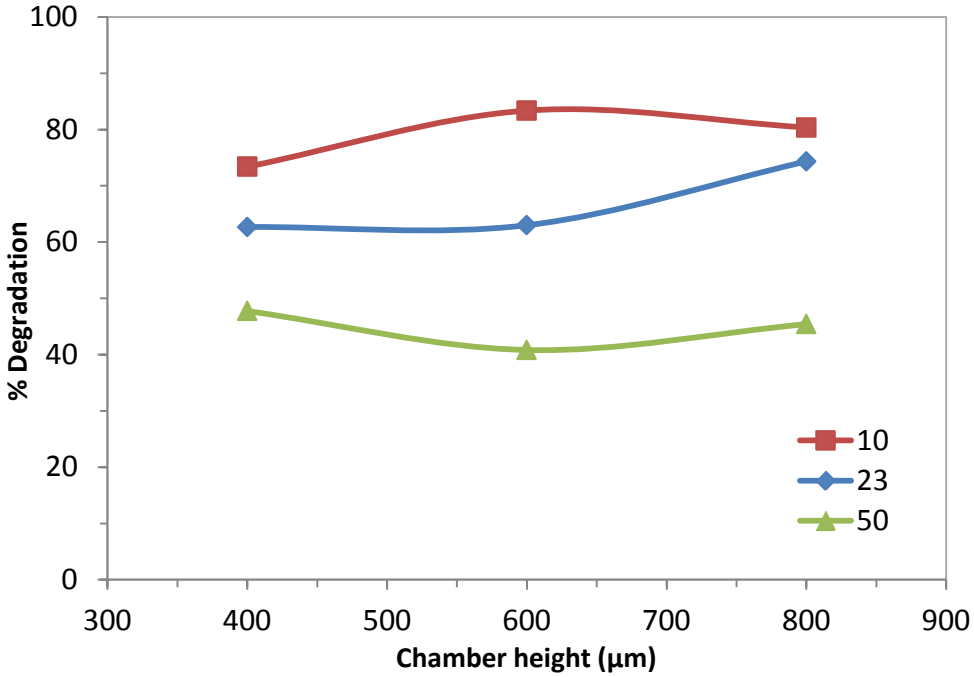

Figure 4.15: Effect of chamber height of the microfluidic devices on its photocatalytic efficiency under each flow rates (10, 20, and 50µL/min).

Figure 4.15 shows the effect of chamber height of the microfluidic device on the photocatalytic efficiency of the MO solutions. It can be observed that under three different flow rates, the change in the degradation results does not follow a single similar trend with increasing chamber height. Thus, we can conclude that the chamber height in the range of 400-800µm does not affect the photocatalytic efficiency of the ZnO nanowires integrated in the micro-chamber. This is possibly due to the fact that the chamber height of the microfluidic device is in the range a few hundred micrometers, which is about one hundred times smaller as compared to the solution height in the bulk reaction (around 1cm). Therefore, in the microfluidic device, the diffusion distance of dye molecules onto the catalyst surface is very short, and the transmission of the incoming light intensity through the dye solution to reach the catalyst surface is very high, neither of which is a limiting factor for the photodegradation efficiency.

Chapter 5

Conclusions and Recommendations

In this chapter, the work completed in the whole project will be summarized and concluded here. Some recommendations for possible improvements in the future studies in similar areas will also be suggested based on the results achieved.

5.1 General Conclusions

In this project, vertically-aligned ZnO nanowires on glass substrate were synthesized by using the facile hydrothermal methods assisted with seeding layer. The obtained samples were characterized by XRD, FE-SEM and UV-Vis Spectrometer to analyze their crystal structure, morphology and UV-Vis transmittance. Methyl Orange (MO) dye in aqueous solution was selected to be the model organic pollutant in waste water to evaluate the photocatalytic activity of the synthesized ZnO nanowire array samples. Their photocatalytic activities under different conditions were measured by the photodegradation rates of MO solution under UV-A irradiation with wavelength of 365nm. Moreover, an effort to miniaturize the photocatalytic degradation process into a micro-chamber based microfluidic device has been made to improve the photocatalytic efficiency.

The prepared ZnO nanowires are all vertically well aligned onto the glass substrate, with an average diameter of around 100nm and an average length of around 1.5μm, and have a hexagonal wurtzite structure with a high degree of crystallinity and anisotropy along the *c*-axis. The nanowires are capable of absorbing 96% of total intensity of the light source used in the experiment with main emission wavelength of 365nm. The synthesis method adopted

in this project to prepare ZnO nanowires is very simple, straightforward, has low cost and does not require high temperature or pressure, allowing for a wider choice of substrates and indicating a greater chance of scaling-up in the industry.

In the application of the prepared ZnO nanowire arrays as photocatalysts for photodegradation of MO solutions, 96% of the MO in aqueous solution was degraded after 4 hours irradiation of UV-A light source at 365nm, based on the absorbance value at 464nm (the peak absorption wavelength of MO molecules) of the MO solutions measured before and after UV irradiation. But no significant degradation of MO was observed in the absence of the photocatalyst. The reproducibility of the experimental methods was evaluated and a very consistent result was obtained, indicating a high reliability of the experimental results achieved. When the pH of the MO solution was increased, the photodegradation rate was found to be improved, due to a higher formation of hydroxyl radicals for decomposition of the dye. For different initial dye concentrations, it can be deduced that the photodegradation rate is reduced when the dye concentration becomes higher. Furthermore, the effect of the growth duration time of the ZnO nanowires on their photoactivity was also investigated and the results indicated a reduction in the photoefficiency for a longer growth time due to a reduction in the aspect ratio of the nanowires. Finally, the used ZnO nanowire photocatalysts were collected and reused for several cycles to test their stability and reusability, and it was found that a high photocatalytic activity was maintained after ten cycles.

A micro-chamber based microfluidic device integrated with vertically-aligned ZnO nanowires was designed and fabricated for highly efficient photocatalysis with large surface-to-volume ratio and continuous flow. As a result, the integrated microfluidic device demonstrated much superior photocatalytic efficiency in photodegradation of MO solutions over the conventional methods using bulk dye solutions. It has also been found that with a lower flow rate, the photoefficiency is higher due to a longer reaction time; while the chamber height of the device does not affect much the photoefficiency. In addition, the fabrication method used here is robust, low cost and has a good potential for scaling up, which could be applicable to many other photocatalytic systems.

5.2 Recommendations

Although the objectives of the project were all met, the scope of study could be much widened and deepened if more time and resource are available. More characterization techniques could be carried out to further analyze the structural properties of the samples. For example, transmission electron microscope (TEM) can be employed to investigate the lattice spacing, crystal size, and exposing lattice plane of the ZnO nanowire structure. The range of the parameters such as pH, initial dye concentration and growth duration time could be set wider to lead to a more comprehensive study. Other growth conditions such as precursor concentration, growth temperature, effect of seeing layer and light intensity could also be investigated in order to achieve a maximum photodegradation rate of MO solution.

More importantly, the microfluidic device could be continuously modified to improve its effectiveness and ease of fabrication. In the previous application of the device for photodegradation of MO solutions, a control experiment could be conducted by using the microfluidic device without UV irradiation or without integration of the ZnO nanowires. The preliminary results presented previously open a gate for many interesting studies about the ZnO nanowire-integrated microfluidic devices to be applied in the photocatalytic systems, such as its effectiveness for parametric studies of ZnO nanowire growth and of photodegradation reactions of many other organic pollutants. A microfluidic model could also be constructed to guide the photocatalytic reactions in the waste water treatment systems. Finally, the potential of scaling up for the device could be realized to accelerate the commercialization of the photocatalysis of organic pollutants.

Bibliography

[1] K. Tanaka, K. Padermpole, and T. Hisanaga, “Photocatalytic degradation of commercial azo dyes,” *Water Research*, vol. 34, no. 1, pp. 327–333, Jan. 2000.

[2] Y. M. Slokar and a. Majcen Le Marechal, “Methods of decoloration of textile wastewaters,” *Dyes and Pigments*, vol. 37, no. 4, pp. 335–356, May 1998.

[3] C. Galindo, P. Jacques, and a Kalt, “Photooxidation of the phenylazonaphthol AO20 on TIO2: kinetic and mechanistic investigations.,” *Chemosphere*, vol. 45, no. 6–7, pp. 997–1005, Nov. 2001.

[4] A. Fujishima, “Electrochemical photolysis of water at a semiconductor electrode,” *Nature*, vol. 238, no. 37, 1972.

[5] L. Li, H. Yang, H. Zhao, J. Yu, J. Ma, L. An, and X. Wang, “Hydrothermal synthesis and gas sensing properties of single-crystalline ultralong ZnO nanowires,” *Applied Physics A*, vol. 98, no. 3, pp. 635–641, Nov. 2009.

[6] S. Chu, G. Wang, W. Zhou, Y. Lin, L. Chernyak, J. Zhao, J. Kong, L. Li, J. Ren, and J. Liu, “Electrically pumped waveguide lasing from ZnO nanowires.,” *Nature nanotechnology*, vol. 6, no. 8, pp. 506–10, Aug. 2011.

[7] X.-M. Zhang, M.-Y. Lu, Y. Zhang, L.-J. Chen, and Z. L. Wang, “Fabrication of a High-Brightness Blue-Light-Emitting Diode Using a ZnO-Nanowire Array Grown on p-GaN Thin Film,” *Advanced Materials*, vol. 21, no. 27, pp. 2767–2770, Jul. 2009.

[8] Z. L. Wang and J. Song, “Piezoelectric nanogenerators based on zinc oxide nanowire arrays.,” *Science (New York, N.Y.)*, vol. 312, no. 5771, pp. 242–6, Apr. 2006.

[9] X. Wang, J. Zhou, J. Song, J. Liu, N. Xu, and Z. L. Wang, “Piezoelectric field effect transistor and nanoforce sensor based on a single ZnO nanowire.,” *Nano letters*, vol. 6, no. 12, pp. 2768–72, Dec. 2006.

[10] Y. C. Kong, D. P. Yu, B. Zhang, W. Fang, and S. Q. Feng, “Ultraviolet-emitting ZnO nanowires synthesized by a physical vapor deposition approach,” *Applied Physics Letters*, vol. 78, no. 4, p. 407, 2001.

[11] Y. C. Kong, D. P. Yu, B. Zhang, W. Fang, and S. Q. Feng, “Ultraviolet-emitting ZnO nanowires synthesized by a physical vapor deposition approach,” *Applied Physics Letters*, vol. 78, no. 4, p. 407, 2001.

[12] B. Cao, W. Cai, G. Duan, Y. Li, Q. Zhao, and D. Yu, “A template-free electrochemical deposition route to ZnO nanoneedle arrays and their optical and field emission properties,” *Nanotechnology*, vol. 16, no. 11, pp. 2567–2574, Nov. 2005.

[13] F. Lu, W. Cai, and Y. Zhang, “ZnO Hierarchical Micro/Nanoarchitectures: Solvothermal Synthesis and Structurally Enhanced Photocatalytic Performance,” *Advanced Functional Materials*, vol. 18, no. 7, pp. 1047–1056, Apr. 2008.

[14] K. Pirkanniemi and M. Sillanpää, “Heterogeneous water phase catalysis as an environmental application: a review.,” *Chemosphere*, vol. 48, no. 10, pp. 1047–60, Sep. 2002.

[15] S. Ahmed, M. G. Rasul, W. N. Martens, R. Brown, and M. a. Hashib, “Heterogeneous photocatalytic degradation of phenols in wastewater: A review on current status and developments,” *Desalination*, vol. 261, no. 1–2, pp. 3–18, Oct. 2010.

[16] A. Mills and S. Le Hunte, “An overview of semiconductor photocatalysis,” *Journal of photochemistry and photobiology A: Chemistry*, vol. 108, no. 1997, pp. 1–35, 1997.

[17] W. Z. Tang and A. Huren, “UV/TiO2 photocatalytic oxidation of commercial dyes in aqueous solutions,” *Chemoshpere*, vol. 31, no. 9, 1995.

[18] N. Daneshvar, D. Salari, and A. Khataee, “Photocatalytic degradation of azo dye acid red 14 in water on ZnO as an alternative catalyst to TiO2,” *Journal of Photochemistry and Photobiology A: Chemistry*, vol. 162, no. 2–3, pp. 317–322, Mar. 2004.

[19] A. A. Khodja, T. Sehili, J. Pilichowski, and P. Boule, “Photocatalytic degradation of 2-phenylphenol on TiO2 and ZnO in aqueous suspensions,” *Journal of Photochemistry and Photobiology A: Chemistry*, vol. 141, pp. 231–239, 2001.

[20] Q. Wan, T. H. Wang, and J. C. Zhao, “Enhanced photocatalytic activity of ZnO nanotetrapods,” *Applied Physics Letters*, vol. 87, no. 8, p. 083105, 2005.

[21] D. S. Bhatkhande, V. G. Pangarkar, and A. A. Beenackers, “Photocatalytic degradation for environmental applications - a review,” *Journal of Chemical Technology & Biotechnology*, vol. 77, no. 1, pp. 102–116, Jan. 2002.

[22] Y. Matatov-Meytal and V. Barelko, “Cloth catalysts for water denitrification: II. Removal of nitrates using Pd–Cu supported on glass fibers,” *Applied Catalysis B: Environmental*, vol. 31, pp. 233–240, 2001.

[23] Y. Zhang, M. K. Ram, E. K. Stefanakos, and D. Y. Goswami, “Synthesis, Characterization, and Applications of ZnO Nanowires,” *Journal of Nanomaterials*, vol. 2012, pp. 1–22, 2012.

[24] S. Linic, P. Christopher, and D. B. Ingram, “Plasmonic-metal nanostructures for efficient conversion of solar to chemical energy.,” *Nature materials*, vol. 10, no. 12, pp. 911–21, Dec. 2011.

[25] M. Fox and M. Dulay, “Heterogeneous photocatalysis,” *Chemical reviews*, vol. 93, pp. 341–357, 1993.

[26] A. Ibhadon and P. Fitzpatrick, “Heterogeneous Photocatalysis: Recent Advances and Applications,” *Catalysts*, vol. 3, no. 1, pp. 189–218, Mar. 2013.

[27] A. Fujishima, T. Rao, and D. Tryk, “Titanium dioxide photocatalysis,” *Journal of Photochemistry and Photobiology C: Photochemistry Reviews*, vol. 1, no. March, pp. 1–21, 2000.

[28] D. H. Lindsley, “Experimental studies of oxide minerals,” *Reviews in Mineralogy and Geochemistry*, vol. 25, no. 1, pp. 69–106, Jan. 1991.

[29] Q. Deng, M. Wei, X. Ding, L. Jiang, B. Ye, and K. Wei, “Brookite-type TiO(2) nanotubes.,” *Chemical communications (Cambridge, England)*, no. 31, pp. 3657–9, Aug. 2008.

[30] U. Diebold, “The surface science of titanium dioxide,” *Surface Science Reports*, vol. 48, no. 5–8, pp. 53–229, Jan. 2003.

[31] R. C. Bhave and B. I. Lee, “Experimental variables in the synthesis of brookite phase TiO2 nanoparticles,” *Materials Science and Engineering: A*, vol. 467, no. 1–2, pp. 146–149, Oct. 2007.

[32] J. Zhuang, W. Dai, Q. Tian, Z. Li, L. Xie, J. Wang, P. Liu, X. Shi, and D. Wang, “Photocatalytic degradation of RhB over TiO2 bilayer films: effect of defects and their location.,” *Langmuir : the ACS journal of surfaces and colloids*, vol. 26, no. 12, pp. 9686–94, Jun. 2010.

[33] I. Dolamic and B. Thomas, “In Situ ATR-IR Study on the Photocatalytic Decomposition of Amino Acids over Au / TiO 2 and TiO 2,” pp. 2228–2234, 2011.

[34] S. Matsushita, T. Miwa, D. Tryk, and A. Fujishima, “New mesostructured porous TiO2 surface prepared using a two-dimensional array-based template of silica particles,” *Langmuir*, no. 24, pp. 6441–6447, 1998.

[35] D. Ollis, E. Pelizzetti, and N. Serpone, “Photocatalyzed destruction of water contaminants,” *Environmental Science Technology*, vol. 25, no. 9, 1991.

[36] A. Linsebigler, G. Lu, and J. Y. Jr, “Photocatalysis on TiO2 surfaces: principles, mechanisms, and selected results,” *Chemical Reviews*, vol. 95, pp. 735–758, 1995.

[37] X. Chen and S. S. Mao, “Titanium dioxide nanomaterials: synthesis, properties, modifications, and applications.,” *Chemical reviews*, vol. 107, no. 7, pp. 2891–959, Jul. 2007.

[38] R. Asahi, T. Morikawa, T. Ohwaki, K. Aoki, and Y. Taga, “Visible-light photocatalysis in nitrogen-doped titanium oxides.,” *Science (New York, N.Y.)*, vol. 293, no. 5528, pp. 269–71, Jul. 2001.

[39] M. Anpo, “The design and development of highly reactive titanium oxide photocatalysts operating under visible light irradiation,” *Journal of Catalysis*, vol. 216, no. 1–2, pp. 505–516, Jun. 2003.

[40] S. U. M. Khan, M. Al-Shahry, and W. B. Ingler, “Efficient photochemical water splitting by a chemically modified n-TiO2.,” *Science (New York, N.Y.)*, vol. 297, no. 5590, pp. 2243–5, Sep. 2002.

[41] C. Di Valentin, G. Pacchioni, H. Onishi, and A. Kudo, “Cr/Sb co-doped TiO2 from first principles calculations,” *Chemical Physics Letters*, vol. 469, no. 1–3, pp. 166–171, Feb. 2009.

[42] M. Ladanov, M. K. Ram, G. Matthews, and A. Kumar, “Structure and opto-electrochemical properties of ZnO nanowires grown on n-Si substrate.,” *Langmuir : the ACS journal of surfaces and colloids*, vol. 27, no. 14, pp. 9012–7, Jul. 2011.

[43] A. Sapkota, A. J. Anceno, S. Baruah, O. V Shipin, and J. Dutta, “Zinc oxide nanorod mediated visible light photoinactivation of model microbes in water.,” *Nanotechnology*, vol. 22, no. 21, p. 215703, May 2011.

[44] B. Dindar and S. Içli, “Unusual photoreactivity of zinc oxide irradiated by concentrated sunlight,” *Journal of Photochemistry and Photobiology A: Chemistry*, vol. 140, no. January, pp. 263–268, 2001.

[45] K. M. Parida, S. S. Dash, and D. P. Das, “Physico-chemical characterization and photocatalytic activity of zinc oxide prepared by various methods.,” *Journal of colloid and interface science*, vol. 298, no. 2, pp. 787–93, Jun. 2006.

[46] J. L. Yang, S. J. An, W. I. Park, G.-C. Yi, and W. Choi, “Photocatalysis Using ZnO Thin Films and Nanoneedles Grown by Metal-Organic Chemical Vapor Deposition,” *Advanced Materials*, vol. 16, no. 18, pp. 1661–1664, Sep. 2004.

[47] J. Chen, C. Li, J. L. Song, X. W. Sun, W. Lei, and W. Q. Deng, “Bilayer ZnO nanostructure fabricated by chemical bath and its application in quantum dot sensitized solar cell,” *Applied Surface Science*, vol. 255, no. 17, pp. 7508–7511, Jun. 2009.

[48] L. Vayssieres, “Growth of Arrayed Nanorods and Nanowires of ZnO from Aqueous Solutions,” *Advanced Materials*, vol. 15, no. 5, pp. 464–466, Mar. 2003.

[49] M. Yeber, J. Rodríguez, J. Freer, and J. Baeza, “Advanced oxidation of a pulp mill bleaching wastewater,” *Chemosphere*, vol. 39, no. 10, pp. 1679–1688, 1999.

[50] N. Serpone, P. Maruthamuthu, P. Pichat, E. Pelizzetti, and H. Hidaka, “Exploiting the interparticle electron transfer process in the photocatalysed oxidation of phenol, 2-chlorophenol and pentachlorophenol: chemical evidence for electron and hole transfer between coupled semiconductors,” *Journal of Photochemistry and Photobiology A: Chemistry*, vol. 85, no. 3, pp. 247–255, Jan. 1995.

[51] G. Marci and V. Augugliaro, “Preparation characterization and photocatalytic activity of polycrystalline ZnO/TiO2 systems. 2. Surface, bulk characterization, and 4-nitrophenol photodegradation in,” *The Journal of Physical Chemistry B*, vol. 105, no. 5, pp. 1033–1040, 2001.

[52] Q. Zhang, C. S. Dandeneau, X. Zhou, and G. Cao, “ZnO Nanostructures for Dye-Sensitized Solar Cells,” *Advanced Materials*, vol. 21, no. 41, pp. 4087–4108, Nov. 2009.

[53] S. Baruah, M. A. Mahmood, M. T. Z. Myint, T. Bora, and J. Dutta, “Enhanced visible light photocatalysis through fast crystallization of zinc oxide nanorods.,” *Beilstein journal of nanotechnology*, vol. 1, pp. 14–20, Jan. 2010.

[54] R. Wang, J. H. Xin, Y. Yang, H. Liu, L. Xu, and J. Hu, “The characteristics and photocatalytic activities of silver doped ZnO nanocrystallites,” *Applied Surface Science*, vol. 227, no. 1–4, pp. 312–317, Apr. 2004.

[55] K. Vanheusden, W. L. Warren, J. a. Voigt, C. H. Seager, and D. R. Tallant, “Impact of Pb doping on the optical and electronic properties of ZnO powders,” *Applied Physics Letters*, vol. 67, no. 9, p. 1280, 1995.

[56] S. Colis, H. Bieber, S. Bégin-Colin, G. Schmerber, C. Leuvrey, and a. Dinia, “Magnetic properties of Co-doped ZnO diluted magnetic semiconductors prepared by low-temperature mechanosynthesis,” *Chemical Physics Letters*, vol. 422, no. 4–6, pp. 529–533, May 2006.

[57] R. Ullah and J. Dutta, “Photocatalytic degradation of organic dyes with manganese-doped ZnO nanoparticles.,” *Journal of hazardous materials*, vol. 156, no. 1–3, pp. 194–200, Aug. 2008.

[58] S. Baruah, R. F. Rafique, and J. Dutta, “Visible Light Photocatalysis By Tailoring Crystal Defects in Zinc Oxide Nanostructures,” *Nano*, vol. 03, no. 05, pp. 399–407, Oct. 2008.

[59] N. Sobana and M. Swaminathan, “The effect of operational parameters on the photocatalytic degradation of acid red 18 by ZnO,” *Separation and Purification Technology*, vol. 56, no. 1, pp. 101–107, Aug. 2007.

[60] B. Neppolian and S. Sakthivel, “Degradation of textile dye by solar light using TiO2 and ZnO photocatalysts,” *Journal of Environmental Science & Health, Part A: Toxic/hazardous Substances and Environmental Engineering*, vol. 34, no. 9, pp. 1829–1838, 1999.

[61] N. V. Kaneva, D. T. Dimitrov, and C. D. Dushkin, “Effect of nickel doping on the photocatalytic activity of ZnO thin films under UV and visible light,” *Applied Surface Science*, vol. 257, no. 18, pp. 8113–8120, Jul. 2011.

[62] S. Sakthivel, B. Neppolian, M. V Shankar, B. Arabindoo, M. Palanichamy, and V. Murugesan, “Solar photocatalytic degradation of azo dye : comparison of photocatalytic efficiency of ZnO and TiO 2,” *Solar Energy Materials & SOlar Cells*, vol. 77, no. 3, pp. 65–82, 2003.

[63] I. N. Martyanov, E. N. Savinov, and K. J. Klabunde, “Influence of solution composition and ultrasonic treatment on optical spectra of TiO2 aqueous suspensions,” *Journal of Colloid and Interface Science*, vol. 267, no. 1, pp. 111–116, Nov. 2003.

[64] S. Martin, “Photochemical mechanism of size-quantized vanadium-doped TiO2 particles,” *The Journal of Physical Chemistry*, vol. 98, no. 51, pp. 13695–13704, 1994.

[65] S. Klosek and D. Raftery, “Visible Light Driven V-Doped TiO 2 Photocatalyst and Its Photooxidation of Ethanol,” pp. 2815–2819, 2001.

[66] M. Cabrera, O. Alfano, and A. Cassano, “Absorption and scattering coefficients of titanium dioxide particulate suspensions in water,” *The Journal of Physical Chemistry*, vol. 100, no. 51, pp. 20043–20050, 1996.

[67] A. Alkauskas and A. Pasquarello, “Band-edge problem in the theoretical determination of defect energy levels: The O vacancy in ZnO as a benchmark case,” *Physical Review B*, vol. 84, no. 12, p. 125206, Sep. 2011.

[68] C. Klingshirn, “ZnO: material, physics and applications.,” *Chemphyschem : a European journal of chemical physics and physical chemistry*, vol. 8, no. 6, pp. 782–803, Apr. 2007.

[69] U. Özgür, Y. I. Alivov, C. Liu, a. Teke, M. a. Reshchikov, S. Doğan, V. Avrutin, S.-J. Cho, and H. Morkoç, “A comprehensive review of ZnO materials and devices,” *Journal of Applied Physics*, vol. 98, no. 4, p. 041301, 2005.

[70] M. Mehrabian, R. Azimirad, K. Mirabbaszadeh, H. Afarideh, and M. Davoudian, “UV detecting properties of hydrothermal synthesized ZnO nanorods,” *Physica E: Low-dimensional Systems and Nanostructures*, vol. 43, no. 6, pp. 1141–1145, Apr. 2011.

[71] C. F. Klingshirn, B. K. Meyer, A. Waag, A. Hoffmann, and J. Geurts, *Zinc Oxide: From Fundamental Properties Towards Novel Applications*. Heidelberg: Springer, 2010, pp. 9–10.

[72] S. J. Cho, D. Maysinger, M. Jain, B. Röder, S. Hackbarth, and F. M. Winnik, “Long-term exposure to CdTe quantum dots causes functional impairments in live cells.,” *Langmuir : the ACS journal of surfaces and colloids*, vol. 23, no. 4, pp. 1974–80, Feb. 2007.

[73] W. Liu, A. B. Greytak, J. Lee, C. R. Wong, J. Park, L. F. Marshall, W. Jiang, P. N. Curtin, A. Y. Ting, D. G. Nocera, D. Fukumura, R. K. Jain, and M. G. Bawendi, “Compact biocompatible quantum dots via RAFT-mediated synthesis of imidazole-based random copolymer ligand.,” *Journal of the American Chemical Society*, vol. 132, no. 2, pp. 472–83, Jan. 2010.

[74] G. Kenanakis and N. Katsarakis, “Light-induced photocatalytic degradation of stearic acid by c-axis oriented ZnO nanowires,” *Applied Catalysis A: General*, vol. 378, no. 2, pp. 227–233, Apr. 2010.

[75] P. Kamat, “Photophysical, photochemical and photocatalytic aspects of metal nanoparticles,” *The Journal of Physical Chemistry B*, pp. 7729–7744, 2002.

[76] B. Weintraub, Z. Zhou, Y. Li, and Y. Deng, “Solution synthesis of one-dimensional ZnO nanomaterials and their applications,” *Nanoscale*, vol. 2, no. 9, pp. 1573–1587, 2010.

[77] Y. Xia, P. Yang, Y. Sun, Y. Wu, B. Mayers, B. Gates, Y. Yin, F. Kim, and H. Yan, “One-Dimensional Nanostructures: Synthesis, Characterization, and Applications,” *Advanced Materials*, vol. 15, no. 5, pp. 353–389, Mar. 2003.

[78] G.-C. Yi, C. Wang, and W. Il Park, “ZnO nanorods: synthesis, characterization and applications,” *Semiconductor Science and Technology*, vol. 20, no. 4, pp. S22–S34, Apr. 2005.

[79] Z. L. Wang, “Ten years’ venturing in ZnO nanostructures: from discovery to scientific understanding and to technology applications,” *Chinese Science Bulletin*, vol. 54, no. 22, pp. 4021–4034, Jul. 2009.

[80] M. K. Kim, D. K. Yi, and U. Paik, “Tunable, flexible antireflection layer of ZnO nanowires embedded in PDMS.,” *Langmuir : the ACS journal of surfaces and colloids*, vol. 26, no. 10, pp. 7552–4, May 2010.

[81] L. Li, T. Zhai, H. Zeng, X. Fang, Y. Bando, and D. Golberg, “Polystyrene sphere-assisted one-dimensional nanostructure arrays: synthesis and applications,” *Journal of Materials Chemistry*, vol. 21, no. 1, p. 40, 2011.

[82] S. Baruah and J. Dutta, “Hydrothermal growth of ZnO nanostructures,” *Science and Technology of Advanced Materials*, vol. 10, no. 1, p. 013001, Jan. 2009.

[83] Z. L. Wang, “Zinc oxide nanostructures: growth, properties and applications,” *Journal of Physics: Condensed Matter*, vol. 16, no. 25, pp. R829–R858, Jun. 2004.

[84] S. Baruah and J. Dutta, “pH-dependent growth of zinc oxide nanorods,” *Journal of Crystal Growth*, vol. 311, no. 8, pp. 2549–2554, Apr. 2009.

[85] Z. Zhang and J. Mu, “Hydrothermal synthesis of ZnO nanobundles controlled by PEO–PPO–PEO block copolymers,” *Journal of Colloid and Interface Science*, vol. 307, no. 1, pp. 79–82, Mar. 2007.

[86] B. D. Yao, Y. F. Chan, and N. Wang, “Formation of ZnO nanostructures by a simple way of thermal evaporation,” *Applied Physics Letters*, vol. 81, no. 4, p. 757, 2002.

[87] Y. Zhang, N. Wang, S. Gao, R. He, S. Miao, J. Liu, J. Zhu, and X. Zhang, “A Simple Method To Synthesize Nanowires,” *Chemistry of Materials*, vol. 14, no. 8, pp. 3564–3568, Aug. 2002.

[88] E. W. Petersen, E. M. Likovich, K. J. Russell, and V. Narayanamurti, “Growth of ZnO nanowires catalyzed by size-dependent melting of Au nanoparticles.,” *Nanotechnology*, vol. 20, no. 40, p. 405603, Oct. 2009.

[89] L. Wang, X. Zhang, S. Zhao, G. Zhou, Y. Zhou, and J. Qi, “Synthesis of well-aligned ZnO nanowires by simple physical vapor deposition on c-oriented ZnO thin films without catalysts or additives,” *Applied Physics Letters*, vol. 86, no. 2, p. 024108, 2005.

[90] L. N. Protasova, E. V. Rebrov, K. L. Choy, S. Y. Pung, V. Engels, M. Cabaj, a. E. H. Wheatley, and J. C. Schouten, "ZnO based nanowires grown by chemical vapour deposition for selective hydrogenation of acetylene alcohols," *Catalysis Science & Technology*, vol. 1, no. 5, p. 768, 2011.

[91] S. Ashraf, A. C. Jones, J. Bacsa, A. Steiner, P. R. Chalker, P. Beahan, S. Hindley, R. Odedra, P. a. Williams, and P. N. Heys, "MOCVD of Vertically Aligned ZnO Nanowires Using Bidentate Ether Adducts of Dimethylzinc," *Chemical Vapor Deposition*, vol. 17, no. 1–3, pp. 45–53, Mar. 2011.

[92] J. S. Wang, C. S. Yang, P. I. Chen, C. F. Su, W. J. Chen, K. C. Chiu, and W. C. Chou, "Catalyst-free highly vertically aligned ZnO nanoneedle arrays grown by plasma-assisted molecular beam epitaxy," *Applied Physics A*, vol. 97, no. 3, pp. 553–557, Oct. 2009.

[93] L. C. Tien, S. J. Pearton, D. P. Norton, and F. Ren, "Synthesis and microstructure of vertically aligned ZnO nanowires grown by high-pressure-assisted pulsed-laser deposition," *Journal of Materials Science*, vol. 43, no. 21, pp. 6925–6932, Sep. 2008.

[94] R. S. Wagner and W. C. Ellis, "Vapor-Liquid-Solid Mechanism of Single Crystal Growth," *Applied Physics Letters*, vol. 4, no. 5, p. 89, 1964.

[95] D.-I. Suh, C. C. Byeon, and C.-L. Lee, "Synthesis and optical characterization of vertically grown ZnO nanowires in high crystallinity through vapor–liquid–solid growth mechanism," *Applied Surface Science*, vol. 257, no. 5, pp. 1454–1456, Dec. 2010.

[96] M. Huang, Y. Wu, H. Feick, and N. Tran, "Catalytic growth of zinc oxide nanowires by vapor transport," *Advanced Materials*, vol. 13, no. 2, pp. 113–116, 2001.

[97] Y. W. Wang, L. D. Zhang, G. Z. Wang, X. S. Peng, Z. Q. Chu, and C. H. Liang, "Catalytic growth of semiconducting zinc oxide nanowires and their photoluminescence properties," *Journal of Crystal Growth*, vol. 234, no. 1, pp. 171–175, Jan. 2002.

[98] S. Y. Li, C. Y. Lee, and T. Y. Tseng, "Copper-catalyzed ZnO nanowires on silicon (100) grown by vapor–liquid–solid process," *Journal of Crystal Growth*, vol. 247, no. 3–4, pp. 357–362, Jan. 2003.

[99] Y. Ding, P. X. Gao, and Z. L. Wang, "Catalyst-nanostructure interfacial lattice mismatch in determining the shape of VLS grown nanowires and nanobelts: a case of Sn/ZnO.," *Journal of the American Chemical Society*, vol. 126, no. 7, pp. 2066–72, Feb. 2004.

[100] W. I. Park, D. H. Kim, S.-W. Jung, and G.-C. Yi, “Metalorganic vapor-phase epitaxial growth of vertically well-aligned ZnO nanorods,” *Applied Physics Letters*, vol. 80, no. 22, p. 4232, 2002.

[101] R. Laudise, “Hydrothermal growth of large sound crystals of zinc oxide,” *Journal of the American Ceramics Society*, vol. 47, no. 1, pp. 9–12, 1964.

[102] M. H. Huang, S. Mao, H. Feick, H. Yan, Y. Wu, H. Kind, E. Weber, R. Russo, and P. Yang, “Room-temperature ultraviolet nanowire nanolasers.,” *Science (New York, N.Y.)*, vol. 292, no. 5523, pp. 1897–9, Jun. 2001.

[103] L. E. Greene, B. D. Yuhas, M. Law, D. Zitoun, and P. Yang, “Solution-grown zinc oxide nanowires.,” *Inorganic chemistry*, vol. 45, no. 19, pp. 7535–43, Sep. 2006.

[104] B. Liu and H. C. Zeng, “Hydrothermal synthesis of ZnO nanorods in the diameter regime of 50 nm.,” *Journal of the American Chemical Society*, vol. 125, no. 15, pp. 4430–1, Apr. 2003.

[105] C. Wu, L. Shen, H. Yu, Q. Huang, and Y. C. Zhang, “Synthesis of Sn-doped ZnO nanorods and their photocatalytic properties,” *Materials Research Bulletin*, vol. 46, no. 7, pp. 1107–1112, Jul. 2011.

[106] S. K. Lim, S. H. Hwang, and S. Kim, “Microemulsion synthesis and characterization of aluminum doped ZnO nanorods,” *Crystal Research and Technology*, vol. 45, no. 7, pp. 771–775, Apr. 2010.

[107] A. Sugunan, H. C. Warad, M. Boman, and J. Dutta, “Zinc oxide nanowires in chemical bath on seeded substrates: Role of hexamine,” *Journal of Sol-Gel Science and Technology*, vol. 39, no. 1, pp. 49–56, May 2006.

[108] W. Bahnemann, M. Muneer, and M. M. Haque, “Titanium dioxide-mediated photocatalysed degradation of few selected organic pollutants in aqueous suspensions,” *Catalysis Today*, vol. 124, no. 3–4, pp. 133–148, Jun. 2007.

[109] M. Qamar, M. Saquib, and M. Muneer, “Titanium dioxide mediated photocatalytic degradation of two selected azo dye derivatives, chrysoidine R and acid red 29 (chromotrope 2R), in aqueous suspensions,” *Desalination*, vol. 186, no. 1–3, pp. 255–271, Dec. 2005.

[110] M. Qamar, M. Saquib, and M. Muneer, “Photocatalytic degradation of two selected dye derivatives, chromotrope 2B and amido black 10B, in aqueous suspensions of titanium dioxide,” *Dyes and Pigments*, vol. 65, no. 1, pp. 1–9, Apr. 2005.

[111] M. Saquib, M. Abu Tariq, M. M. Haque, and M. Muneer, “Photocatalytic degradation of disperse blue 1 using UV/TiO2/H2O2 process.,” *Journal of environmental management*, vol. 88, no. 2, pp. 300–6, Jul. 2008.

[112] M. A. Tariq, M. Faisal, and M. Muneer, “Semiconductor-mediated photocatalysed degradation of two selected azo dye derivatives, amaranth and bismarck brown in aqueous suspension.,” *Journal of hazardous materials*, vol. 127, no. 1–3, pp. 172–9, Dec. 2005.

[113] M. Abu Tariq, M. Faisal, M. Saquib, and M. Muneer, “Heterogeneous photocatalytic degradation of an anthraquinone and a triphenylmethane dye derivative in aqueous suspensions of semiconductor,” *Dyes and Pigments*, vol. 76, no. 2, pp. 358–365, 2008.

[114] M. Faisal, M. Abu Tariq, and M. Muneer, “Photocatalysed degradation of two selected dyes in UV-irradiated aqueous suspensions of titania,” *Dyes and Pigments*, vol. 72, no. 2, pp. 233–239, Jan. 2007.

[115] M. Haque and M. Muneer, “TiO2-mediated photocatalytic degradation of a textile dye derivative, bromothymol blue, in aqueous suspensions,” *Dyes and Pigments*, vol. 75, no. 2, pp. 443–448, 2007.

[116] N. H. Salah, M. Bouhelassaa, S. Bekkouche, and A. Boultii, “Study of photocatalytic degradation of phenol,” *Desalination*, vol. 166, pp. 347–354, 2004.

[117] A. E. Cassano and O. M. Alfano, “Reaction engineering of suspended solid heterogeneous photocatalytic reactors,” *Catalysis Today*, vol. 58, no. 2–3, pp. 167–197, May 2000.

[118] V. Pareek and S. Chong, “Light intensity distribution in heterogenous photocatalytic reactors,” *Asia-Pacific Journal of Chemial Engineering*, vol. 3, pp. 171–201, 2008.

[119] J. Herrmann, “Heterogeneous photocatalysis: fundamentals and applications to the removal of various types of aqueous pollutants,” *Catalysis Today*, vol. 53, no. 1, pp. 115–129, Oct. 1999.

[120] G. Al-Sayyed, J. D’Oliveira, and P. Pichat, “Semiconductor-sensitized photodegradation of 4-chlorophenol in water,” *Journal of Photochemistry and Photobiology A: Chemistry*, vol. 58, pp. 99–114, 1991.

[121] N. Venkatachalam, M. Palanichamy, and V. Murugesan, “Sol–gel preparation and characterization of alkaline earth metal doped nano TiO2: Efficient photocatalytic degradation of 4-chlorophenol,” *Journal of Molecular Catalysis A: Chemical*, vol. 273, no. 1–2, pp. 177–185, Aug. 2007.

[122] P. R. Shukla, S. Wang, H. M. Ang, and M. O. Tadé, “Photocatalytic oxidation of phenolic compounds using zinc oxide and sulphate radicals under artificial solar light,” *Separation and Purification Technology*, vol. 70, no. 3, pp. 338–344, Jan. 2010.

[123] S. Hong, C. Ju, and C. Lim, “A photocatalytic degradation of phenol over TiO2 prepared by sol-gel method,” *Journal of Industrial and Engineering Chemistry*, vol. 7, no. 2, pp. 99–104, 2001.

[124] M. H. Priya and G. Madras, “Photocatalytic degradation of nitrobenzenes with combustion synthesized nano-TiO2,” *Journal of Photochemistry and Photobiology A: Chemistry*, vol. 178, no. 1, pp. 1–7, Feb. 2006.

[125] S. K. Pardeshi and a. B. Patil, “A simple route for photocatalytic degradation of phenol in aqueous zinc oxide suspension using solar energy,” *Solar Energy*, vol. 82, no. 8, pp. 700–705, Aug. 2008.

[126] R. W. Matthews, “Purification of water with near—u.v. illuminated suspensions of titanium dioxide,” *Water Research*, vol. 24, no. 5, pp. 653–660, May 1990.

[127] R. Matthews, “Kinetics of photocatalytic oxidation of organic solutes over titanium dioxide,” *Journal of Catalysis*, vol. 272, pp. 264–272, 1988.

[128] A. Mills and S. Morris, “Photomineralization of 4-chlorophenol sensitized by titanium dioxide: a study of the initial kinetics of carbon dioxide photogeneration,” *Journal of Photochemistry and Photobiology A: Chemistry*, vol. 71, no. 1, pp. 75–83, Mar. 1993.

[129] K. Selvam, M. Muruganandham, I. Muthuvel, and M. Swaminathan, “The influence of inorganic oxidants and metal ions on semiconductor sensitized photodegradation of 4-fluorophenol,” *Chemical Engineering Journal*, vol. 128, no. 1, pp. 51–57, Mar. 2007.

[130] A. A. Adesina, “Industrial exploitation of photocatalysis: progress, perspectives and prospects,” *Catalysis Surveys from Asia*, vol. 8, no. 4, pp. 265–273, Dec. 2004.

[131] M. A. Barakat, H. Schaeffer, G. Hayes, and S. Ismat-Shah, “Photocatalytic degradation of 2-chlorophenol by Co-doped TiO2 nanoparticles,” *Applied Catalysis B: Environmental*, vol. 57, no. 1, pp. 23–30, Apr. 2005.

[132] S. Lathasree, A. N. Rao, B. SivaSankar, V. Sadasivam, and K. Rengaraj, “Heterogeneous photocatalytic mineralisation of phenols in aqueous solutions,” *Journal of Molecular Catalysis A: Chemical*, vol. 223, no. 1–2, pp. 101–105, Dec. 2004.

[133] H. K. Singh, M. Saquib, M. M. Haque, M. Muneer, and D. W. Bahnemann, “Titanium dioxide mediated photocatalysed degradation of phenoxyacetic acid and 2,4,5-

trichlorophenoxyacetic acid, in aqueous suspensions," *Journal of Molecular Catalysis A: Chemical*, vol. 264, no. 1–2, pp. 66–72, Mar. 2007.

[134] M. M. Haque, M. Muneer, and D. W. Bahnemann, "Semiconductor-mediated Photocatalyzed degradation of a herbicide derivative, chlorotoluron, in aqueous suspensions.," *Environmental science & technology*, vol. 40, no. 15, pp. 4765–70, Aug. 2006.

[135] P. Watts and C. Wiles, "Micro reactors: a new tool for the synthetic chemist.," *Organic & biomolecular chemistry*, vol. 5, no. 5, pp. 727–32, Mar. 2007.

[136] Z. He, Y. Li, Q. Zhang, and H. Wang, "Capillary microchannel-based microreactors with highly durable ZnO/TiO2 nanorod arrays for rapid, high efficiency and continuous-flow photocatalysis," *Applied Catalysis B: Environmental*, vol. 93, no. 3–4, pp. 376–382, Jan. 2010.

[137] G. Charles and S. Corbel, "Design of a micro-channel reactor for decomposition of organic pollutants in waste water treatment," *Design and …*, pp. 4–7, 2009.

[138] Z. Han, J. Li, W. He, S. Li, Z. Li, J. Chu, and Y. Chen, "A microfluidic device with integrated ZnO nanowires for photodegradation studies of methylene blue under different conditions," *Microelectronic Engineering*, vol. 111, pp. 199–203, Nov. 2013.

[139] Z. Meng, X. Zhang, and J. Qin, "A high efficiency microfluidic-based photocatalytic microreactor using electrospun nanofibrous TiO2 as a photocatalyst.," *Nanoscale*, vol. 5, no. 11, pp. 4687–90, Jun. 2013.

[140] J. Kim, Z. Li, and I. Park, "Direct synthesis and integration of functional nanostructures in microfluidic devices.," *Lab on a chip*, vol. 11, no. 11, pp. 1946–51, Jun. 2011.

[141] J. Joo, B. Y. Chow, M. Prakash, E. S. Boyden, and J. M. Jacobson, "Face-selective electrostatic control of hydrothermal zinc oxide nanowire synthesis.," *Nature materials*, vol. 10, no. 8, pp. 596–601, Aug. 2011.

[142] S. Xu, C. Lao, B. Weintraub, and Z. L. Wang, "Density-controlled growth of aligned ZnO nanowire arrays by seedless chemical approach on smooth surfaces," *Journal of Materials Research*, vol. 23, no. 08, pp. 2072–2077, Jan. 2008.

[143] T. Otto, W. Habicht, E. Dinjus, and M. Zimmerman, "Catalyst Characterization with FESEM/EDX by the Example of Silver-Catalyzed Epoxidation of 1, 3-Butadiene," in *Scanning Electron Microscopy*, Dr. Viache., 2012.

[144] S. Chakrabarti and B. K. Dutta, “Photocatalytic degradation of model textile dyes in wastewater using ZnO as semiconductor catalyst.,” *Journal of hazardous materials*, vol. 112, no. 3, pp. 269–78, Aug. 2004.

[145] F. Zhang, J. Zhao, T. Shen, H. Hidaka, E. Pelizzetti, and N. Serpone, “Ti02-assisted photodegradation of dye pollutants II . Adsorption and degradation kinetics of eosin in Ti02 dispersions under visible light irradiation,” *Applied Catalysis B: Environmental*, vol. 15, pp. 147–156, 1998.

[146] S. K. Kansal, A. H. Ali, S. Kapoor, and D. W. Bahnemann, “Synthesis of flower like zinc oxide nanostructure and its application as a photocatalyst,” *Separation and Purification Technology*, vol. 80, no. 1, pp. 125–130, Jul. 2011.

[147] N. Daneshvar, D. Salari, and M. Behnasuady, “DECOMPOSITION OF ANIONIC SODIUM DODECYLBENZENE SULFONATE BY UV/TIO2 AND UV/H202 PROCESSES A-COMPARISON OF REACTION RATES,” *Iranian Journal of Chemistry & Chemical Engineering*, vol. 21, no. 1, p. 55, 2002.

[148] C. Galindo, P. Jacques, and A. Kalt, “Photodegradation of the aminoazobenzene acid orange 52 by three advanced oxidation processes : UV / H 2 O 2 , UV / TiO 2 and VIS / TiO 2 Comparative mechanistic and kinetic investigations,” vol. 130, pp. 35–47, 2000.

[149] S. Baruah and J. Dutta, “Effect of seeded substrates on hydrothermally grown ZnO nanorods,” *Journal of Sol-Gel Science and Technology*, vol. 50, no. 3, pp. 456–464, Feb. 2009.